https://ntrs.nasa.gov/search.jsp?R=19660022821 2020-03-16T21:15:00+00:00Z

A STATISTICAL MODEL FOR APPLICATION OF MANEUVER FLIGHT LOADS DATA TO STRUCTURAL DESIGN CRITERIA

By Alan P. Berens, Larry E. Clay,
and F. Joseph Giessler

August 1965

GPO PRICE $ _____

CFSTI PRICE(S) $ _____

Hard copy (HC) 3.00

Microfiche (MF) .75

ff 653 July 65

Report No. 970-65-4

Prepared Under Contract No. NASw-970 by

TECHNOLOGY INCORPORATED
DAYTON, OHIO

for

NATIONAL AERONAUTICS AND SPACE ADMINISTRATION
WASHINGTON, D. C.

N66 32111 (ACCESSION NUMBER) (THRU)

102 (PAGES) 1 (CODE)

CR-76426 (NASA CR OR TMX OR AD NUMBER) 02 (CATEGORY)

FACILITY FORM 602

A STATISTICAL MODEL FOR APPLICATION OF MANEUVER FLIGHT LOADS DATA TO STRUCTURAL DESIGN CRITERIA

By Alan P. Berens, Larry E. Clay,
and F. Joseph Giessler

Distribution of this report is provided in the interest of information exchange. Responsibility for the contents resides in the author or organization that prepared it.

Prepared Under Contract No. NASw-970 by
TECHNOLOGY INCORPORATED
DAYTON, OHIO

for

NATIONAL AERONAUTICS AND SPACE ADMINISTRATION

FOREWORD

This report covers research conducted by Technology Incorporated, Dayton, Ohio, to determine the feasibility of using a proposed statistical maneuver model to predict the distribution of maneuver load peaks at any point in an aircraft's structure. The research was conducted for the Office of Advanced Research and Technology, National Aeronautics and Space Administration, and authorized under Contract NASw-970. Mr. Harvey H. Brown, chief, Loads and Structures Branch, was the project monitor. Personnel of Technology Incorporated having the prime responsibility in this program were Mr. William B. Walcott, director of the Astronautics Division, who acted as the project supervisor, and Mr. Larry E. Clay, research engineer, who served as the project engineer. Research began on 1 July 1964 and ended on 27 August 1965.

The authors gratefully acknowledge the assistance of the following personnel of Technology Incorporated: Mr. Cyril G. Peckham, director of the Data Processing Division; Mr. Thomas J. Hogan, scientific programmer; Mr. Robert J. Papajcik, scientific programmer; Mr. John F. Nash, supervisor of data reduction; and Mr. Chris E. Passerello, technical assistant.

ABSTRACT

A study was conducted to test the feasibility of using a proposed statistical maneuver model of aircraft center-of-gravity motions to predict for a given maneuver type the distribution of maneuver load peaks at any point in an aircraft's structure. Proven feasibility of this model would permit more meaningful application of maneuver flight loads data to structural design criteria. Consequently, a statistical maneuver model was derived for a data sample consisting of 318 descending left turns selected from available F-105D eight-channel flight loads data. From this model, distributions of peak loads were predicted for the shear load at three different locations in the F-105D structure. As evidence of the feasibility of the model, the predicted distributions compared very favorably with "observed" distributions of the loads of peaks obtained from three load time histories calculated for each of the 318 maneuvers.

author!

CONTENTS

ILLUSTRATIONS

ILLUSTRATIONS (cont'd.)

ILLUSTRATIONS (cont'd.)

ILLUSTRATIONS (cont'd.)

ILLUSTRATIONS (cont'd)

TABLES

TABLES (cont'd)

SYMBOLS

a_i	linear acceleration of structural element i, feet/second^2
a_x	linear acceleration in x-direction, feet/second^2
a_y	linear acceleration in y-direction, feet/second^2
a_z	linear acceleration in z-direction, feet/second^2
b	wing span, feet
g	acceleration due to gravity, feet/second^2
I_x	moment of inertia about x-axis, slug-feet^2
I_y	moment of inertia about y-axis, slug-feet^2
I_z	moment of inertia about z-axis, slug-feet^2
I_{xz}	product of inertia, slug-feet^2
L_i	inertia force on structural element i, pounds
L_{yA}	lateral airload on wing-fuselage combination, pounds
L_{yv}	lateral airload on vertical tail, pounds
L_{zA}	normal airload on wing-fuselage combination, pounds
L_{zF}	normal airload on fuselage, pounds
L_{zH}	normal airload on horizontal tail, pounds
L_{zw}	normal airload on wing, pounds
m	mass, slugs
m(y)	mass distribution of structure per foot of span, slugs/foot
n_x	longitudinal load factor
n_y	lateral load factor
$n_y'(c)$	corrected distribution of normalized lateral load factors

n_z	normal load factor
$n_z'(c)$	corrected distribution of normalized normal load factors
p	roll rate, degrees/second
$\dot{p}$	roll acceleration, degrees/second^2
$\dot{p}'(c)$	corrected distribution of normalized roll accelerations
$P(\,)$ or $P\{\,\}$	indicates probability of indicated event
q	pitch rate, degrees/second
$\dot{q}$	pitch acceleration, degrees/second^2
$\dot{q}'(c)$	corrected distribution of normalized pitch acceleration
r	yaw rate, degrees/second
$\dot{r}$	yaw acceleration, degrees/second^2
$\dot{r}'(c)$	corrected distribution of normalized yaw acceleration
V	shear load, pounds
V_{6A}	wing shear load at station 6A, pounds
V_{RHT}	horizontal tail shear load at the root station, pounds
V_{RVT}	vertical tail shear load at the root station, pounds
V_y	shear load at y, pounds
W	instantaneous gross weight of aircraft, pounds
W_D	design gross weight of aircraft, pounds
w_i	weight of structural element i, pounds
x	coordinate axis

x_{yA}	distance along x-axis from aircraft c. g. to point of action of L_{yA}, feet
x_{yv}	distance along x-axis from aircraft c. g to point of action of L_{yv}, feet
x_{zA}	distance along x-axis from aircraft c. g. to point of action of L_{zA}, feet
x_{zH}	distance along x-axis from aircraft c. g. to point of action of L_{zH}, feet
y	coordinate axis
y_i	distance from xz plane to c. g. of structural element i, feet
y_w	distance along y-axis from aircraft c. g. to point of action of L_{zw}, feet
z	coordinate axis
z_v	distance parallel to z-axis from x-axis to point of action of L_{yv}, feet
α	limit of a summation
β	limit of a summation
ΔL_{zw}	differential airload on wing, pounds
θ_{1y}	percent of L_{zA} contributing to V_y airload
θ_{2y}	percent of ΔL_{zw} contributing to V_y airload
θ	Euler angle for pitch relative to space-fixed coordinate system
ϕ	Euler angle for roll relative to space-fixed coordinate system
Ψ	Euler angle for yaw relative to space-fixed coordinate system
$\omega_1(y)$	percent of L_{zA} per foot of span
$\omega_2(y)$	percent of ΔL_{zw} per foot of span
$( )^*$	indicates simplified relation

Subscripts

c. g.	for aircraft center of gravity
i	for element i
i, j, k	summation indices

1. INTRODUCTION AND BACKGROUND

This study was conducted to test the feasibility of using a proposed statistical maneuver model to predict for a given maneuver type the distribution of maneuver load peaks at any point in an aircraft's structure. Since the specification of design loads is the primary objective of the design criteria, such a model, if proved feasible, would certainly enhance the structural design criteria. At the onset, the requirements specified in existing structural design criteria were examined to determine the specific aspects of these requirements to which the model could be applied advantageously.

1.1 Design Criteria Requirements

Aircraft structural design criteria have been defined in previous reports as "those documented requirements compliance with which is believed to assure a high level of structural integrity in operational aircraft." Included among these "documented requirements" are requirements to withstand loads imposed on the structure by maneuvering and atmospheric turbulence while the aircraft is in flight. These flight loads may be divided into four groups—maneuvering static design limit loads, gust design limit static loads, maneuvering fatigue loads, and gust fatigue loads.

Early aircraft design criteria dealt only with static design limit loads, that is, loads whose duration is not considered important. To ensure that these loads were calculated properly, the design criteria specified a set of critical design maneuver flight conditions for which the designer had to derive a set of static ultimate design loads for the various structural components (wing, fuselage, vertical tail, horizontal tail, etc.). Upon completion of the flight test aircraft, the aircraft manufacturer was required to perform demonstration flights in which the aircraft was subjected to each of the critical design maneuver flight conditions specified in the design criteria. In addition to the aircraft's demonstrating its capability of operating satisfactorily under the prescribed flight conditions, data collected during flight evidenced the degree of accuracy attained in calculating the design structural loads. This procedure, which provides a quick and relatively inexpensive check on the ultimate design load values, serves as the basis of present military design criteria.

Besides the set of critical design maneuver flight conditions, the design criteria specified the design maximum gust conditions which the designer also had to consider in calculating the static ultimate design loads. Atmospheric turbulence can provide a critical design flight condition for (1) a cargo or bomber type of aircraft having a relatively low design load

factor or (2) a high-performance type of aircraft which encounters a gust while performing a high load factor maneuver.

In addition to static ultimate design loads, the designer must calculate the effects of repeated, or fatigue, maneuver and gust loadings on the structure. The design criteria governing his calculations for the effects of repeated maneuver loads is a loads frequency spectrum derived from three-channel (airspeed, altitude and normal acceleration) maneuver data recorded on service aircraft during normal operation. This type of spectrum indicates the frequency of loads at various load levels expressed as percentages of positive and negative design load factors. And the design criteria governing the designer's calculations for the effects of repeated gust loads is a gust input spectrum expressed in the form of a power spectral density.

Before the accumulation of appreciable flight time, each new aircraft type is subjected to a cyclic fatigue test on the ground. This test is based on a loading spectrum calculated from the maneuver load spectrum and the gust input spectrum specified in the design criteria. The test is continued until a failure occurs in the primary structure. Using the fatigue test data and early service flight loads data (including suitable scatter factors to compensate for the limited sample size), an estimate is made of the safe service life for the aircraft type.

The major deficiency of the present design criteria is their inability to account for asymmetrical fatigue loads since such loads cannot be derived from the spectrum of normal accelerations. Instances of fatigue failures in tail surfaces indicate the need for design criteria using a fatigue spectrum based on asymmetrical loads. Also, a quantitative estimate of the probability of exceeding given percentages of the design maximum asymmetrical loads would be desirable.

1.2 Application of Flight Loads Data to Design Criteria

To calculate aircraft loads from the rigid-body equations of motion requires recording at least eight parameters. The eight listed in Table 1 were used in this program.

Three other required parameters—$\dot{p}$ (roll angular acceleration), $\dot{q}$ (pitch angular acceleration), and $\dot{r}$ (yaw angular acceleration)—can be derived by differentiating the recorded analog traces of p, q, and r. The dynamic and static pressures are used to derive airspeed, altitude, and Mach number. Substituting these data in the rigid-body equations of motion will yield structural loads for any part of the aircraft.

TABLE 1

Eight-Channel Recorded Parameters

n_x—longitudinal c.g. acceleration (positive forward)

n_y—lateral c.g. acceleration (positive right)

n_z—vertical c.g. acceleration (positive up)

p —roll angular velocity (positive right wing down)

q —pitch angular velocity (positive nose up)

r —yaw angular velocity (positive nose right)

P_d—dynamic pressure

P_a—static pressure

Because of the expense and complexity of recording and processing eight-channel oscillograph data, only a limited amount of this type of data now exists. However, digital recorders (predominantly magnetic tape) will soon be in service to record, in volume, eight-channel data in a form compatible with digital computers. Obviously, the handling of a large amount of eight-channel data requires a computer program to reduce the data into a meaningful form and a method of statistically calculating distributions of loads from distributions of the basic parameters to avoid the excessive expense of re-processing all the data points each time a load spectrum calculation is needed. This program was intended primarily to test the feasibility of a proposed method of statistically calculating the loads.

Since 1954 various reports have proposed several methods of calculating the structural loads from eight-channel data. All methods involve the use of statistical techniques because of the huge size of the data sample and the variations in the sample due to the uncontrollable effects of different pilot techniques, atmospheric turbulence, geographic topology, and weather conditions.

A commonly proposed statistical technique utilizes probability density functions of discrete samples of the parameters (usually the parameter peak values). This method, known as the "peak-count method," has some serious shortcomings, two of which are described below:

(1) The number of load peaks on some aircraft components is not necessarily related to the number of recorded parameter peaks. For example, since vertical tail

loads can be considered a function of n_y, $\dot{r}$, and $\dot{p}$, it would seem reasonable to correlate vertical tail load peaks with peaks of each of these parameters. However, Figure 1 shows a case where n_y and $\dot{r}$ peak at slightly different times with only a single corresponding vertical tail load peak. In other instances, a single vertical tail load peak still appears when only one of the n_y and $\dot{r}$ parameters peaks outside the threshold. Consequently, the total number of vertical tail load peaks is probably more than the total number of either the n_y or $\dot{r}$ peaks but less than the sum of the totals.

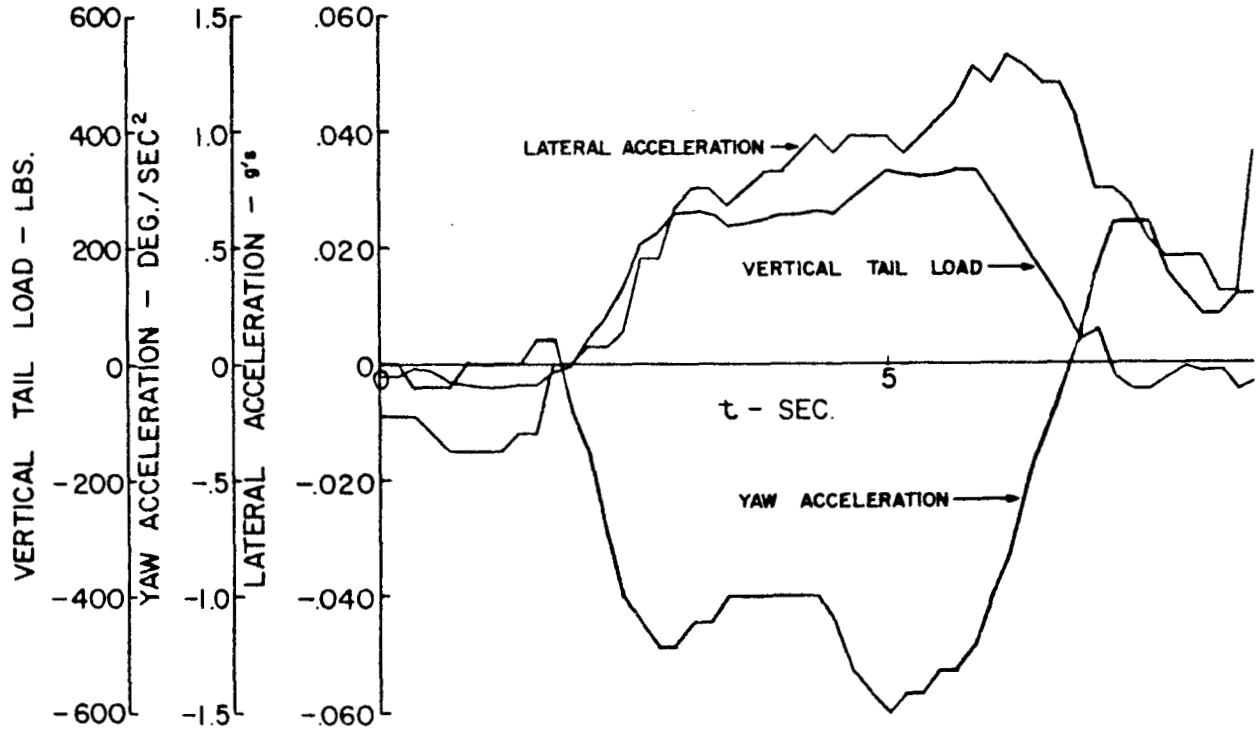

Figure 1. Sample Time Histories for Tail Load, Yaw Acceleration, and Lateral Acceleration

(2) Structural load peaks do not necessarily coincide in time with the peak of one of the basic parameters. For example, Figure 1, which is a time-history plot for a portion of a left turn, shows the vertical tail load peak occurring between the n_y and $\dot{r}$ peaks. During the reduction of data to peak-count form, the parameter values corresponding to the vertical tail load peak are discarded whenever the peaks of the former do not occur simultaneously with the peaks of the latter.

These shortcomings indicate that the peak-count method cannot adequately predict structural load distributions.

1.3 Proposed Statistical Maneuver Model

The proposed statistical model is limited to maneuver loads. As discussed later, the distribution of gust loads to be combined with the calculated maneuver loads must be determined by other means such as a power spectral density technique.

The basic unit in maneuver flight loads data is the maneuver itself—the result of the pilot's effort to change his flight path. If the data were broken down into the different types of maneuvers performed and if all the loads associated with each maneuver type were calculated, the loads spectrum for each flight and each mission and finally for the entire life of the aircraft could be constructed from these maneuver loads. This procedure requires two steps:

(1) Each maneuver type must be represented by an accurate set of parameter time histories applicable to all maneuvers of the same type.

(2) The number and type of maneuvers performed during each flight, mission type, and life of the aircraft must be estimated.

Since all aircraft generally perform the same type of maneuvers, the sets of parameter time histories determined for the maneuver types of one aircraft could be applied to other aircraft types if the effects of the configuration of the instrumented aircraft could be removed from the data. Since this extension is an important part of the proposed application of flight loads to design criteria, a third step is required:

(3) The data for each maneuver type must be normalized to remove the effects of aircraft configuration and the factors used to perform the normalizing must be recorded.

The flow chart in Figure 2 presents the basic program to establish design criteria from maneuver loads in the light of the foregoing discussion. Normalized time histories of the various parameters for each maneuver type are derived from the data of one aircraft type. From these time histories, distributions of normalized parameters are derived to form a statistical model. Then, combining the model with the distributions of recorded parameter peak values and with the aircraft aerodynamic and

inertial properties yields an expected distribution of structural loads. Applying the statistical model to other aircraft types does not require recalculating the distributions of normalized parameters.

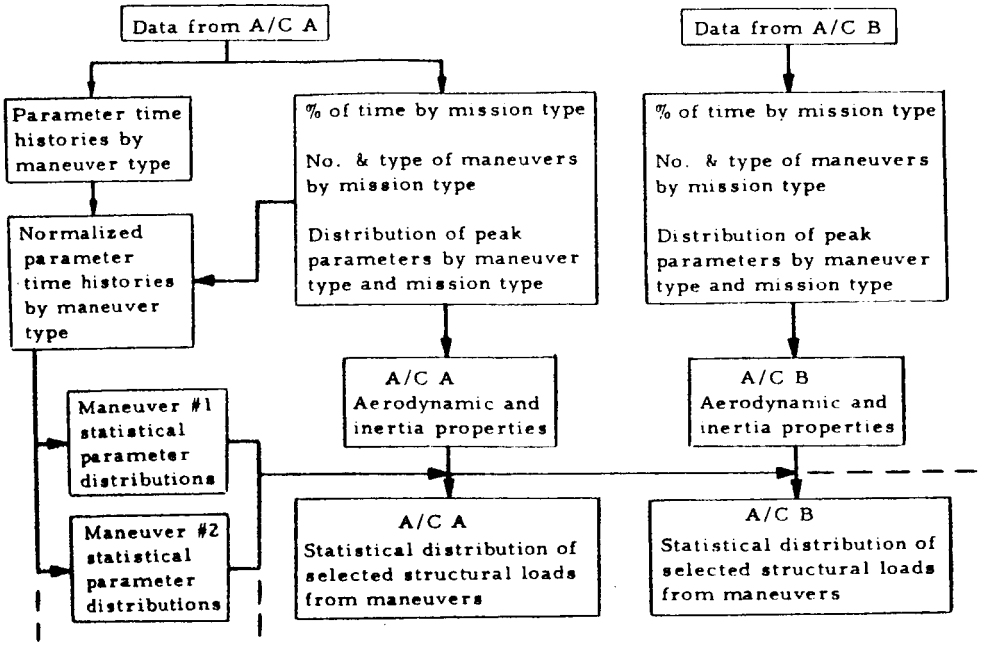

Figure 2. Flow Chart of Proposed Basic Program

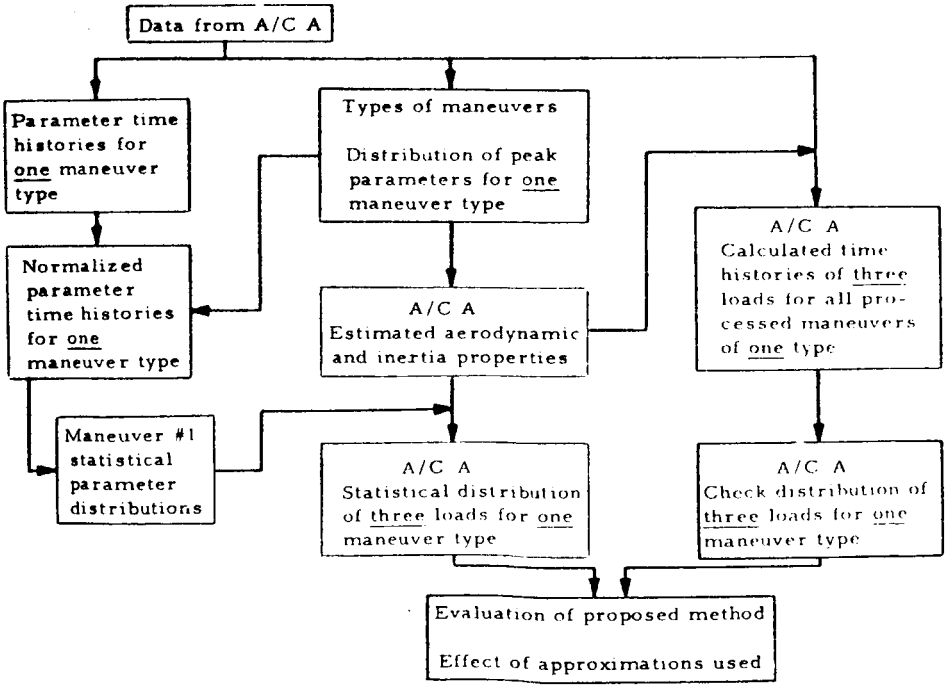

Figure 3. Flow Chart Showing Major Phases of Proposed Basic Program Included in This Study

The flow chart in Figure 3 indicates the phases of the basic program covered in this study. A sample of 318 descending left turns was derived from eight-channel data recorded on F-105D aircraft. The time scales were transformed to align the parameter traces, and the parameter time histories were normalized by using the peak values. From the distributions of the normalized parameters at specified transformed times, the distribution of parameter peaks, and the estimated aerodynamic and inertial properties, distributions of peak loads were calculated statistically. From time histories of these loads calculated for each individual descending left turn, actual distributions of peak loads were derived to check the statistical calculations.

2. DISCUSSION

2.1 F-105D Eight-Channel Data

The eight-channel data selected to illustrate the proposed statistical model were recorded during the normal operation of F-105D aircraft based at Wheelus Air Base, Libya; Kadena Air Base, Okinawa; and Nellis Air Force Base, Nevada. A view of the F-105D aircraft is shown in Figure 4.

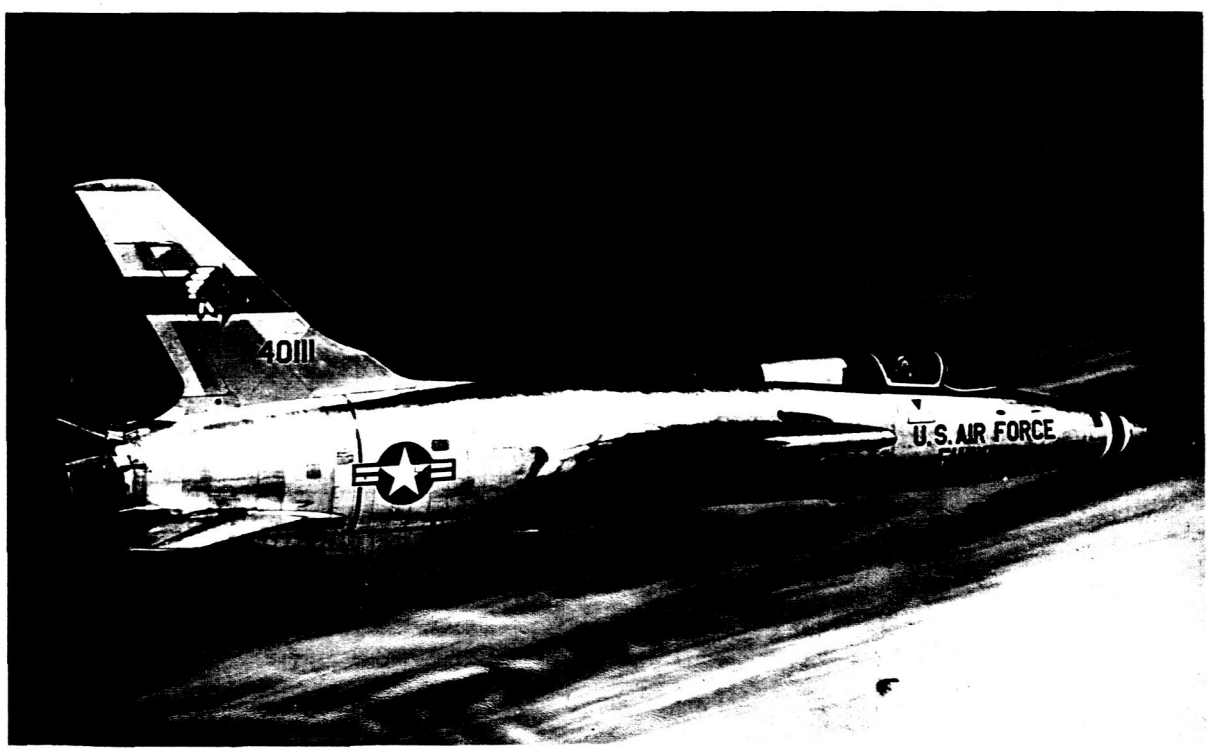

Figure 4. View of the F-105D Airplane

The instrumentation system consisted of an oscillograph recorder, bridge control units, three strain gage accelerometers, three potentiometer rate gyros, and two strain gage pressure transducers. The three accelerometers were mounted at the approximate location of the aircraft's center of gravity and aligned with the major axes of the aircraft. The three rate gyros were aligned to measure the angular rates around each of the aircraft's major axes. The pressure transducers were connected to the aircraft's pitot-static system to sense the dynamic and static pressures. When the landing gear was retracted, the oscillograph operated continuously and recorded data at a paper speed of about 24 inches per minute. The data was recorded on a roll of photosensitive paper 3-5/8 inches wide and up to 400 feet long. Sample portions of data are shown elsewhere in this report.

2.2 Selected Data Sample

The statistical maneuver model for calculating structural load distributions developed in this study was tested by using a sample of one maneuver type, namely, the descending left turn. The reasons for selecting this maneuver type were twofold.

(1) Since the maneuver is asymmetrical, it induces tail and aileron loads.

(2) Since the data from a descending left turn is relatively difficult to process because of the significant variations in such data from maneuver to maneuver, this maneuver type provided a good means of testing the practicality of the proposed method.

From the available data, about 450 hours of both training and operational eight-channel flight loads data, a sample of 318 descending left turns performed in 40 flights was selected. A summary of the flight conditions, aircraft configurations, and air bases associated with the data sample is included in Appendix A. During the selection of the maneuver type to serve as the sample, types found easily identifiable and occurring frequently are listed in Table 2.

Further study of the maneuver types may reveal that some similar types of maneuvers among those listed above may be combined into a single type. Such combining of types would greatly simplify maneuver recognition and permit compiling a good sample of a maneuver type from a smaller amount of flight data.

TABLE 2

Observed Maneuver Types

Ascending left turn	Ascending right turn
Descending left turn	Descending right turn
Level left turn	Level right turn
Symmetrical pull-up	Right yaw
Right rolling pull-up	Left yaw
Left rolling pull-up	
Longitudinal acceleration	Coordinated roll
Longitudinal deceleration	

The type and number of maneuvers recorded depends on the mission flown. For example, the number of maneuvers per flight hour in the F-105 data is greater in the bombing and gunnery missions than in the navigation or ferrying missions. Table 3 lists the maneuver types observed in a typical F-105D bombing and gunnery mission.

TABLE 3

Summary of Maneuvers in a Typical Flight

Base:	Wheelus Air Base, Libya
Mission:	Nuclear and conventional bombing and ground gunnery
Total flight time:	72.6 minutes
Breakdown of maneuvers:	
34 right turns	1 toss bomb maneuver
12 left turns	1 yawing maneuver
8 rolling pull-ups	2 accelerations to Mach 0.9
2 symmetrical pull-ups	2 decelerations to low air speed

As described in Appendix B, each of the observed maneuver types has distinctive trace patterns.

2.3 Data Reduction

2.3.1 Calculation Procedure for Basic Parameters

Data editing, the first phase of the data reduction, consisted primarily of identifying all maneuvers to be processed, indicating the start and end of each of these maneuvers, and determining the normal or null values for each trace. Figure 5, a reproduction of part of an oscillograph, shows a typical descending left turn with its extremities marked. As mentioned previously, Appendix B describes the trace pattern defining each of the maneuver types. The roll rate trace primarily defines the maneuver length since, in the performance of this maneuver, the pilot first rolls the aircraft in the direction of the turn and finally rolls it back to the wings-level position. Near normal values for the n_z and yaw rate traces serve to check the extremities of the maneuver length. As shown in Figure 5, the start and end of the maneuvers were marked, respectively, before the first negative deflection of the roll rate trace and after the positive peak of this trace. Measurements of the traces during the calibration and straight-and-level flight yielded the normal values for the traces.

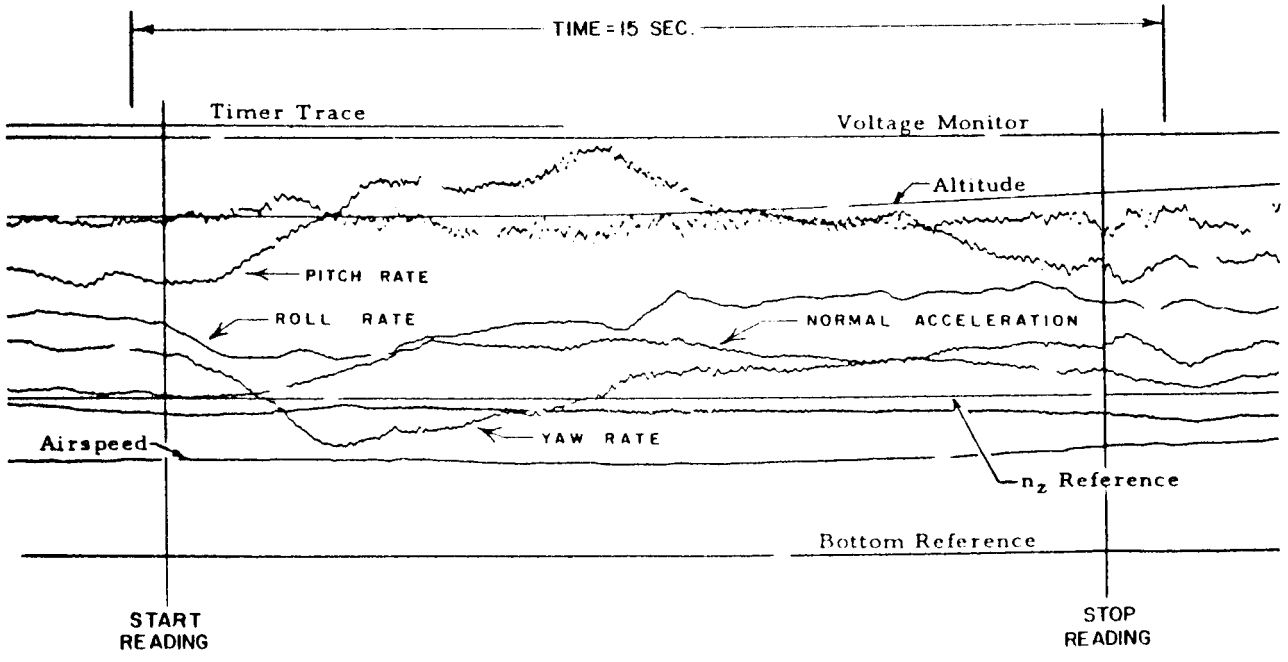

Figure 5. Oscillogram Showing Typical Descending Left Turn

A semiautomatic oscillogram reader was used to measure all the data traces about every 0.2 second throughout the maneuver period. Then the digital output was transcribed onto magnetic tape in a format compatible with the IBM 7094 computer.

To provide flexibility in this study, the computer performed calculations in several steps. In the first step, the following parameters were calculated: time in seconds; calibrated airspeed in knots; pressure altitude in feet; the three linear accelerations at the center of gravity—n_x, n_y, and n_z; the three angular rates—p (roll), q (pitch), and r (yaw); the three angular accelerations—$\dot{p}$, $\dot{q}$, and $\dot{r}$ (which were calculated by differentiating p, q, and r with respect to time); and the three Eulerian angles—Ψ, θ, ϕ (which gave the aircraft's orientation with respect to the earth's coordinate system). All angular parameters were expressed in degrees.

The Eulerian angles were calculated by integrating the values of p, q, and r which were measured about every 0.2 second. As with any integration of this type, any minor errors introduced by the sampling frequency, calibration, and measurement of the normal parameter values became large when the integration covers an appreciable period. As a consequence, significant errors could have been introduced into the values for the angles Ψ, θ, and ϕ when the integration for a maneuver was completed. These values, nevertheless, indicated the type of maneuver performed and whether the turn was 45, 90, or 180 degrees.

The angular accelerations, $\dot{p}$, $\dot{q}$, and $\dot{r}$, at each point were calculated by differentiating the angular rate traces approximated by a parabola defined by the point and its two adjacent points.

This approximate method of differentiation theoretically becomes more accurate as the time interval between readings decreases. However, the sampling rate was fixed at about five readings per second because of the data recording at a paper speed of 24 inches per minute. With this fixed sampling rate, the data sample could not reflect the actual trace when the parameter deflected at frequencies above 0.5 cps (see Appendix D). Even with the frequency limitation imposed by the sampling rate, some peaks at the higher frequencies (above 1 cps) appeared in the angular accelerations when the angular rate traces were differentiated. Since these higher frequency peaks occur primarily at the lower altitudes, they have been attributed to atmospheric turbulence, structural dynamic effects, and occasionally close formation flights. Although these three types of response are important, they are independent of the maneuver types covered by the proposed statistical model and will have to be obtained from another source. It is envisioned that the load contributions causing these higher frequency responses may be superimposed on the load distributions calculated from the statistical model. This problem is discussed further in Section 2.5.5. Since these effects are not considered part of the basic maneuvers, the angular rate traces were smoothed prior to differentiation to eliminate the higher frequencies. The smoothing

involved a seven-point weighted filter consisting of the reading and three points immediately before and after it, the points nearest the reading being most significant in smoothing the reading. Appendix D completely describes the filtering process and its effect on the data.

2.3.2 Loads Equations

Approximate structural loads for the F-105D aircraft were calculated during the program to demonstrate the use of the proposed statistical model. The calculated loads include the vertical shear load at right Wing Station 136.6, the vertical shear load at the root of the right horizontal tail surface, and the lateral shear load at the root of the vertical tail. Figure 6 illustrates the location of these load points on the aircraft. The shaded areas indicate the portions of the aircraft which contribute airloads and inertia loads to the calculated shears.

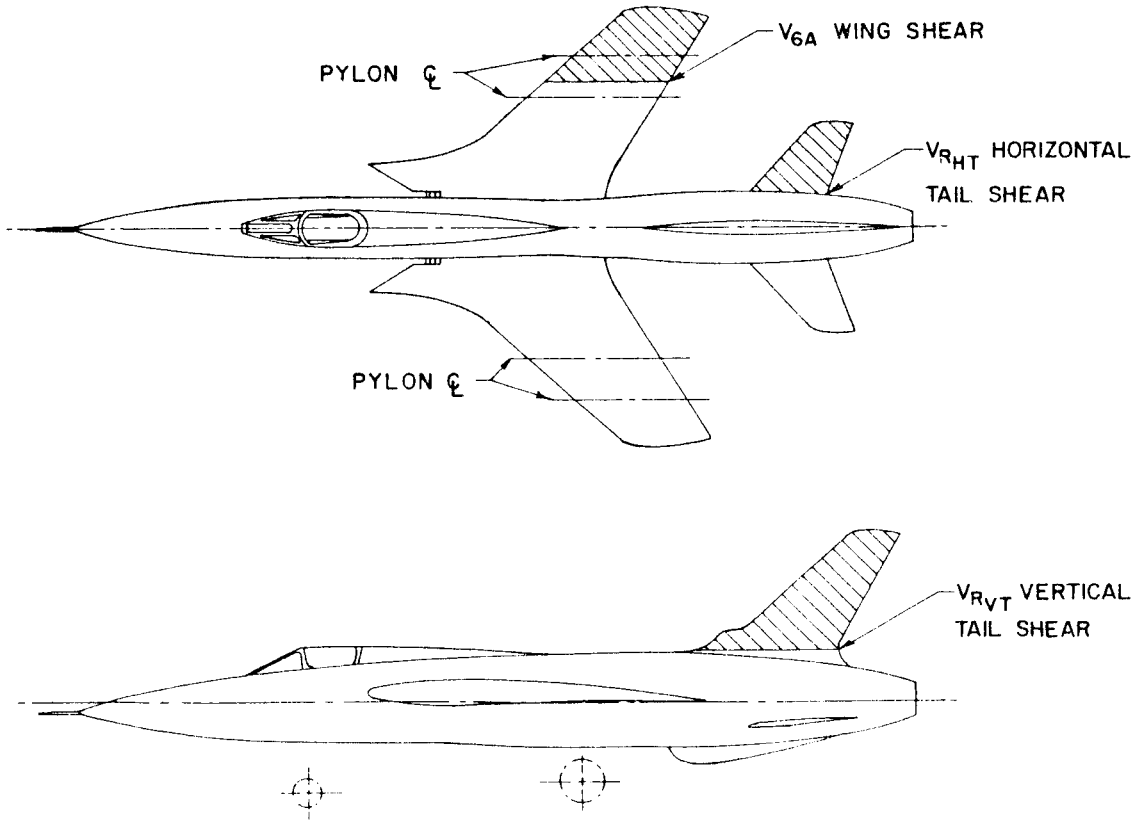

Figure 6. Two-View Drawing of F-105D Airplane Indicating Locations of Calculated Structural Loads

The following simplified loads equations, developed in Appendix C, were used to calculate a time history of the loads during each descending left turn in the data sample and to predict the load spectrums from the statistical model:

(1) Simplified equation for the wing shear load at Station 136.6 (also called Location 6A):

$$V^{*}_{6A} = .15547\ Wn_z + .000138\ I_y\dot{q} - .000596\ I_x\dot{p} - n_z \sum_{i=1}^{n} w_i + .01745\ \dot{p} \left(\sum_{i=1}^{n} w_i \frac{y_i}{g} \right)$$

(2) Simplified equation for the vertical tail shear load at root:

$$V^{*}_{RVT} = .1061\ Wn_y - .000741\ I_z\dot{r} + .000741\ I_{xz}\dot{p} - 889\ n_y - 3.244\ \dot{p}$$

(3) Simplified equation for the horizontal tail shear load at root:

$$V^{*}_{RHT} = - .0307\ Wn_z - .000472\ I_y\dot{q} - 349\ n_z + 3.86\ \dot{q} + .993\ \dot{p}$$

The following assumptions were made in these approximate equations:

(1) The center of gravity is fixed.

(2) The shape (not the magnitude) of the aerodynamic distributions and the aerodynamic centers for each aerodynamic surface are fixed. This premise assumes no significant variation in Mach number and dynamic pressure and ignores the change in the centers of pressure due to control deflections, angle of attack, angle of yaw, and roll angle.

(3) The aircraft responds as a rigid body.

(4) The contribution of second order terms is insignificant.

The aircraft gross weights and moments of inertia were evaluated for each descending left turn, as described in Appendix C. To calculate more accurate loads requires that the constant coefficients used in the equations be functions of Mach number and dynamic pressure.

Although more accurate loads would be required for designing aircraft, the above equations are sufficiently complete for illustrating the use of the statistical model presented in this study.

2.4 Description of Statistical Maneuver Model

Any technical progress in using flight loads data to estimate structural loads obviously requires some type of statistical description of the data leading to a distribution of the loads. Moreover, if statistical quantities are to describe populations meaningfully, the universe of flight loads data must be so stratified into subpopulations that each subpopulation may be precisely defined and that the innate variation in the universe may be reduced. As discussed above, the descending left turn was selected as a trial subpopulation; and a model to predict the distributions of peaks of load cycles in this subpopulation was formulated.

The essential feature of the model is its accounting for the time change of the statistical properties of the basic parameters within the population of descending left turns. Consequently, distributions of parameters are maintained at various time slices and not used until the critical times have been determined. The only statistical assumption in the model is the independence of all random variables; that is, if two distributions are to be combined in any fashion, these distributions are assumed to be independent.

The application of the model consisted basically of four steps: data reduction, normalization, derivation of statistical description, and calculation of loads distributions. Also included in this study was the comparison of distributions derived from the model with those distributions "observed" from load time histories of each descending left turn. The steps are illustrated in detail by a complete application of the model to a wing load, a vertical tail load, and a horizontal tail load during descending left turns.

2.4.1 Data Available

Since the data reduction process was discussed above, this section assumes the completion of the data reduction step and the availability of the time histories of the basic parameters in correct units for each of 318 descending left turns (hereafter referred to as "maneuvers" since no other maneuver type was processed in this study).

2.4.2 Normalization

Obviously, the maneuvers vary in length. To maintain

the distributions of values at various time slices, therefore, requires first aligning the basic parameters as much as possible so that these distributions may have definite meaning. Figures 7 and 8 display, respectively, the p and ṙ traces for 10 maneuvers. Although these traces show that the time slice values would have no meaning, the degree of shape similarity among the traces indicates that the traces could be interrelated advantageously if the time axis for each maneuver were transformed. Again, although the maximum amplitudes of the traces are related to the aircraft type and would vary from type to type, normalizing of the amplitudes, it is hypothesized, would make the parameters independent of the aircraft type. Consequently, the time and amplitude were normalized to align the traces. Strictly speaking, however, the amplitudes for this one aircraft type did not have to be normalized.

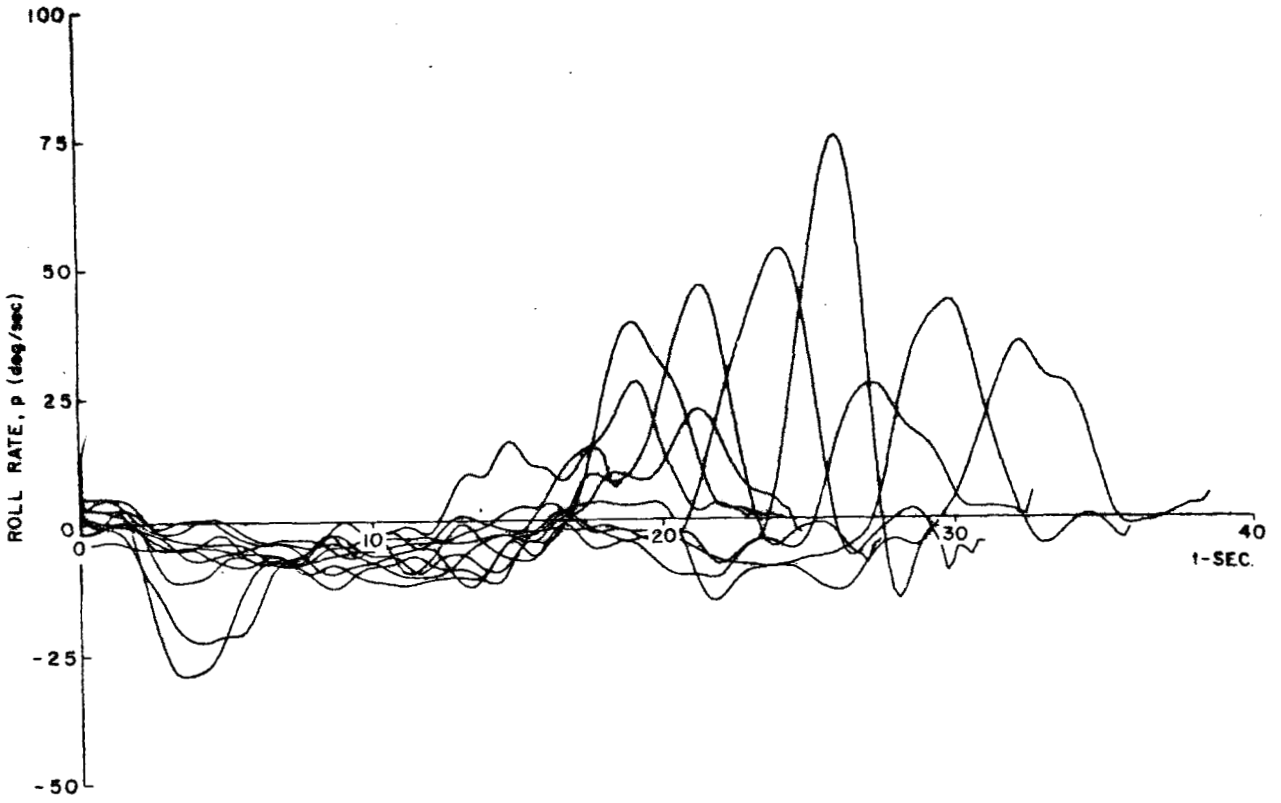

Figure 7. Plots of Non-Normalized Roll Rate versus Time for Ten Descending Left Turns

The horizontal, or time scale, normalization factor for all parameters within a maneuver was derived from the p trace. Since the estimated time of a descending left turn had a very high correlation with the difference between the time of peak positive p ($t_{p_{max}}$) and the time when the p trace first goes negative (t_{p-}), the time transformation

was given by

$$t' = \frac{t - t_{p-}}{t_{p_{max}} - t_{p-}}$$

These terms were chosen for normalizing because of the ease of identifying the terms among the data. In the normalized time scale, $t' = 0$ corresponds to the time when the p trace first goes negative (which is actually the start of the maneuver), and $t' = 1$ corresponds to the time when the p trace reaches its maximum value. All calculations were carried to $t' = 1.1$ which is longer than the average actual maneuver length.

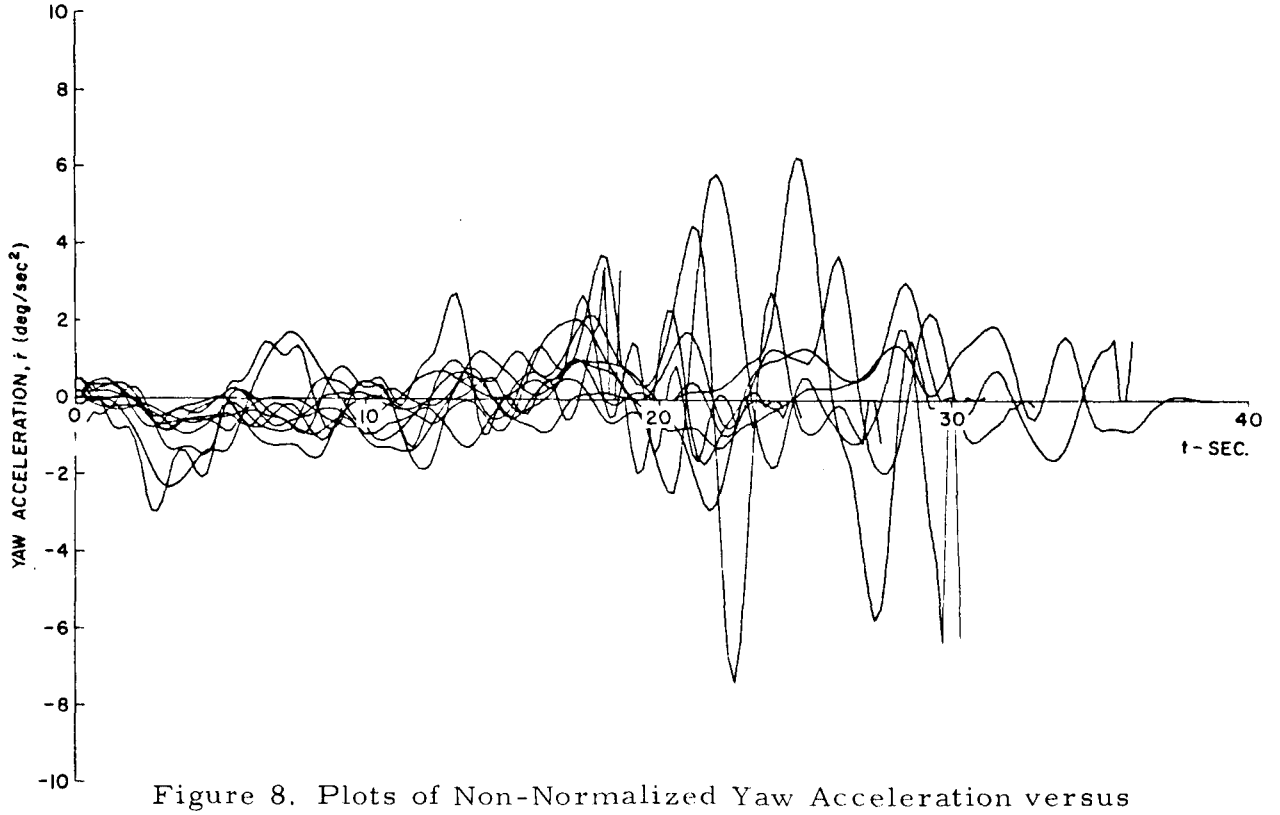

Figure 8. Plots of Non-Normalized Yaw Acceleration versus Time for Ten Descending Left Turns

The amplitudes of the traces were normalized individually with each trace being divided by its absolute deviation from zero. The absolute deviation was selected as a normalization factor over either the maximum or minimum value because the trace representing a particular parameter may never become negative during one maneuver and positive during another maneuver. The absolute deviation also circumvents the possibility of a normalization factor involving a zero division, and, finally, all normalized amplitudes will fall between ± 1.

Figures 9 and 10 showing the result of the normalization on the traces of Figures 7 and 8 indicate considerable variation still existing. However, since the remaining variation is due primarily to pilot technique, it cannot be removed. (Although the traces could be better aligned by a different time normalization factor for each parameter, the relative magnitudes between traces within a maneuver would be lost.) As a further example of the variation from pilot to pilot, Figure 11 presents the roll rate traces for descending left turns performed by two different pilots. As can be seen, one pilot rolled into the turn much faster than the other and pulled out of the turn more slowly. Obviously, when the traces are normalized, the early negative p peaks will be spread further apart. As illustrated in Figure 12, two maneuvers performed by a pilot during a single flight exhibit the same type of variation. Since the effect of pilot technique cannot be eliminated, it can only be measured and recorded in the form of statistical distributions.

Primes are used to denote transformed (normalized) values.

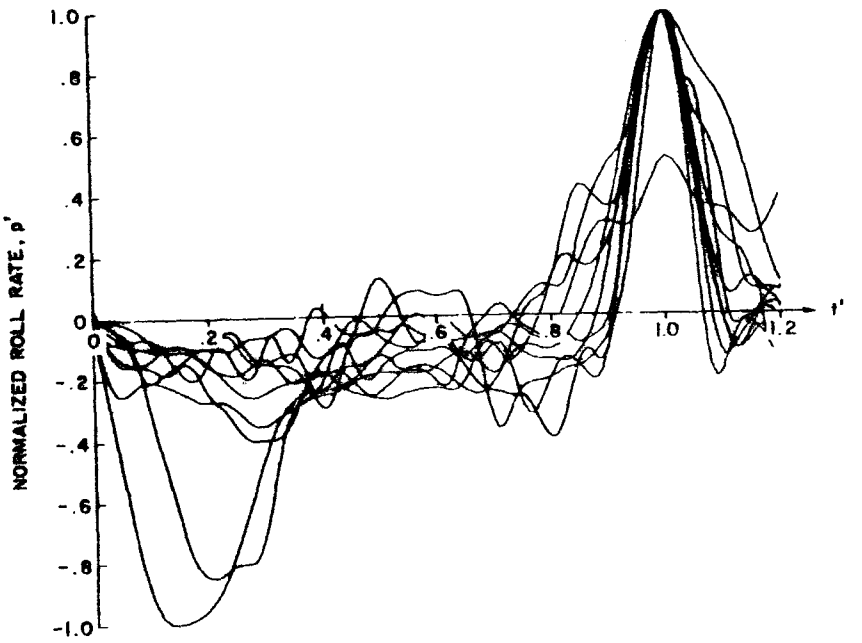

Figure 9. Plots of Normalized Roll Rate versus Normalized Time for Ten Descending Left Turns

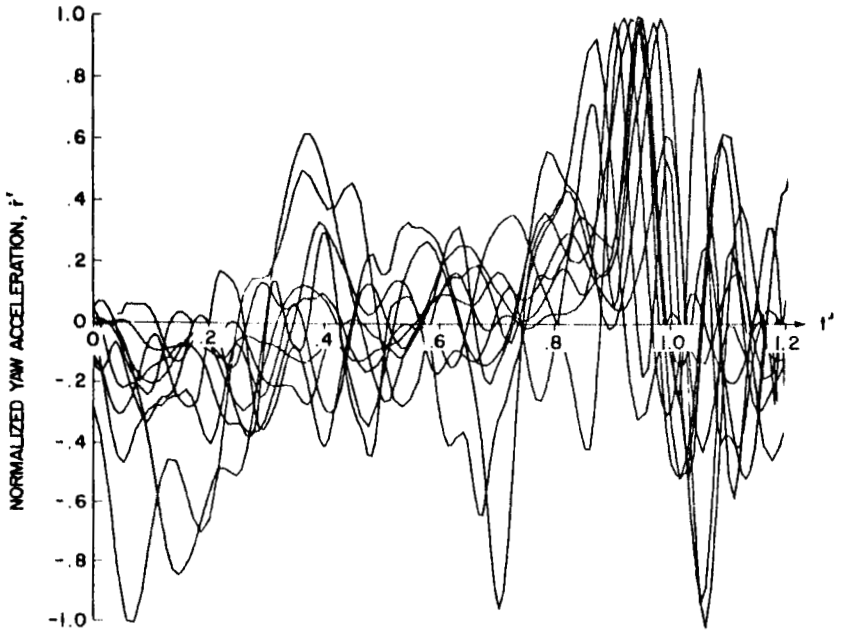

Figure 10. Plots of Normalized Yaw Acceleration versus Normalized Time for Ten Descending Left Turns

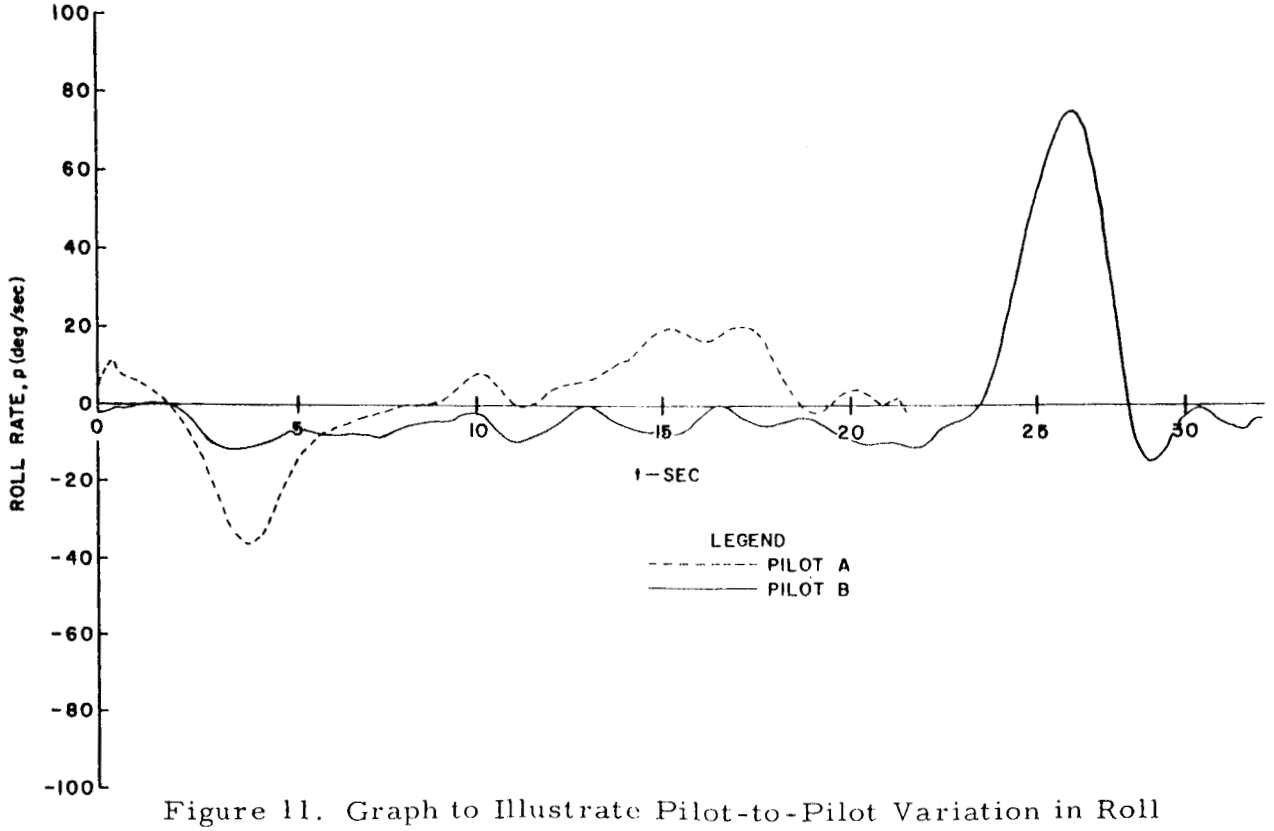

Figure 11. Graph to Illustrate Pilot-to-Pilot Variation in Roll Rate Trace During Descending Left Turns

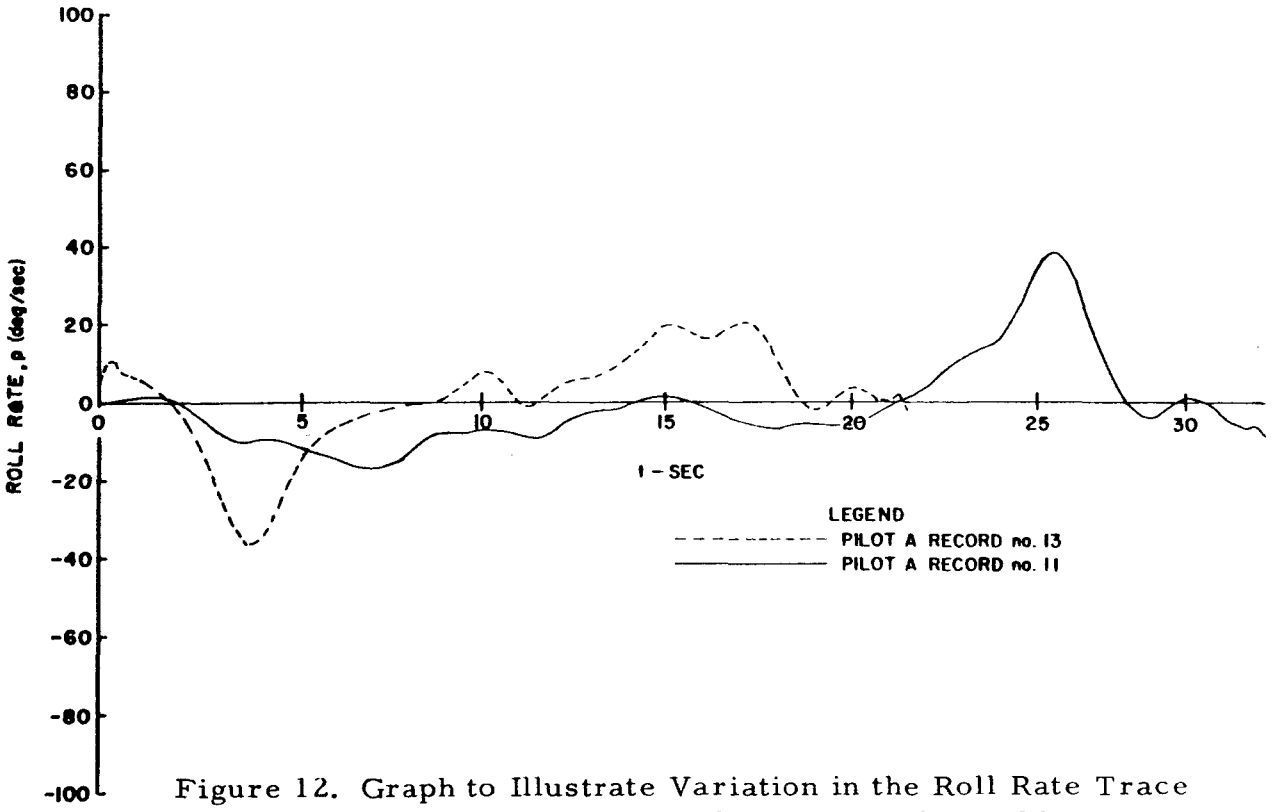

Figure 12. Graph to Illustrate Variation in the Roll Rate Trace During Descending Left Turns Performed by the Same Pilot

2.4.3 Derivation of Statistical Description

Since the normalized values are unitless, they cannot, of course, be used to generate distributions of loads. Denormalization, therefore, requires retaining sufficient information from the original data. The distributions to be denormalized include the distributions of amplitude normalizing factors for each parameter, the distribution of maneuver lengths, the distribution of "constants" or conditions (weight, Mach number, and moments of inertia) which appear in the loads equation, and the average of the positive and negative peak transformed values. The last was used to develop a time adjustment factor, as discussed later.

From the normalized parameter traces, distributions at 25 different times were derived. These distributions were considered sufficient to develop the distribution of any load during descending left turns. The time slice values chosen include all multiples of $t' = 0.05$ from 0 to 1.1 and the two values $t' = 0.975$ and $t' = 1.025$ which are critical with respect to the peaks of some parameters. The means of these 25 distributions yielded an average normalized time history for each of the parameters.

Figures 13 through 21 present the average time histories of 9 basic parameters. Since the data were processed in batches, three independent sets of data and a composite of them were plotted to permit data comparisons. Set I, the first set of processed data, contains 68 maneuvers; Set II contains 132; and Set III contains 118. In addition, on each figure is a corrected composite of the three sets. (Corrected composites for n_x, p, q, and r are not shown since these parameters were not used during this program.) The corrected average trace was derived from the average trace by adjusting each value so that the positive peak of the average transformed time history agreed with the average of the individual transformed positive peak values and the negative peak of the average transformed time history agreed with the average of the individual transformed negative peak values. Depending on their signs, all other values were adjusted proportionately. The means of adjustment was the time adjustment factor which was introduced to account for the peak values not aligning perfectly in the transformed time scale.

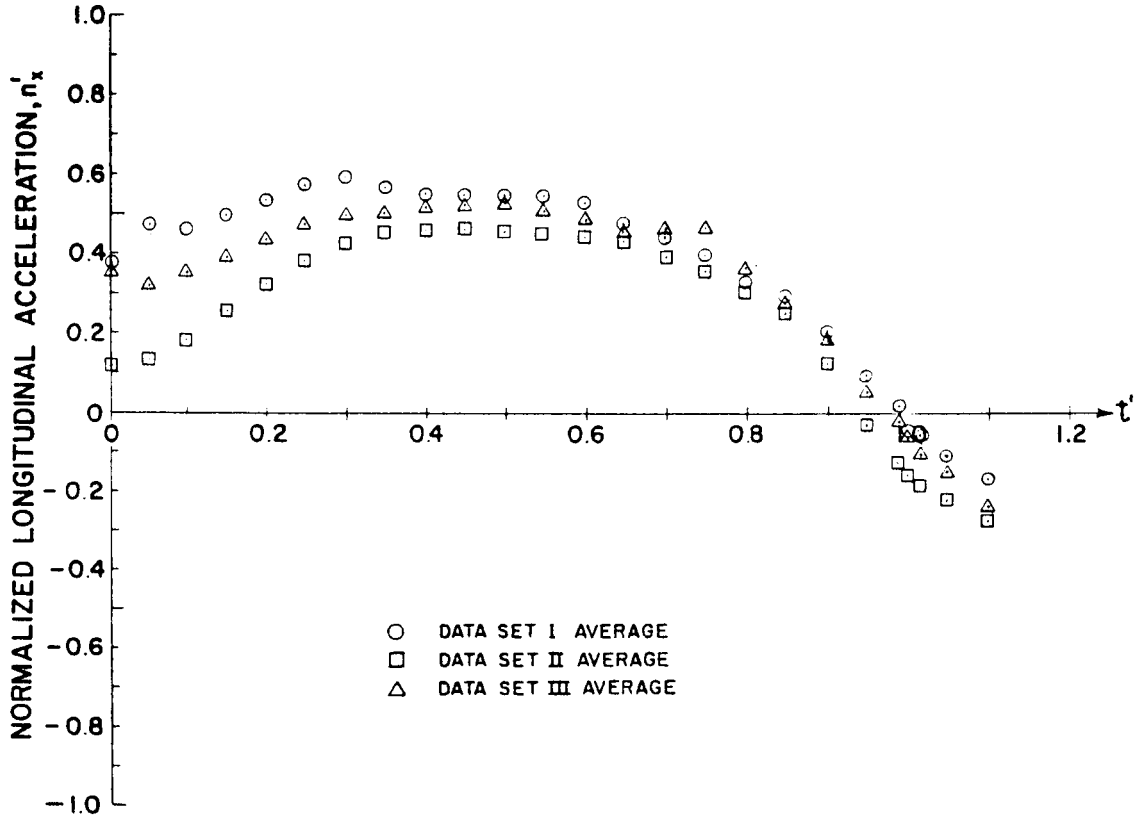

Figure 13. Plots of n_x Average Normalized Time History for Three Indpendent Data Sets

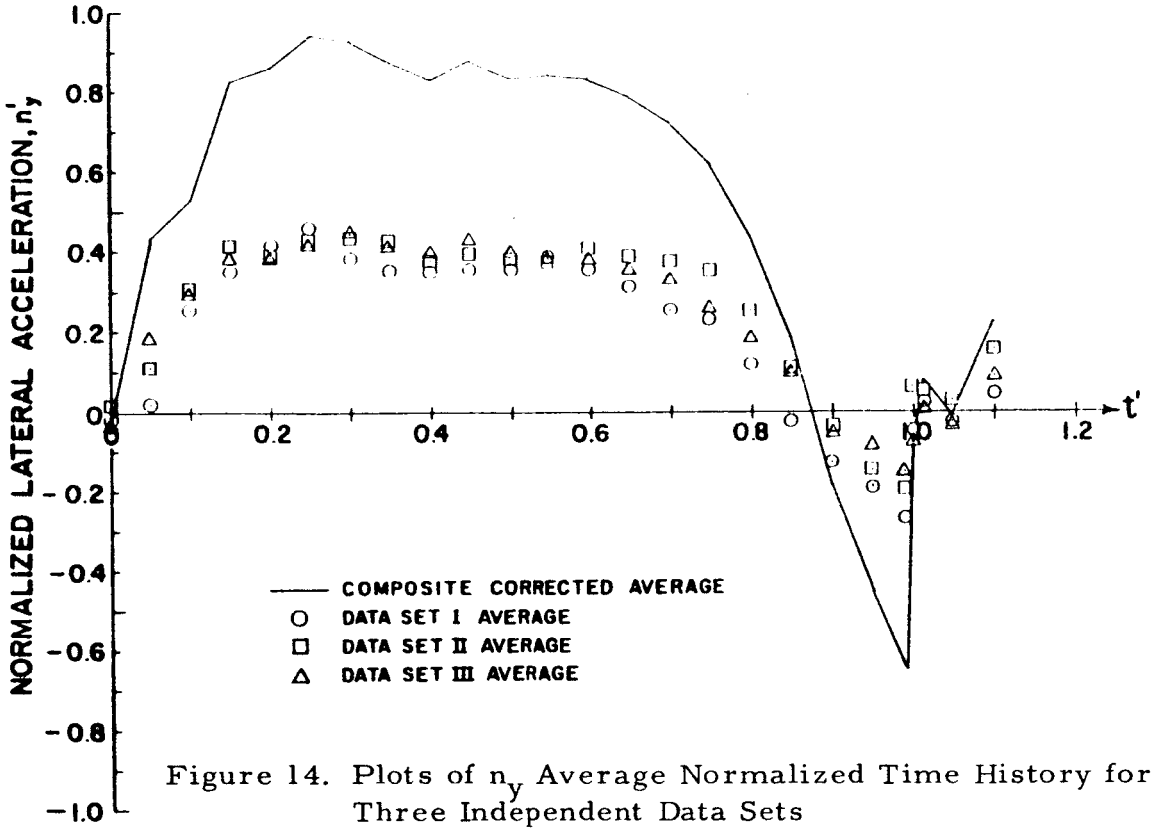

Figure 14. Plots of n_y Average Normalized Time History for Three Independent Data Sets

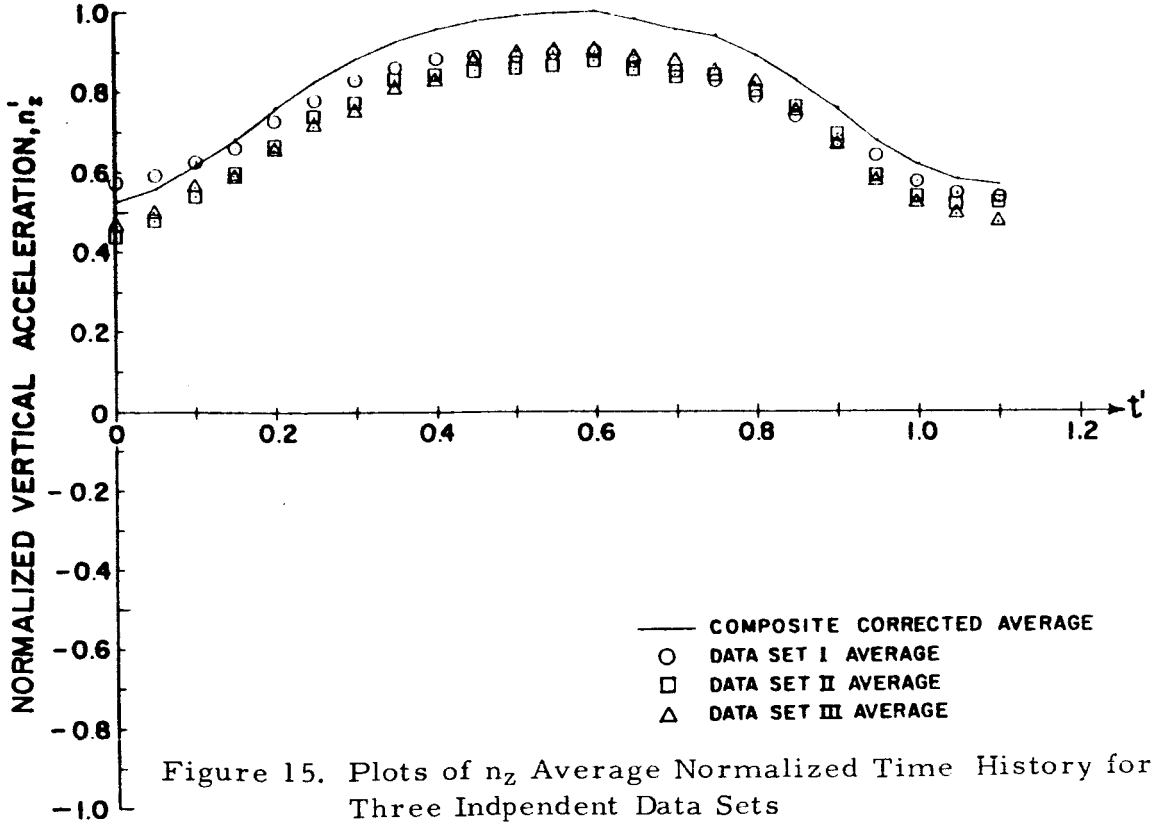

Figure 15. Plots of n_z Average Normalized Time History for Three Indpendent Data Sets

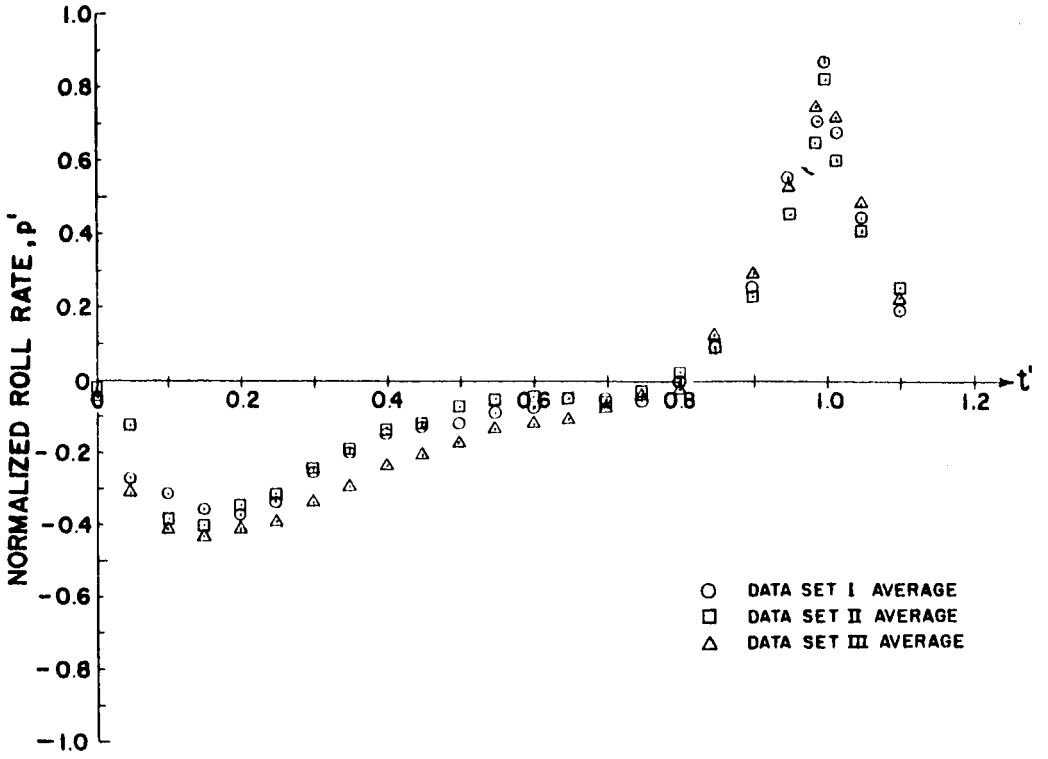

Figure 16. Plots of p Average Normalized Time Histories for Three Independent Data Sets

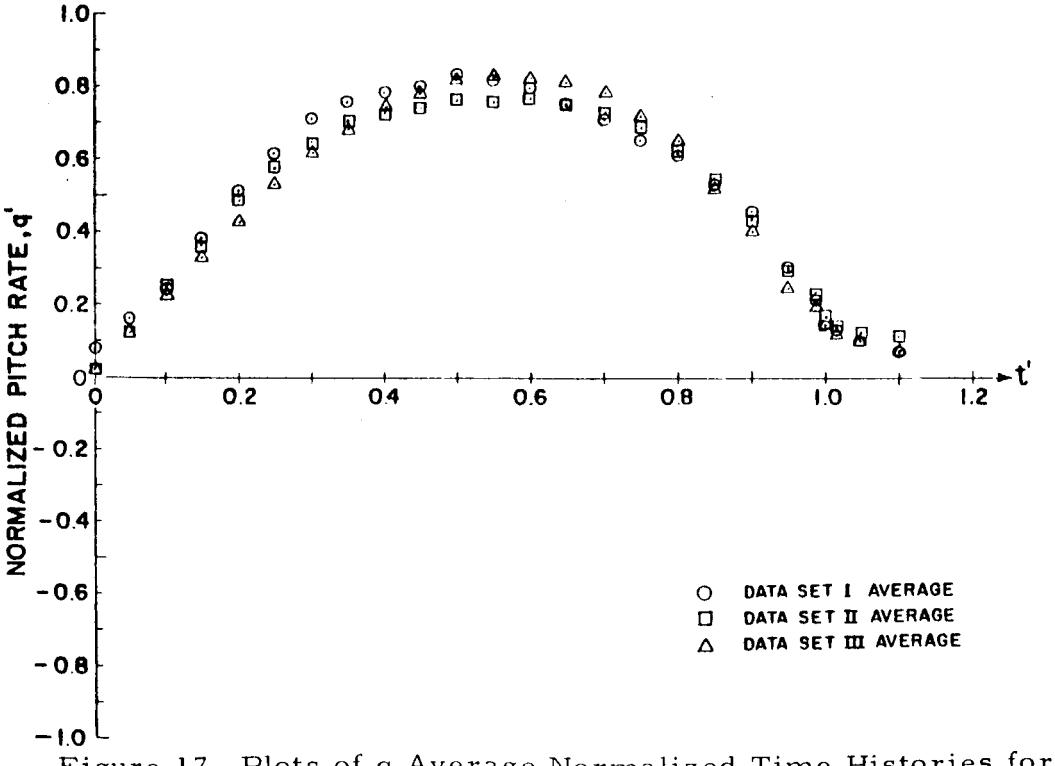

Figure 17. Plots of q Average Normalized Time Histories for Three Independent Data Sets

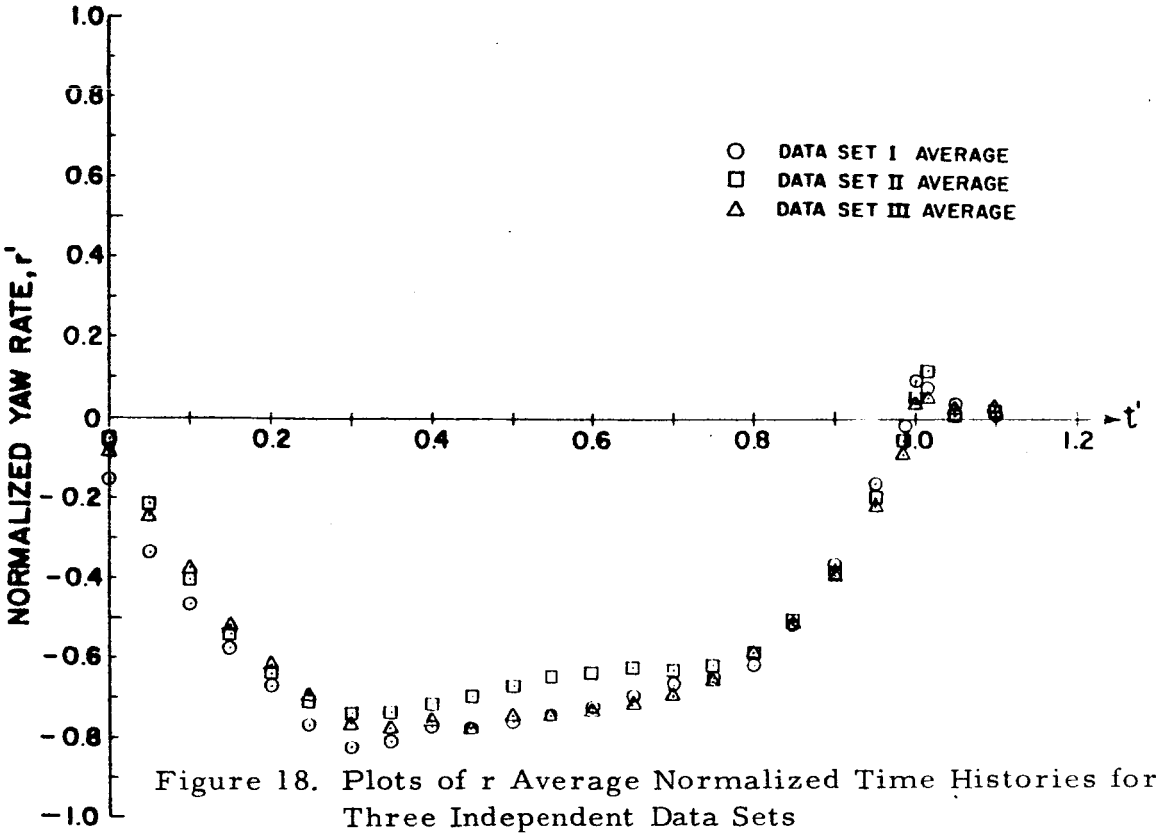

Figure 18. Plots of r Average Normalized Time Histories for Three Independent Data Sets

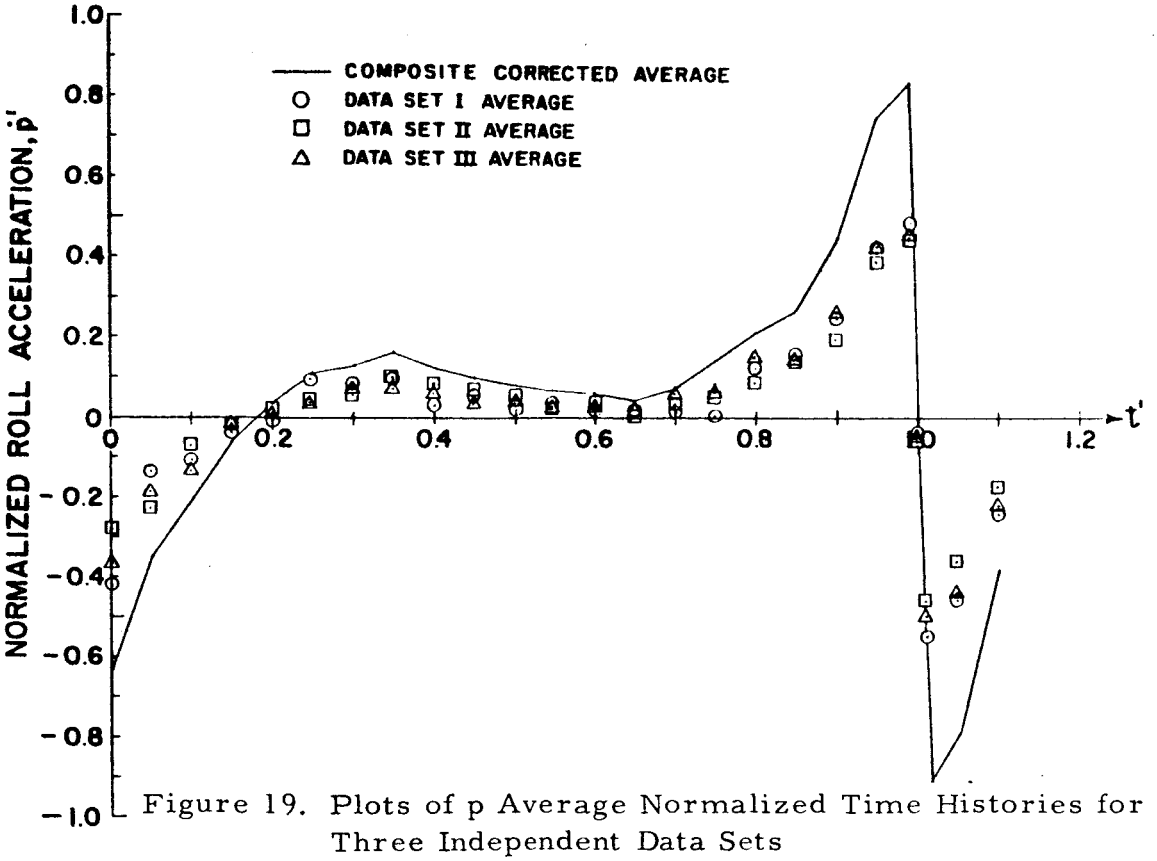

Figure 19. Plots of p Average Normalized Time Histories for Three Independent Data Sets

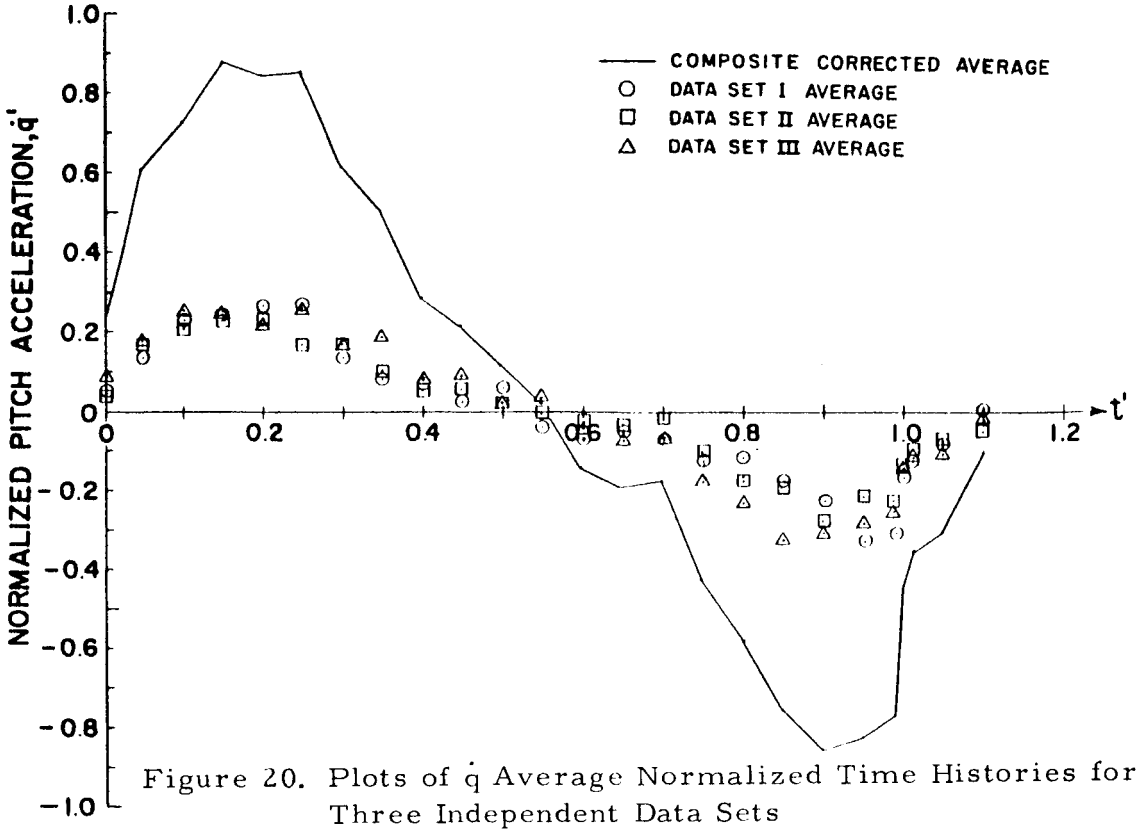

Figure 20. Plots of $\dot{q}$ Average Normalized Time Histories for Three Independent Data Sets

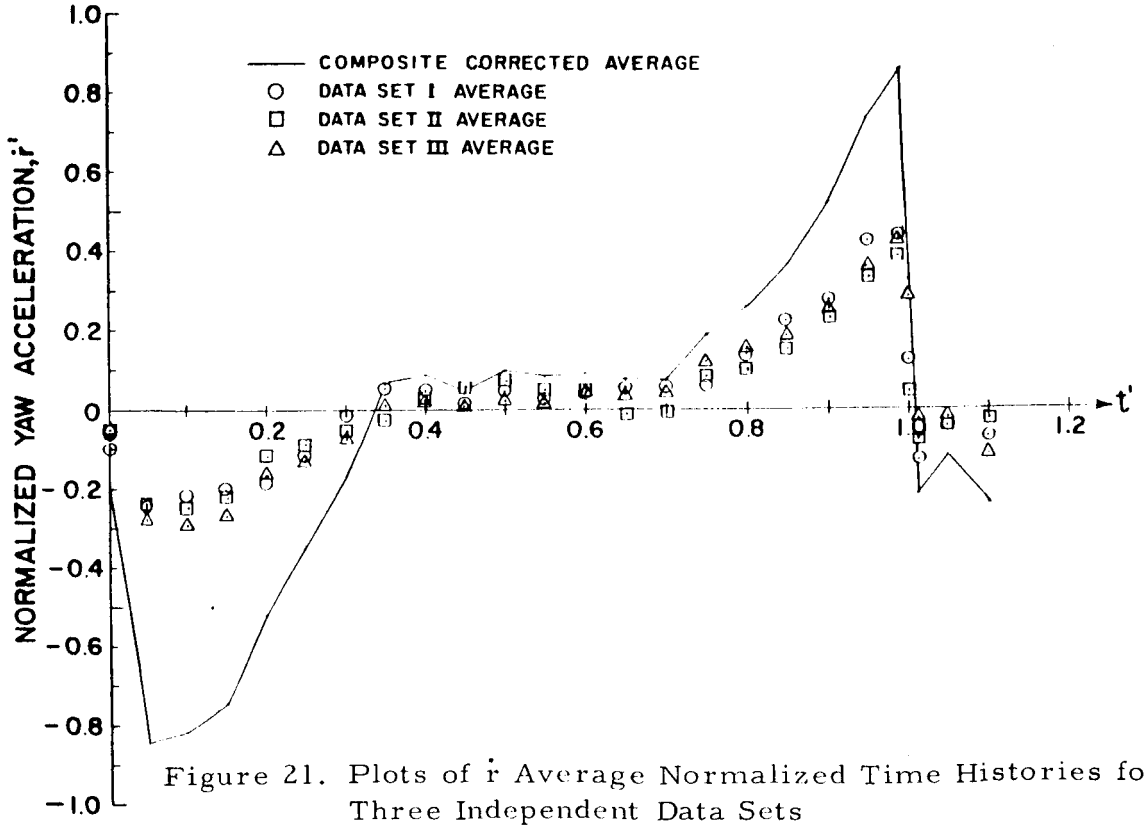

Figure 21. Plots of $\dot{r}$ Average Normalized Time Histories for Three Independent Data Sets

The corrected average traces represent the best estimate of the relationship between the parameters during a descending left turn. By introduction of an average parameter value, therefore, an average descending left turn can be described and an average time history of a load can be generated. Through the simplified equations developed in Appendix C, the average wing (V^*_{6A}), root horizontal tail (V^*_{RHT}), and root vertical tail (V^*_{RVT}) loads were calculated for Condition 1; these loads are displayed in Figures 22, 23 and 24, respectively. These figures indicate that the wing load passes through one long positive load cycle, the horizontal tail load passes through one long negative load cycle, and the vertical tail passes through a load cycle having an early positive peak and a late negative peak. The average traces for Condition 2 exhibited identical behavior. The distribution of the peak values of these load cycles fully describes the loads distributions in an average descending left turn. The times of the average load peak values were then selected as critical times; and the distributions of the transformed parameter values at these critical times were corrected, denormalized and used to generate the distributions of the peak values of the load cycles. This process is illustrated in Figure 25 where it is assumed that $\dot{r}$ and n_y are the only contributors to the vertical tail load. The $\dot{r}$ and n_y distributions were recorded at several time slices; then, after the time of the load peak had been determined, the distributions at this time slice were used to calculate the peak loads distributions.

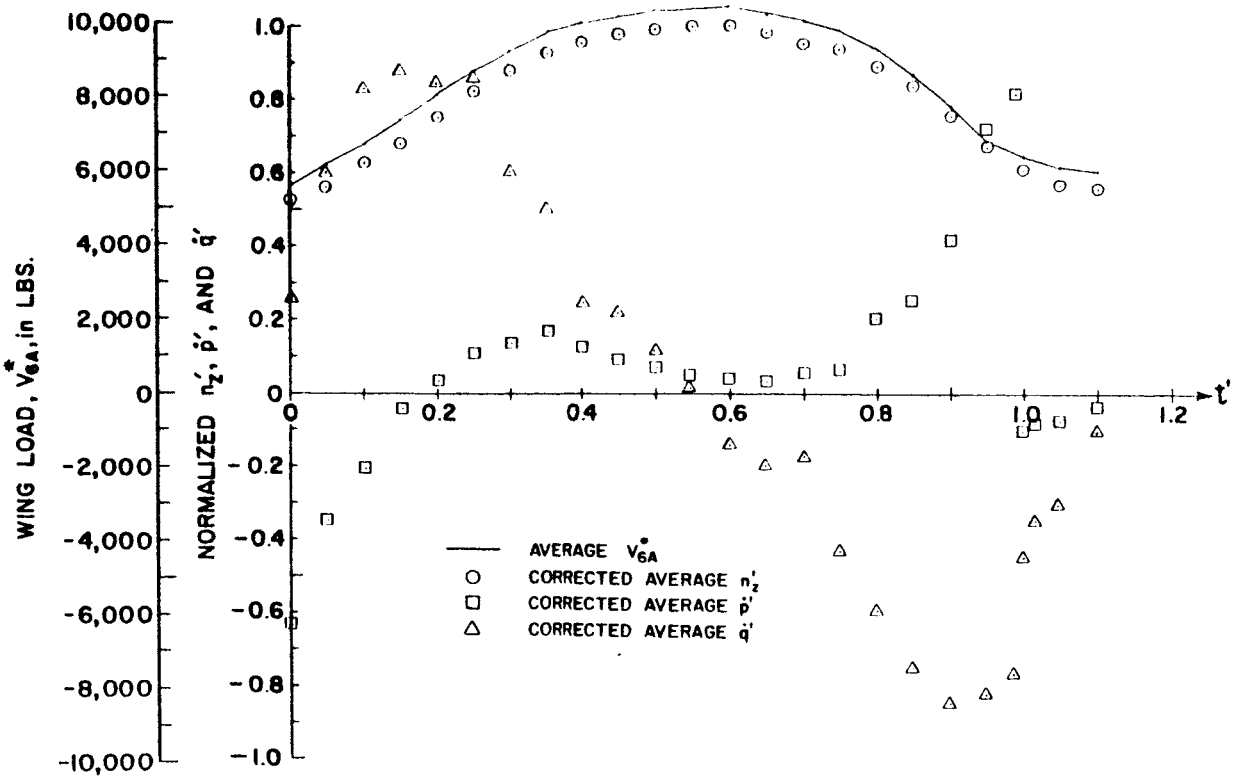

Figure 22. Graph of Average Wing Load Time History Calculated from Average Normalized Time Histories of n_z, $\dot{p}$, and $\dot{q}$

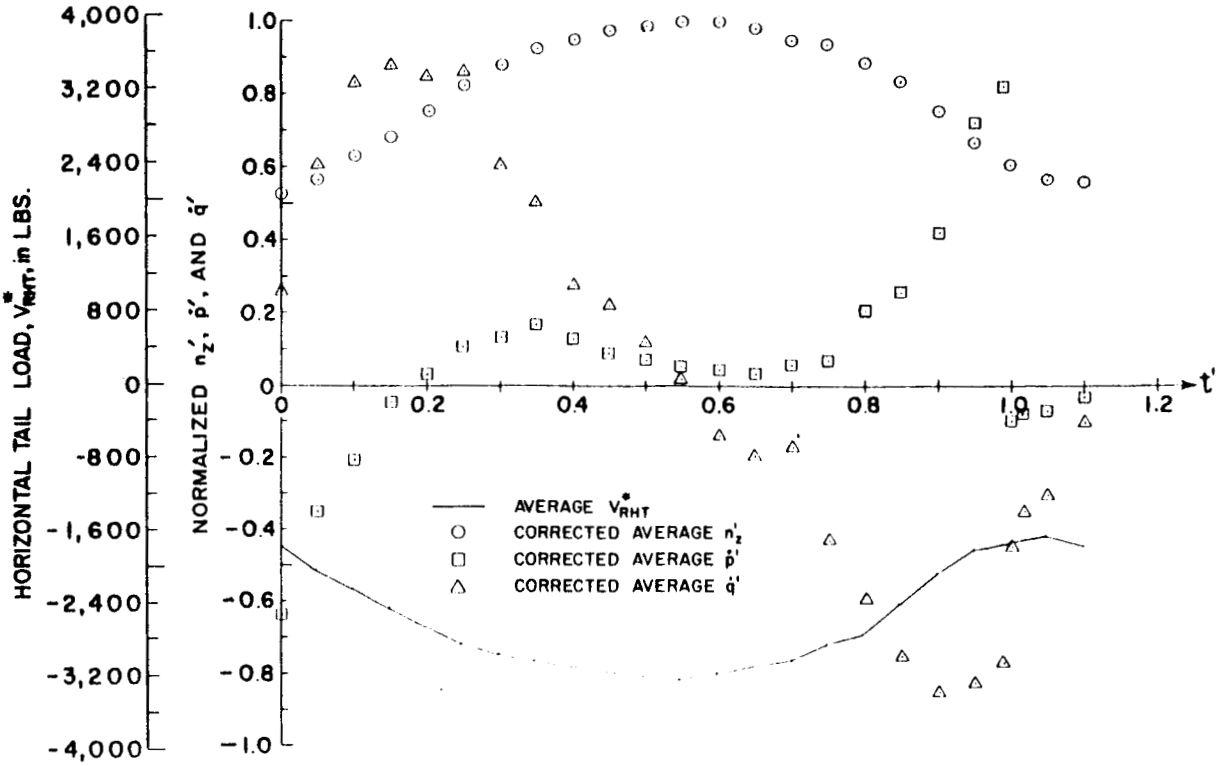

Figure 23. Graph of Average Horizontal Tail Load Time History Calculated from Average Normalized Time Histories of n_z, $\dot{p}$, and $\dot{q}$

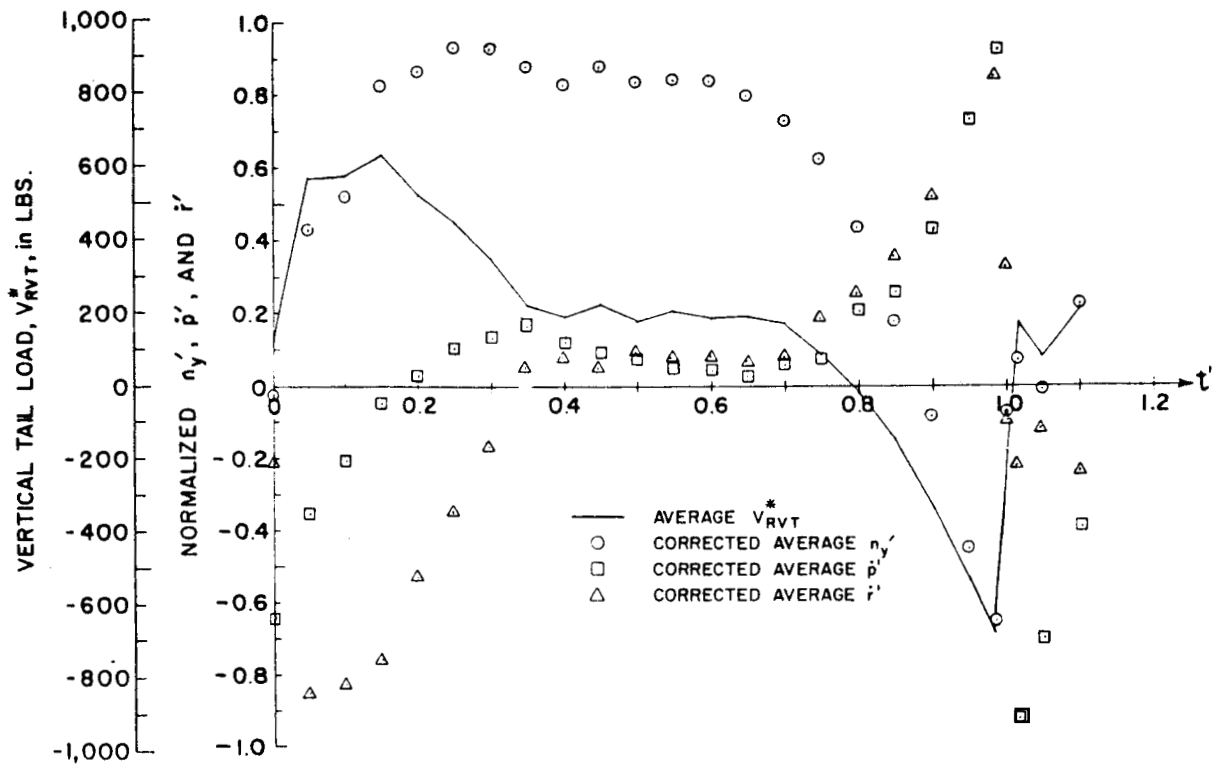

Figure 24. Graph of Average Vertical Tail Load Time History Calculated from Average Normalized Time Histories of n_y, $\dot{p}$, and $\dot{r}$

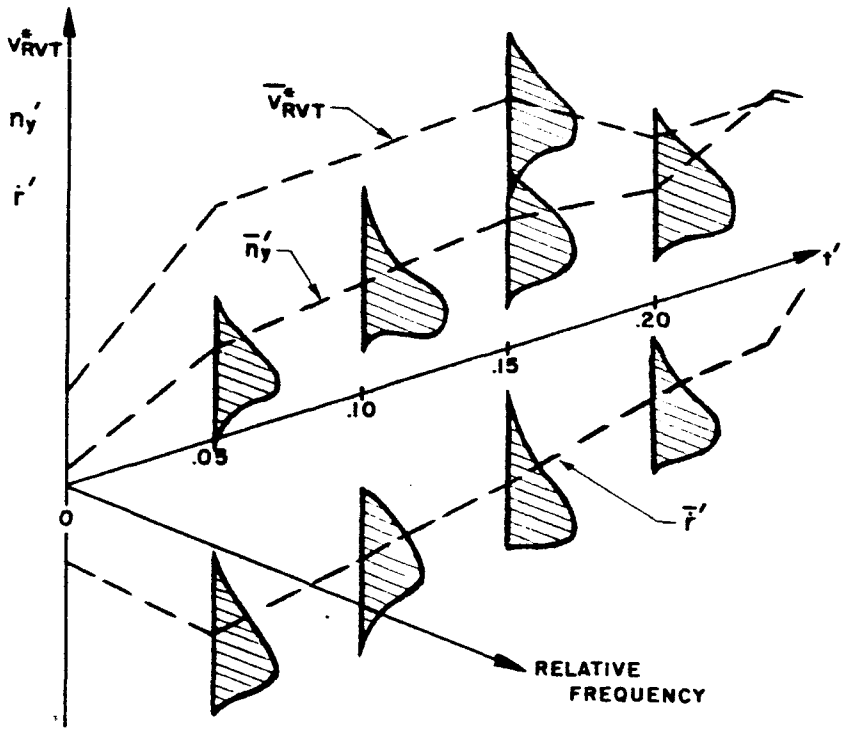

Figure 25. Example of Normalized Parameter and Load Distributions at the Selected Times

In summary, the statistical description of the data consists of the following:

(1) The distribution of peak values which are used in denormalization.

(2) The distribution of maneuver lengths which can be used to reintroduce real time.

(3) The distribution of "constants" or conditions which appear in the loads equation.

(4) The average positive and negative peak transformed values which determine the time adjustment factor.

(5) The distributions of transformed values at 25 preselected times which are used to generate distributions of the peaks of load cycles at the critical times.

(6) The corrected mean time history of all parameters which are used to generate average loads which, in turn, determine the critical time of loads.

2.4.4 Calculation of Loads Distributions

According to the statistical description given in Section 2.4.3, directives for the derivation of peak loads distributions consist of the following two steps:

(1) For a particular load, denormalize the time slice distributions for each relevant parameter at the time of critical load by adding the time adjustment factor to the normalized values and finding the distribution of the product of the distribution of corrected normalized parameter values and the distribution of peak parameter values. For a given t', the time adjustment factor is simply the corrected mean minus the uncorrected mean at that t'. The distribution of the product is found empirically by assuming independence. Consequently, distributions displaying the relative magnitude of the parameters at the time slice of interest result.

(2) Utilizing the particular loads equation, determine the empirical distribution of the load by combining the contributions from the parameters as indicated by the loads equation. The following equations show a typical calculation for a vertical tail load:

$$\overset{*}{V}_{RVT} = 2741\, n_y - 161\, \dot{r} - 1.74\, \dot{p}$$

$$P\left\{ V_{RVT} \leq A \right\} = P\left\{ 2741\, n_y - 161\, \dot{r} - 1.74\, \dot{p} \leq A \right\}$$

$$= \sum_{i=1}^{m} \sum_{j=1}^{B} \sum_{k=1}^{\alpha} P_{n_y}(n_{y_i})\, P_{\dot{r}}(\dot{r}_j)\, P_{\dot{p}}(\dot{p}_k)$$

where

$P_\zeta(')$ denotes probability mass function for parameter ζ

α denotes greatest value of k for which

$$\dot{p}_k \geq \frac{1}{1.74}\left(A - 2741\, n_{y_i} + 161\, \dot{r}_j\right)$$

β denotes greatest value of j for which

$$\dot{r}_j \geq \frac{1}{161} (A - 2741\ n_{yi})$$

m denotes greatest value of i

The method for the calculation of the distributions of the peaks of the load cycles will be explained in detail by carrying out the procedure for the wing load, the horizontal tail load, and the vertical tail load. All 318 maneuvers are represented in these calculations. But the results from the three sets comprising the composite data sample are presented in Appendix E for comparison.

In this study the maneuvers were separated into two conditions depending upon whether the gross weight was above or below 36,000 pounds. Table 12 in Appendix A lists the average values of the calculated "constants". Different peak distributions were maintained for each of the conditions since the peak distributions could reflect the pilot's intention to adjust his flying habits in accordance with the gross weight. Given as follows for the two conditions are the appropriate loads equations for the wing load:

Condition 1: $V_{6A}^{*} = 4567\ n_z + 27.8\ \dot{q} - 7.46\ \dot{p}$

Condition 2: $V_{6A}^{*} = 5109\ n_z + 28.4\ \dot{q} - 8.66\ \dot{p}$

Figure 22 indicates that the single peak of the one load cycle during a descending left turn occurs on the average at $t' = .60$. Therefore, the n_z', $\dot{q}'$, and $\dot{p}'$ distributions at $t' = .60$ are denormalized. The normalized, peak, and denormalized parameter distributions for Condition 1 are presented in Table 4. The distribution at the top is the normalized distribution with the correction factor added; the middle distribution is the distribution of peak or normalizing factors; and the distribution at the bottom represents the product of the other two distributions.

Figure 26 displays for each of the two conditions the predicted and observed distributions of the peaks of the load cycle. The abscissa of this figure is load in pounds and the ordinate is the probability of a peak of a load cycle being less than or equal to the indicated load. Through the above equations, the observed distributions were determined from time history calculations of the load for each maneuver. The figure shows excellent agreement between the predicted and observed distributions. Since a Kolmogoroff-Smirnov test failed to reject the hypothesis of the equality of the two distributions at a level of significance of .05, the distributions from the present sample are not significantly different.

TABLE 4

Distributions of n_z, $\dot{p}$ and $\dot{q}$ at $t' = 0.60$ for Condition 1
Used in Predicting the Peak Wing Load Distribution

n'_z (c)	Class Midpoint	1.085	1.035	.985	.935	.885	.835	.760	.660					
	Relative Frequency	.3836	.2075	.1289	.0881	.0786	.0472	.0449	.0220					
Peak n_z	Class Midpoint	1.2	1.4	1.6	1.8	2.0	2.2	2.4	2.6	2.8	3.0	3.2	3.4	
	Relative Frequency	.0054	.0272	.0435	.1250	.1196	.1576	.2337	.1141	.0543	.0652	.0380	.0163	
n_s	Class Midpoint	1.0	1.2	1.4	1.6	1.8	2.0	2.2	2.4	2.6	2.8	3.0	3.2	3.4	3.6
	Relative Frequency	.0038	.0103	.0346	.0746	.1000	.1338	.1801	.1667	.1435	.0718	.0338	.0448	.0246	.0096
$\dot{p}'$ (c)	Class Midpoint	.72	.52	.32	.17	.07	.03	-.13	-.28	-.48	-.68			
	Relative Frequency	.0063	.0252	.0943	.1384	.2767	.2298	.1006	.1069	.0157	.0063			
Peak $\dot{p}$	Class Midpoint	10	20	30	40	50	60	70						
	Relative Frequency	.1685	.4130	.2120	.1196	.0598	.0163	.0109						
$\dot{p}$	Class Midpoint	35	25	15	7.5	2.5	-2.5	-7.5	-15	-25	-35			
	Relative Frequency	.0014	.0074	.0381	.0915	.4024	.3275	.0902	.0344	.0060	.0011			
$\dot{q}'$ (c)	Class Midpoint	.802	.602	.402	.202	.002	-.198	-.398	-.598	-.798	-.998			
	Relative Frequency	.0063	.0094	.0566	.1101	.2830	.2893	.1447	.0535	.0252	.0220			
Peak $\dot{q}$	Class Midpoint	1.0	2.0	3.0	4.0	5.0	6.0	7.0	8.0	9.0				
	Relative Frequency	.0217	.1359	.3370	.2500	.1086	.0707	.0335	.0272	.0054				
$\dot{q}$	Class Midpoint	7.0	5.0	3.0	1.0	-1.0	-3.0	-5.0	-7.0					
	Relative Frequency	.0006	.0043	.0455	.4150	.1567	.0662	.0091	.0018					

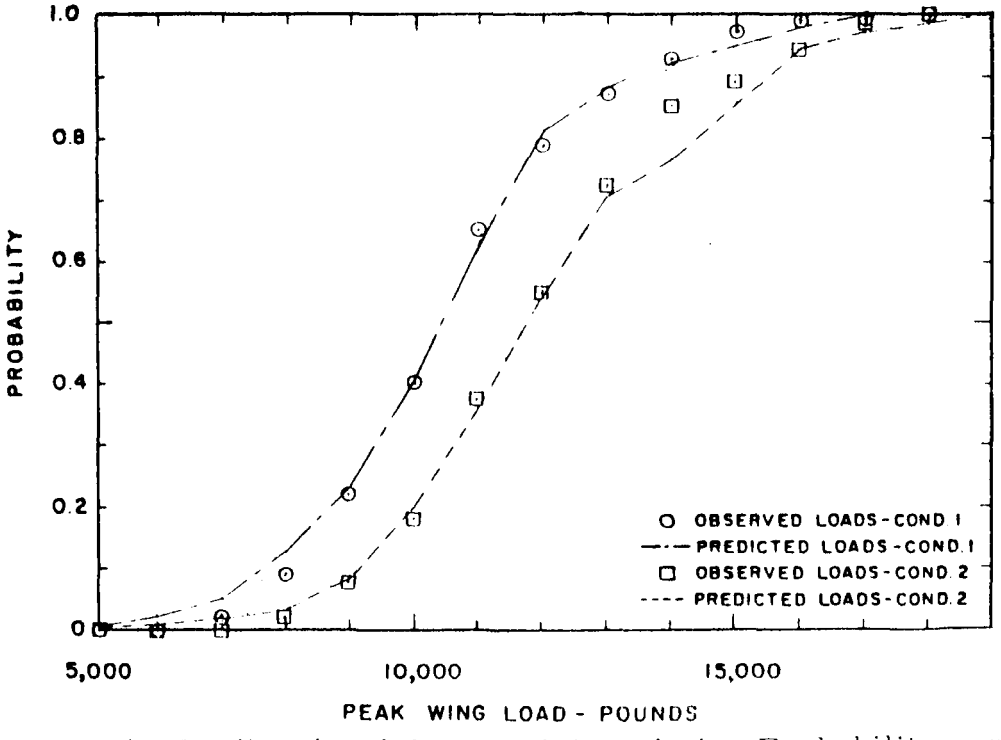

Figure 26. Predicted and Observed Cumulative Probability versus Peak Wing Load for Weight Condition 1 (185 turns) and Weight Condition 2 (133 turns)

Given as follows for the two conditions are the appropriate loads equations for the horizontal tail load:

Condition 1: $V^{*}_{RHT} = -1399\ n_z - 91.1\ \dot{q} + .993\ \dot{p}$

Condition 2: $V^{*}_{RHT} = -1506\ n_z - 93.1\ \dot{q} + .993\ \dot{p}$

Figure 23 shows that on the average one negative load cycle appears on the horizontal tail and that the negative peak occurs at $t' = 0.55$ Therefore, the n_z', $\dot{p}'$, and $\dot{q}$ distributions at $t' = 0.55$ are denormalized. Table 5 presents the normalized, peak, and denormalized parameter distributions analogously to Table 4.

TABLE 5

Distributions of n_z, $\dot{p}$ and $\dot{q}$ at $t' = .55$ for Condition 1 Used in Predicting the Negative Peak Horizontal Tail Load Distribution

n'_z (c)	Class Midpoint	1.085	1.035	.985	.935	.885	.835	.760	.660					
	Relative Frequency	.3774	.2130	.1164	.0975	.0755	.0283	.0755	.0126					
Peak n_z	Class Midpoint	1.2	1.4	1.6	1.8	2.0	2.2	2.4	2.6	2.8	3.0	3.2	3.4	
	Relative Frequency	.0054	.0272	.0435	.1250	.1196	.1576	.2337	.1141	.0543	.0652	.0380	.0163	
n_z	Class Midpoint	1.0	1.2	1.4	1.6	1.8	2.0	2.2	2.4	2.6	2.8	3.0	3.2	3.4	3.6
	Relative Frequency	.0039	.0100	.0310	.0813	.1031	.1305	.1509	.1657	.1406	.0594	.0448	.0447	.0244	.0097
$\dot{p}'$ (c)	Class Midpoint	.522	.372	.272	.172	.072	-.028	-.128	-.228	-.328	-.528			
	Relative Frequency	.0126	.0346	.0975	.1635	.2673	.2233	.1101	.0472	.0283	.0157			
Peak $\dot{p}$	Class Midpoint	10	20	30	40	50	60	70						
	Relative Frequency	.1685	.4130	.2120	.1196	.0598	.0163	.0109						
$\dot{p}$	Class Midpoint	25	15	7.5	2.5	-2.5	-7.5	-15	-25					
	Relative Frequency	.0036	.0460	.1444	.3816	.3427	.0587	.0195	.0036					
$\dot{q}'$ (c)	Class Midpoint	.914	.714	.564	.464	.364	.264	.164	.064	-.036	-.136	-.236	-.336	-.486	-.686
	Relative Frequency	.0063	.0220	.0314	.0377	.0409	.0566	.1321	.1648	.1887	.1069	.0818	.0597	.0503	.0157
Peak $\dot{q}$	Class Midpoint	1.0	2.0	3.0	4.0	5.0	6.0	7.0	8.0	9.0					
	Relative Frequency	.0217	.1359	.3370	.2500	.1086	.0707	.0435	.0272	.0054					
$\dot{q}$	Class Midpoint	7.0	5.0	3.0	1.0	-1.0	-3.0	-5.0						
	Relative Frequency	.0005	.0057	.0516	.4391	.4682	.0327	.0022						

Figure 27 displays for the two conditions the predicted and observed peak load distributions for the horizontal tail. Again there is excellent agreement, and the two sample distributions are not significantly different. For these curves, the ordinate represents the probability of exceeding the indicated load or the probability of being less than the absolute value of the load.

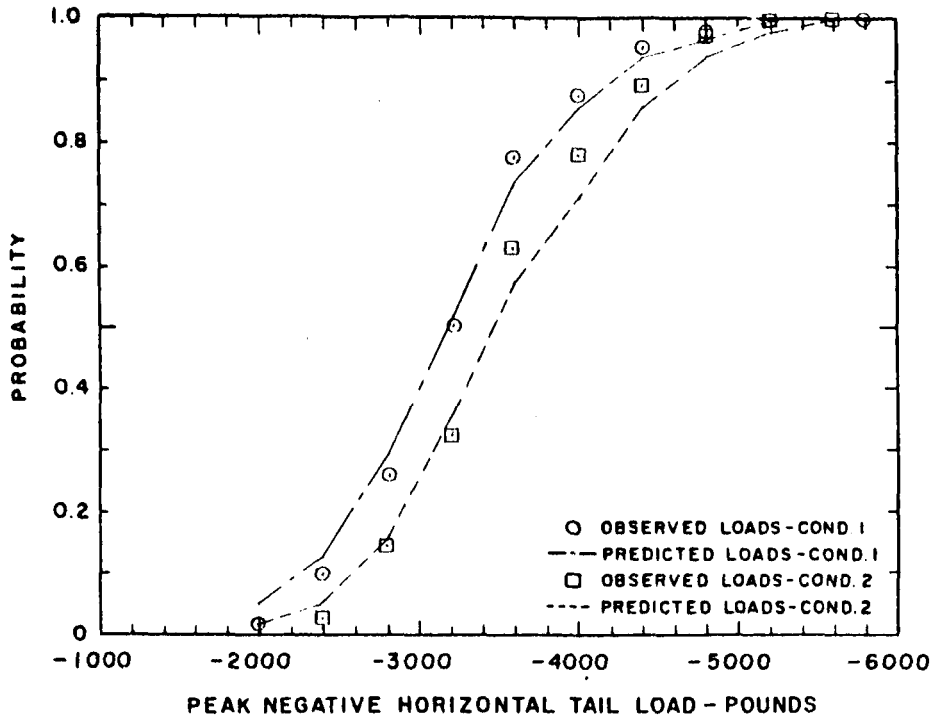

Figure 27. Predicted and Observed Cumulative Probability versus Peak Horizontal Tail Load for Weight Condition 1 (185 turns) and Weight Condition 2 (133 turns)

Given as follows for the two conditions are the appropriate loads equations for the vertical tail load:

Condition 1: $V^{*}_{RVT} = 2741\ n_y - 161\ \dot{r} - 1.74\ \dot{p}$

Condition 2: $V^{*}_{RVT} = 3110\ n_y - 165\ \dot{r} - 1.78\ \dot{p}$

Reference to Figure 24 indicates that the average load cycle on the vertical tail consists of a positive peak at $t' = 0.15$ and a negative peak at $t' = 0.975$. Consequently, since two distributions of peak values are important for the vertical tail, two sets of parameter values must be derived. Tables 6 and 7 present analogously to Table 4 the normalized, peak, and denormalized parameter distributions for $t' = 0.15$ and $t' = 0.975$, respectively.

Figures 28 and 29 present, respectively, the predicted and observed peak load distributions for $t' = 0.15$ and $t' = 0.975$ for the two conditions. Again, the differences in the distributions are not statistically significant.

TABLE 6

Distributions of n_y, $\dot{p}$ and $\dot{r}$ at t' = .15 for Condition 1 Used in Predicting the Position Peak Vertical Tail Distribution

n'_y (c)	Class Midpoint	1.399	1.299	1.199	1.099	.999	.899	.799	.699	.599	.499	.349	.149	-.051
	Relative Frequency	.0440	.0472	.0629	.0881	.0975	.1069	.0912	.1164	.1101	.1038	.1101	.0126	.0094
Peak n_y	Class Midpoint	.03	.05	.07	.09	.11	.13	.15	.17	.19				
	Relative Frequency	.0543	.1685	.2011	.2283	.1630	.0543	.0701	.0380	.0217				
n_y	Class Midpoint	.25	.23	.21	.19	.17	.15	.13	.11	.09	.07	.05	.03	.01	-.01
	Relative Frequency	.0020	.0048	.0073	.0111	.0192	.0360	.0535	.0776	.1502	.1905	.2144	.1767	.0472	.0094
$\dot{p}'$ (c)	Class Midpoint	.879	.679	.479	.279	.079	-.121	-.321	-.521	-.721	-.921			
	Relative Frequency	.0063	.0220	.1006	.1101	.2264	.3019	.0818	.0818	.0252	.0440			
Peak $\dot{p}$	Class Midpoint	10	20	30	40	50	60	70						
	Relative Frequency	.1685	.4130	.2120	.1196	.0598	.0163	.0109						
$\dot{p}$	Class Midpoint	45	35	25	15	5	-5	-15	-25	-35	-45	-55		
	Relative Frequency	.0014	.0032	.0162	.0678	.3774	.3926	.0957	.0332	.0090	.0030	.0015		
$\dot{r}'$ (c)	Class Midpoint	-.226	-.376	-.476	-.576	-.676	-.776	-.876	-.976	-1.076	-1.176	-1.276	-1.376	-1.476
	Relative Frequency	.0723	.0755	.1226	.1509	.1289	.1006	.0597	.0629	.0472	.0252	.0503	.0535	.0503
Peak $\dot{r}$	Class Midpoint	1.0	2.0	3.0	4.0	5.0	6.0	7.0	8.0	9.0				
	Relative Frequency	.0598	.2717	.3424	.1413	.0707	.0598	.0326	.0054	.0163				
$\dot{r}$	Class Midpoint	-.25	-.75	-1.25	-1.75	-2.5	-3.5	-4.5	-5.5	-6.5	-7.5	-8.5	-9.5	-10.5	-11.5
	Relative Frequency	.0357	.1189	.1775	.1377	.2563	.1050	.0800	.0408	.0184	.0112	.0099	.0028	.0023	.0031

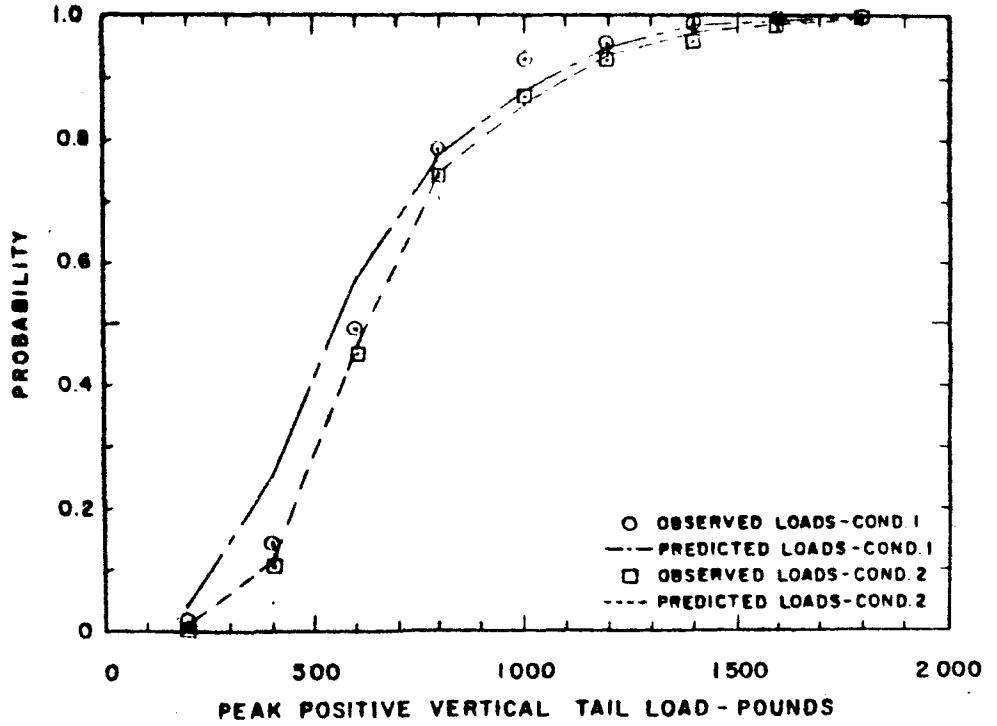

Figure 28. Predicted and Observed Cumulative Probability versus Peak Positive Vertical Tail Load for Weight Condition 1 (185 turns) and Weight Condition 2 (133 turns)

TABLE 7

Distributions of n_y, $\dot{p}$ and $\dot{r}$ at t' = .975 for Condition 1 Used in Predicting the Negative Peak Vertical Tail Distribution

n'_y (c)	Class Midpoint	.444	.244	.044	-.156	-.306	-.406	-.506	-.606	-.706	-.806	-.906	-1.006	-1.156	-1.356
	Relative Frequency	.0157	.0063	.0346	.0912	.0692	.0975	.1352	.1038	.1006	.0566	.0629	.0597	.0849	.0818
Peak n_y	Class Midpoint	.03	.05	.07	.09	.11	.13	.15	.17	.19					
	Relative Frequency	.0543	.1685	.2011	.2283	.1630	.0543	.0701	.0380	.0217					
n_y	Class Midpoint	.075	.045	.015	-.015	-.045	-.075	-.105	-.135	-.165	-.195	-.225	-.255		
	Relative Frequency	.0020	.0113	.0432	.2255	.3151	.1883	.1049	.0656	.0265	.0102	.0049	.0018		
$\dot{p}'$ (c)	Class Midpoint	1.264	1.064	.864	.664	.464	.264	.064							
	Relative Frequency	.1541	.1541	.2610	.2512	.1415	.0220	.0157							
Peak $\dot{p}$	Class Midpoint	10	20	30	40	50	60	70							
	Relative Frequency	.1685	.4130	.2120	.1196	.0598	.0163	.0109							
$\dot{p}$	Class Midpoint	75	65	55	45	35	25	17.5	12.5	7.5	2.5				
	Relative Frequency	.0059	.0145	.0319	.0367	.1172	.2233	.1786	.1896	.1585	.0432				
$\dot{r}'$ (c)	Class Midpoint	1.388	1.288	1.188	1.088	.988	.888	.788	.688	.588	.488	.338	.138	-.062	
	Relative Frequency	.1698	.0723	.0692	.0660	.0597	.0535	.1069	.0786	.0786	.0692	.0943	.0409	.0409	
Peak $\dot{r}$	Class Midpoint	1.0	2.0	3.0	4.0	5.0	6.0	7.0	8.0	9.0					
	Relative Frequency	.0598	.2717	.3424	.1413	.0707	.0598	.0326	.0054	.0163					
$\dot{r}$	Class Midpoint	12.5	11.5	10.5	9.5	8.5	7.5	6.5	5.5	4.5	3.5	2.5	1.5	0.5	-0.5
	Relative Frequency	.0028	.0021	.0015	.0095	.0139	.0138	.0265	.0558	.1030	.1248	.2501	.2386	.1166	.0408

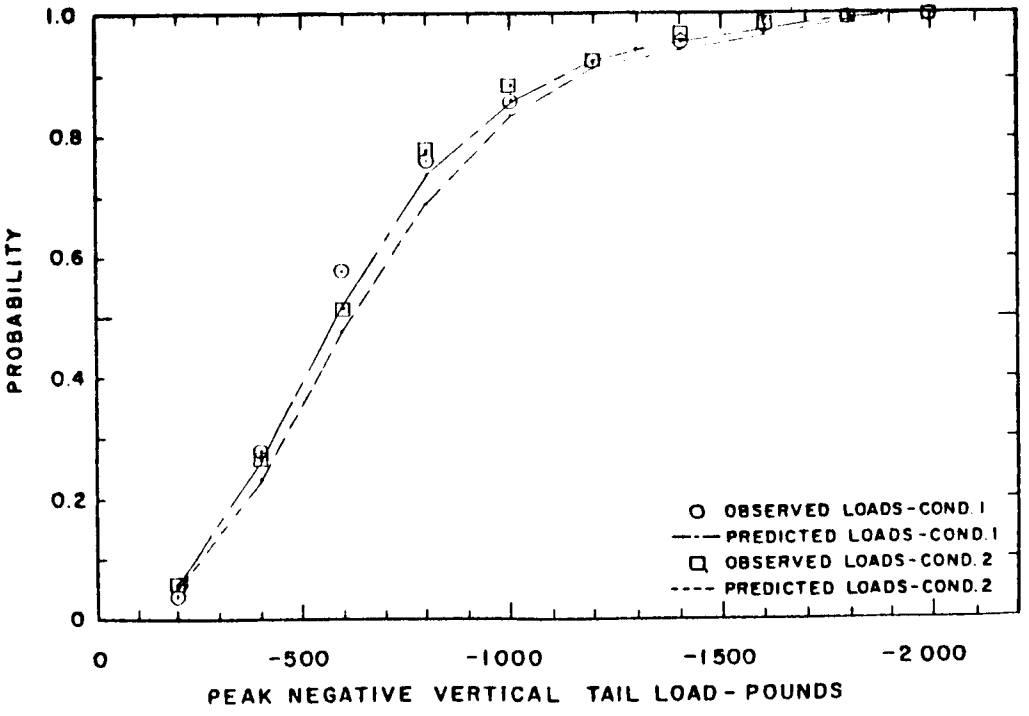

Figure 29. Predicted and Observed Cumulative Probability versus Peak Negative Vertical Tail Load for Weight Condition 1 (185 turns) and Weight Condition 2 (133 turns)

Since the level-flight (n_z = 1.0) vertical tail load is zero, the load peaks for Conditions 1 and 2 oscillate about the same value. Therefore, the load probability calculations can be carried one step further by combining the distributions for the two conditions by a weighted average of the curves for each condition. Figure 30 and 31 present these weighted composites and the composite observed distributions for t' = 0.15 and t' = 0.975, respectively. Similar composites for the wing and horizontal tail loads would have no particular meaning since different conditions imply different level-flight loadings.

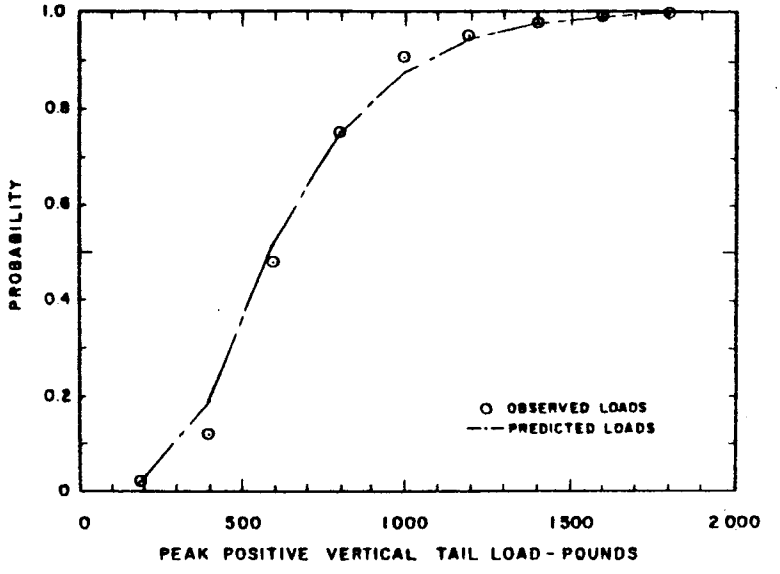

Figure 30. Predicted and Observed Cumulative Probability versus Peak Positive Vertical Tail Load for Composite of 318 Turns

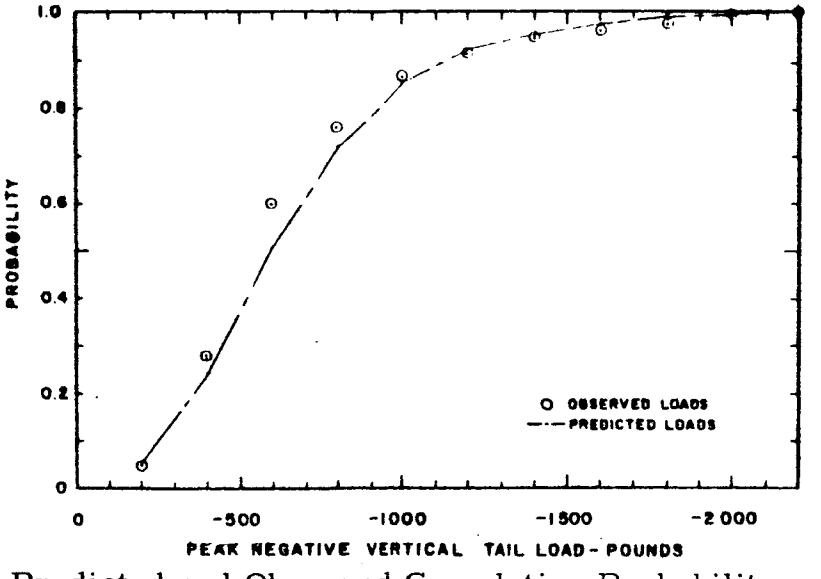

Figure 31. Predicted and Observed Cumulative Probability versus Peak Negative Vertical Tail Load for Composite of 318 Turns

The discrepancies between the predicted and observed distributions can be attributed to three major factors:

(1) The invalidness of the assumption that all random variables are independent of one another. Although a method was developed to account for their interdependence, the attendant increase in the complexity and size of the sample would likely negate its use.

(2) The peculiarities existing in the empirical distributions which could be removed only by increasing the sample size.

(3) The use of the same average "constants" to predict loads distributions while the observed distributions were derived from load time histories which used different "constants" for each particular maneuver.

2.5 Applications of Statistical Maneuver Model to Design Criteria

The present effort has demonstrated the form of the statistical model of normalized parameters for one maneuver type and the prediction of three sample maneuver load probability curves by using equations for two flight conditions for the F-105D airplane. However, this effort is only a partial solution to the problem of applying the model to design criteria.

2.5.1 Calculation of Maneuver Fatigue Loads Spectrum

The prediction of an accurate maneuver fatigue loads spectrum for an aircraft by using the statistical model requires the following:

(1) A set of distributions of normalized parameter values at selected time slices for all maneuver types.

(2) The distribution of parameter peak values by maneuver type, by flight condition, by mission type, and by air base.

(3) The distribution of each type of maneuver by flight condition, by mission type, and by air base.

Items (1) and (2) permit the calculation of probability curves for predicted maneuver loads for each maneuver type, flight condition, mission type, and air base combination. Using this set of probability curves and Item (3) yields a predicted maneuver loads distribution,

or fatigue spectrum, giving the magnitude and number of peak maneuver loads at each level of a steady level-flight (n_z = 1.0) load.

The probability curves (Figures 26 through 31) in the previous section can be used to illustrate the prediction of a maneuver loads fatigue spectrum. For demonstration purposes, assume that a typical F-105D airplane will perform 14,000 descending left turns during its lifetime and that this is the only maneuver type performed. Assume further that 8,000 of these turns will be in Condition 1 and the remaining 6,000 will be in Condition 2. With these assumptions, the maneuver loads fatigue spectrum for the wing load, or wing shear, at location 6A, was calculated. The level-flight (n_z = 1.0) wing loads for Conditions 1 and 2 are 4567 and 5109 pounds, respectively. The number and ranges of maneuver peak loads at level-flight loads of 4567 and 5109 pounds were calculated from the probability curves for Condition 1 and 2 in Figure 26 and the assumed distribution of maneuvers by condition. Figure 32 illustrates the calculated wing load fatigue spectrum. The value at the top of each column represents the number of cycles in that peak load range.

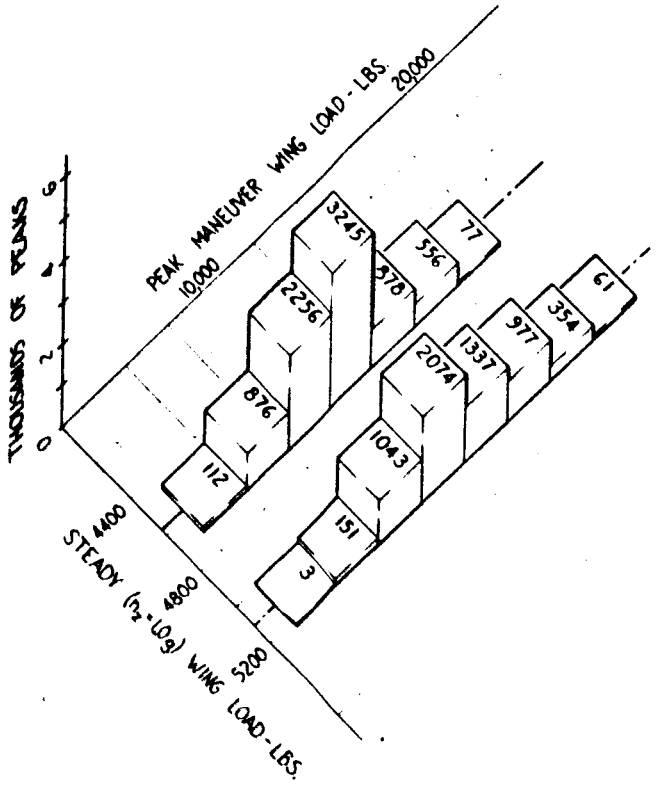

Figure 32. Maneuver Fatigue Load Spectrum of Wing Shear Load (V_{6A}) Representing 14,000 Descending Left Turns

Figure 33 depicts the horizontal tail load, or shear load at the root of the horizontal tail, fatigue spectrum which was calculated by using the same assumptions. The level-flight (n_Z = 1.0) horizontal tail loads for Conditions 1 and 2 are -1399 and -1506 pounds, respectively.

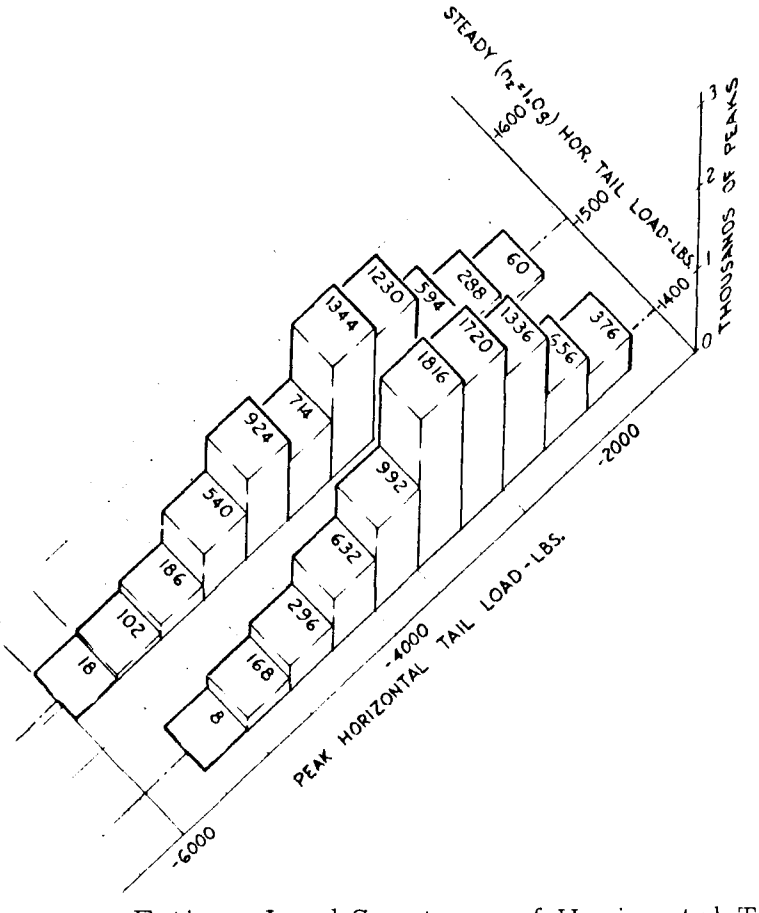

Figure 33. Maneuver Fatigue Load Spectrum of Horizontal Tail Shear Load (V_{RHT}) Representing 14,000 Descending Left Turns

For the vertical tail load, or shear load at the root of the vertical tail, a slightly different calculation technique was used because the level-flight (n_Z = 1.0) load is zero for all flight conditions. For the vertical tail load, a composite probability curve (see Figures 30 and 31) was calculated by weighting the probability curves for Conditions 1 and 2 (see Figures 28 and 29) by the percentage of maneuvers performed in each condition and then combining the curves. Two composite curves were required, one for positive maneuver load peaks and one for negative maneuver load peaks, since one peak occurred in each direction during the descending left turn. Since the vertical tail load probability curve already contains the distribution of maneuvers by flight condition, only the total

number of maneuvers (14,000) is required to calculate the fatigue spectrum for the maneuver loads. Figure 34 illustrates the vertical tail maneuver load spectrum with both the positive and negative load peaks shown. Note that the total number of peaks indicated is 28,000, 14,000 being positive and 14,000 negative. The rest of this section discusses the effect of mission type, air base, and flight condition on the statistical model and the methods of handling these effects in the design criteria.

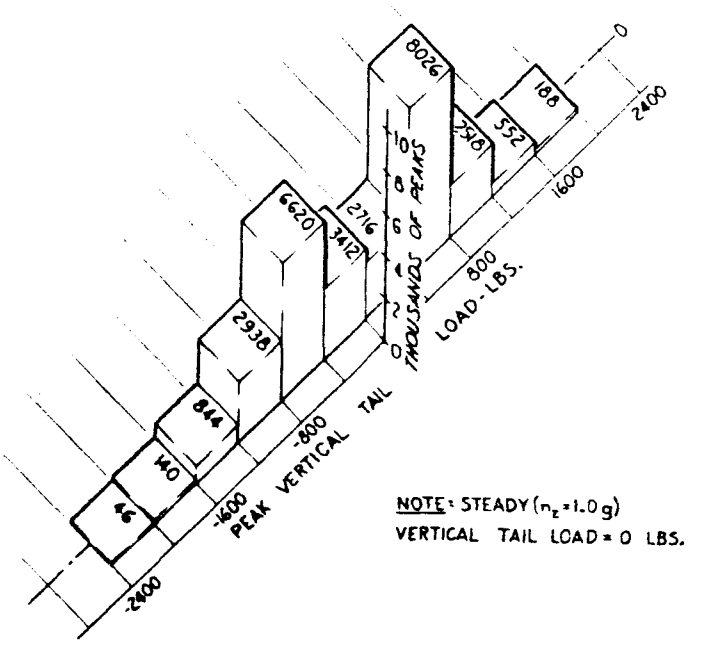

Figure 34. Maneuver Fatigue Load Spectrum of Vertical Tail Shear Load (V_{RVT}) Representing 14,000 Descending Left Turns

2.5.2 Effect of Mission and Base

The type of missions flown by an aircraft and the base from which the aircraft operates are significant factors in the distribution of the loads encountered. For example, the difference between the load distribution on an aircraft performing mostly ground gunnery and bombing missions and an aircraft flying primarily cross-country ferry missions can be a factor of two in the amplitude of maneuver loads and a factor of twenty in the frequency of maneuver loads. The proximity of an air base to practice gunnery and bombing ranges can affect the maneuver load distribution of the aircraft stationed at the air base. Obviously, aircraft stationed at an air base close to such ranges have an appreciably higher percentage of flight time making passes over the target and a correspondingly lower percentage of time maintaining the relatively inactive cruise condition than aircraft located at an air base remote from the ranges.

Since the percentage differences can be very significant, they should be included in a comprehensive design criteria.

Design criteria can be developed only from data descriptive of the number of maneuvers and percentages of time spent by operational aircraft in various air base-mission conditions. Since operational requirements of future aircraft must be projected with some uncertainty, the design criteria should prescribe such a fatigue spectrum that the new aircraft be capable of performing some minimum percentage of its flight time in the more severe air base-mission conditions, such as those in the ground support mission performed from Wheelus Air Base, Libya.

2.5.3 Effect of Variation in Flight Conditions

The parameters comprising the flight conditions which primarily affect the magnitude and distribution of loads incurred by an aircraft are gross weight, moments of inertia, mass distribution, altitude and Mach number. These parameters determine the coefficients in the airloads and inertia loads equations. Through changes in the slopes of the lift and side force curves versus angles of attack and yaw, respectively, and changes in the centers of pressure of the aerodynamic surfaces, Mach number and altitude determine the distribution of airloads. The magnitude of all vertical airloads are dependent on the gross weight. The moments of inertia affect the centers of pressure and airload distribution because they establish the control deflections required to produce given angular motions. Finally, changes in the mass distribution (due to various store locations and fuel burnoff) produce corresponding changes in the distribution of inertia loads in the structure. Therefore, the variations in the flight conditions cause variation in the maneuver peak load magnitudes. Since the number of maneuvers of each type for each flight condition is primarily a function of flight performance, the design criteria cannot prescribe such numbers because of the uncertainty of future flight performance. Therefore, the aircraft designer must determine for his particular aircraft the distribution of maneuvers for the various flight conditions. To make the design requirements less stringent, the designer often imposes operational restrictions to prevent certain maneuvers in some of the more severe flight conditions. These restrictions, however, must be chosen so that the performance of the required mission is in no way compromised. An example of such a restriction is the limitation of some fighter aircraft to 6.0-g normal accelerations when flying with full external fuel tanks. These tanks are normally empty by the time the aircraft is in the target area but can be dropped instantly should an unexpected combat situation develop.

To determine the distribution of maneuvers by flight condition, the designer must develop mission profiles for each mission type.

These profiles indicate the percentage of mission time expected for each flight condition and the order in which the conditions occur. Then the designer can superimpose the required maneuvers on the mission profile to project a more realistic distribution of maneuvers by flight condition. Since such mission profiles have been used in the design of new aircraft, they should not pose any problems.

2.5.4 Effect of Aircraft Type and Configurations

The proposed statistical model was designed specifically to eliminate the effects of aircraft type from the normalized maneuver parameter time histories. How effective this elimination may be can be revealed only by comparing the normalized data of F-105D aircraft with that of a different aircraft type. Although results from the proposed model are quite encouraging, data from many aircraft types must be tested before the model may be incorporated in the aircraft design criteria.

Even though the effects of aircraft type are removed from the normalized maneuver parameter time histories, the normalizing factors, or parameter peak values, for each maneuver type will still depend on the aircraft type. Consequently, the design criteria must include a distribution of parameter peak values by maneuver type for each general category of aircraft so that the designer can apply the statistical model to his particular type of aircraft. Of course, the distribution of parameter peak values must be sufficiently flexible to permit its application to aircraft with radically different design features, such as the variable sweep wings of the F-111, and to aircraft with a specialized mission, such as the high-altitude U-2 airplanes. In such applications, the designer must choose the appropriate distribution of parameter peak values.

The configuration of an aircraft should not affect the proposed statistical model except in the calculation of its load distributions. "Configurations," as used in this report, denotes the possible arrangements of internal and external stores on a single airplane. Since a configuration determines the distribution of the airplane's mass, it establishes the distribution of loads in the airplane's structure. The designer must be certain that his aircraft flying with the most burdensome configuration will withstand the load spectrum for each mission type. The configuration normally changes during flight by the dropping of stores and the consumption of the fuel load. To some degree, therefore, the pilot can control a configuration change as well as the maneuvers to be performed in a particular configuration. Consequently, the designer may specify some operational limits on the maneuvers performed with the more severe configurations so that unusual loading conditions will not penalize the overall design. An example

of this is the operational limit placed on normal accelerations for some fighter-bombers when heavy stores are carried externally. Of course, any operational limitations must be approved by the user.

2.5.5 Effect of Gusts, Formation Flying, and Structural Elasticity

As applied to the recorded parameter traces, the term "maneuver" normally denotes the smooth low-frequency deflections with peaks lasting two seconds or more. Whenever these traces are ragged with random high-frequency deflections, the input is attributed to the effects of turbulence unless the pilot was engaged in close formation flying where he must continually adjust his control input to maintain a precise position relative to the lead aircraft. Because of the randomness of these inputs, they are not likely to affect the average parameter time histories derived from the statistical model. Their inclusion in the model, however, would significantly increase the width of the distribution of parameter values about the average and, consequently, make it more difficult to determine the true maneuver input. In addition, since the airload distribution of a gust input is different from the airload distribution of a maneuver, or control surface, input, a different loads equation would be needed to predict the distribution of loads. Therefore, so that the maneuver loads could be predicted more accurately, the high-frequency responses were removed from the data by using a fixed sampling rate for all traces and a weighted filter for the angular rate traces (see Appendix D).

The calculation of fatigue load distributions from high-frequency inputs, such as those produced by gusts and formation flying, requires different statistical techniques from those used in the proposed statistical model. The randomness of these inputs lends itself to a power spectral density analysis. Since the time transformation factors are recorded in the statistical models of maneuvers, it should be possible, from the power spectral density analysis of the gusts and formation flying, to calculate the high-frequency loads spectrum expected during maneuvers and to superimpose these loads on the calculated maneuver loads. Although time during this study did not permit investigating this procedure, some method of combining gusts with the statistical maneuver model should be possible.

The amplification and attenuation of structural loads caused by the elasticity of the aircraft's structure poses one of the most difficult problems in flight loads analysis. The extent to which the true structural loads differ from the calculated "rigid-body" loads and the recorded aircraft motions differ from the actual center-of-gravity motions depends on the flexibility of the aircraft structure. On a relatively rigid

airplane, such as the F-105D, the difference is very small; but on a flexible airplane, such as the B-52, the difference can be quite significant. The dynamic loads are a function of the input frequency as well as the aircraft flexibility. For the low-frequency maneuver inputs, the dynamic load distributions should not be significantly different from the rigid-body load distributions even on the flexible aircraft types. Therefore, the proposed statistical maneuver model should not be significantly affected by structural elasticity. For the higher frequency inputs from gusts and formation flying, however, a dynamic analysis must be used. To calculate dynamic loads requires knowledge of the frequency and amplitude of the gust and control surface inputs and the complete structural response characteristics of the airframe. In some analyses, a dynamic amplification factor is used to predict the dynamic loads from rigid-body loads; but this method is less accurate. When the gust data are combined with data in the statistical maneuver model, the dynamic loads must be considered.

3. SUMMARY AND CONCLUSIONS

This study formed a statistical maneuver model and demonstrated its use in predicting a fatigue load spectrum. The model was derived from a data sample of 318 descending left turns performed by F-105D aircraft. Aspects of the proposed statistical model shown to be feasible are as follows:

(1) From the trace patterns appearing in eight-channel data, maneuver types can be distinguished and categorized.

(2) The parameter traces of all maneuvers of the same type can be approximately aligned by transforming the time scale. In the processing of the sample of 318 descending left turns, the averages derived for the transformed parameter traces were almost identical for each of three independent groups of turns.

(3) The statistical maneuver model permits an accurate prediction of distributions of structural load peaks from eight-channel data. The predicted peak loads spectrum for three particular structural locations on the F-105D airplane compared very favorably with the "observed" load time histories.

One important potential of the proposed method—the extension of the application of the statistical maneuver model from one aircraft type to another—could not be tested in this study because no suitable eight-channel data from another aircraft type was available.

4. RECOMMENDATIONS

In the light of the foregoing study, the following recommendations are proposed:

(1) To test the feasibility of using a single statistical maneuver model for all types of aircraft, eight-channel data should be recorded on either a small light aircraft, such as a Cessna 182, or a large heavy aircraft, such as a B-52 or a C-141, and reduced to a form compatible with the statistical model.

(2) All available F-105D eight-channel data should be processed to obtain a larger sample of the descending left turn, to test the statistical maneuver model for all maneuver types, to permit a more comprehensive use of the various flight conditions in the calculation of loads, and to test the feasibility of a program covering all maneuver types.

(3) The feasibility of automatically processing the eight-channel data on a high-speed computer to derive the statistical maneuver model should be determined.

(4) Methods of combining gust inputs with the proposed statistical maneuver model should be investigated.

(5) A method of calculating the effects of aircraft structural elasticity on the predicted loads distributions should be developed.

APPENDIX A

DATA SAMPLE

The data sample used to demonstrate the proposed statistical model consists of 318 descending left turn maneuvers performed during 40 flights of F-105D aircraft operating from three Air Force bases. Since this maneuver type occurs most frequently in a ground support mission, most of the 40 flights were of this mission type. Giving the breakdown of these data, Table 8 shows the number of flights originating from each base and the number of maneuvers performed during these flights.

TABLE 8

Breakdown of Data Sample by Air Base

Base	No. of Flights	No. of Maneuvers
Nellis	21	194
Kadena	13	63
Wheelus	6	61
Total	40	318

The effect of sample size on the statistical model was investigated by separating the data sample into three independent sets and then comparing each set with the others and with a composite of all the sets. The number of maneuvers in each set and the breakdown of maneuvers by base within each set is given in Table 9.

TABLE 9

Distribution of Descending Left Turns by Set

Set	Nellis	Kadena	Wheelus	Total
I	46	22		68
II	75	17	26	118
III	73	24	35	132
Total	194	63	61	318

TABLE 10

Takeoff Configurations of F-105D Aircraft Observed During 40 Flights

Configuration	No. of Maneuvers	No. of Flights	Bomb Bay	Center Line Pylon	Right In-Board Pylon	Left In-Board Pylon	Right Out-Board Pylon	Left Out-Board Pylon
1	20	5	Full fuel tank	Store dispenser	Full fuel tank	Full fuel tank	Rocket (M) launcher	Rocket (M) launcher
2	27	2	Full fuel tank	Store dispenser	Full fuel tank	Full fuel tank	Rocket (L) launcher	Rocket (L) launcher
3	4	1	Full fuel tank	Store dispenser	Full fuel tank	Full fuel tank	No store	No store
4	30	3	Full fuel tank	Store dispenser	Empty fuel tank	Empty fuel tank	Rocket (M) launcher	Rocket (M) launcher
5	13	2	Full fuel tank	Store dispenser	Empty fuel tank	Empty fuel tank	No store	No store
6	16	2	Full fuel tank	Store dispenser	No store	No store	Rocket (M) launcher	Rocket (M) launcher
7	65	6	Empty fuel tank	Store dispenser	Full fuel tank	Full fuel tank	Rocket (M) launcher	Rocket (M) launcher
8	7	2	Empty fuel tank	Store dispenser	Full fuel tank	Full fuel tank	Rocket (L) launcher	Rocket (L) launcher
9	3	1	Empty fuel tank	Store dispenser	Full fuel tank	Full fuel tank	No store	No store
10	15	3	Ballast	Store dispenser	Full fuel tank	Full fuel tank	Rocket (L) launcher	Rocket (L) launcher
11	6	1	Ballast	No store	Full fuel tank	Full fuel tank	GAM	GAM
12	7	2	Ballast	No store	Full fuel tank	Full fuel tank	GAM	No store
13	6	1	Ballast	No store	Partial fuel tank	Partial fuel tank	Incend. bomb	Incend. bomb
14	7	1	No store	Store dispenser	Full fuel tank	Full fuel tank	Rocket (M) launcher	Rocket (M) launcher
15	70	7	No store	Store dispenser	Partial fuel tank	Partial fuel tank	Rocket (L) launcher	Rocket (L) launcher
16	2	1	No store	Store dispenser	Partial fuel tank	Partial fuel tank	Incend. bomb	Incend. bomb
	318	40						

The F-105D aircraft, a fighter-bomber, has a large number of possible configurations of internal and external stores. Table 10 lists the various takeoff configurations which existed in the data sample. Moreover, a configuration was changed whenever external stores were dropped. The variation of configuration affects the aircraft's mass distribution, moments of inertia and, to a certain extent, airload distribution. Although the effects of configuration variation in the mass distribution and moments of inertia were calculated for each descending left turn maneuver, the effects

on airload distribution due to the placement of stores were ignored in this study since they were considered negligible compared to the total airloads.

The 318 maneuvers were performed under various flight conditions of gross weight, moments of inertia, altitude, and Mach number. The coefficients in the loads equations, developed in Appendix C, are functions of the respective flight conditions. Consequently, before these equations may be applied to the maneuvers to calculate their loads, the flight conditions of each maneuver must be determined and the coefficients appropriate to each flight condition must be calculated.

For the statistical prediction of the distribution of load peaks, the moments of inertia and mass distributions were assumed to be functions of gross weight only. The 318 maneuvers were grouped by weight according to the listing in Table 11 (Figure 35 shows this grouping as the percentage of maneuvers with weights below given values). Then, with the 36,000-lb. level serving as the best dividing point, the maneuvers with weights below this level were grouped to form the maneuvers in Condition 1 and those above to comprise the maneuvers in Condition 2. Next, with the average gross weights computed for the weights below and above the 36,000-lb. level, the moments of inertia and mass distributions for Conditions 1 and 2 were calculated, as listed in Table 12. Finally, the average gross weights and calculated moments of inertia and mass distributions were used to calculate the coefficients in the loads equations for the two conditions, as shown in the equations presented in Section 2.4.4.

TABLE 11

Distribution of Descending Left Turns by Gross Weight Range

Weight Range (lbs)	Set I	Set II	Set III	Composite
Below 32,000	5			5
32,000 to 34,000	19	21	32	72
34,000 to 36,000	30	29	49	108
36,000 to 38,000	6	40	39	85
38,000 to 40,000	6	23	10	39
40,000 and above	2	5	2	9
Total	68	118	132	318

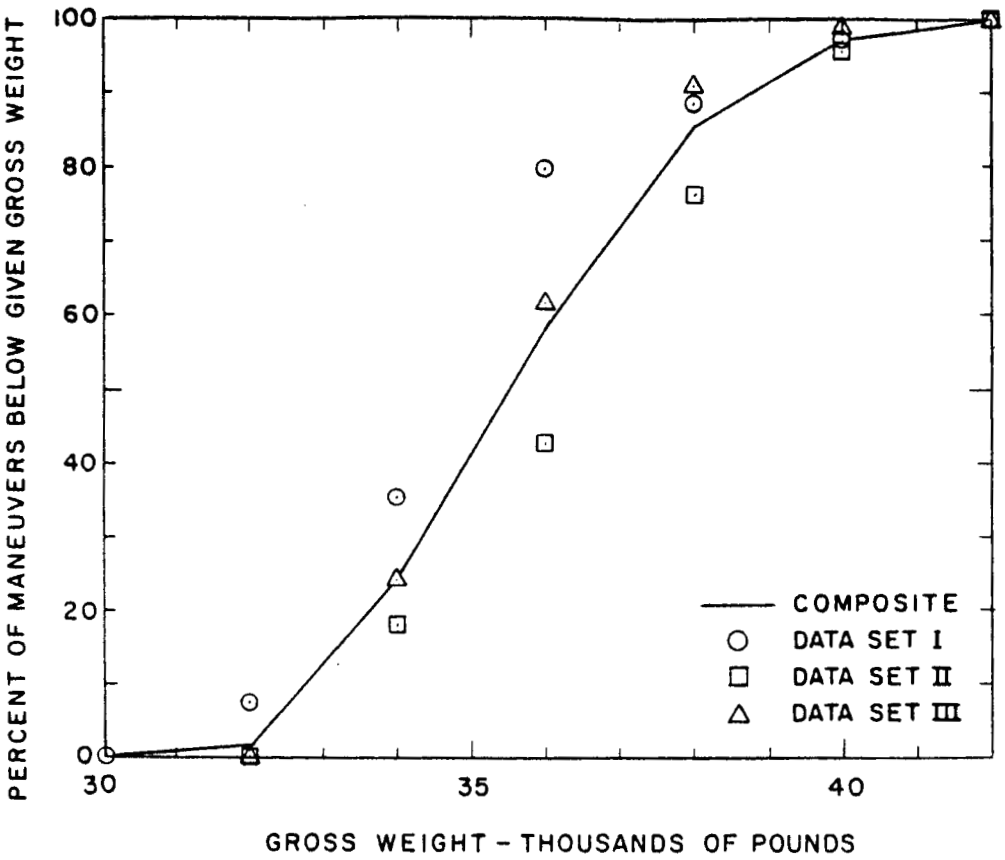

Figure 35. Graph Indicating Percentage of F-105D Descending Left Turns Below Given Gross Weights by Data Set

TABLE 12

Values of Mass Distribution and Moments of Inertia for Conditions 1 and 2

Parameter	Condition 1 (Below 36,000 lbs)	Condition 2 (Above 36,000 lbs)
I_x (slug-ft^2)	22,110	24,220
I_y (slug-ft^2)	201,100	205,500
I_z (slug-ft^2)	217,300	222,200
I_{xz} (slug-ft^2)	2,030	1,973
$\sum_{i=1}^{n} w_i$ (lbs)	751	751
$\sum_{i=1}^{n} w_i \frac{y_i}{g}$ (slug-ft)	328	331

Since most of the 318 turns were performed in ground support missions, most of the Mach numbers fell within the 0.4 to 0.7 range and most of the altitudes were within the sea level to 10,000-foot range. Because of the relatively small sample size, the effects of Mach number and altitude variations in the flight conditions were not accounted for. Of course, the effects of these variations must be considered in calculating accurate design loads. Tables 13 and 14 show the maneuvers distributed by ranges of altitude and Mach number, respectively. Individual values used to determine placement within a range were those existing at the onset of the maneuver. During a descending left turn, the altitude always decreases and the Mach number normally increases slightly. Figures 36 and 37 illustrate the percentage of maneuvers below given altitudes and airspeeds, respectively.

TABLE 13

Distribution of Descending Left Turns by Altitude Range

Altitude Range (feet)	Set I	Set II	Set III	Composite
Below 2,000	4	6	4	14
2,000 to 5,000	7	21	21	49
5,000 to 10,000	34	56	67	157
10,000 to 15,000	23	35	39	97
15,000 to 20,000	—	—	1	1
Total	68	118	132	318

TABLE 14

Distribution of Descending Left Turns by Mach Number Range

Mach No. Range	Set I	Set II	Set III	Composite
Below .4	1			1
.4 to .5	20	6	11	37
.5 to .6	34	84	89	207
.6 to .7	13	26	31	70
.7 to .8	—	2	1	3
Total	68	118	132	318

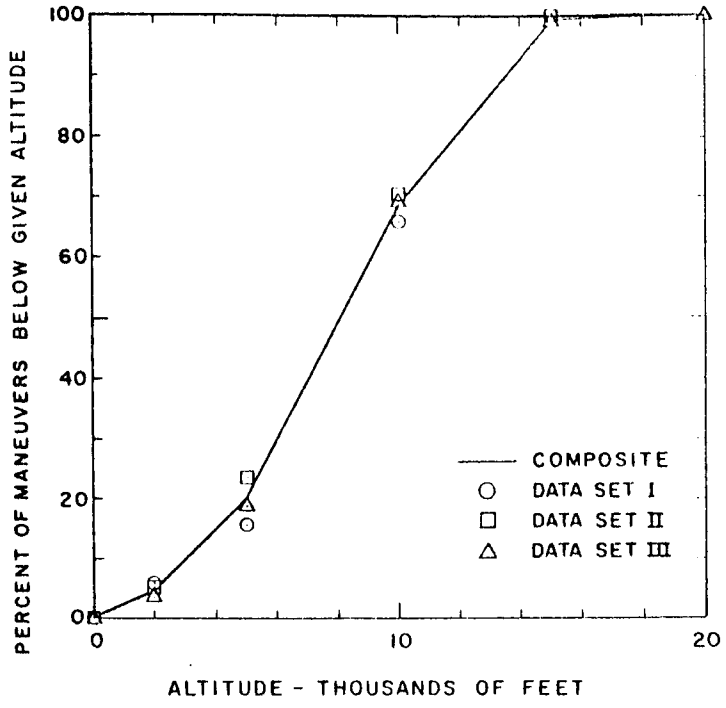

Figure 36. Graph Indicating Percentage of F-105D Descending Left Turns Below Given Altitudes by Data Set

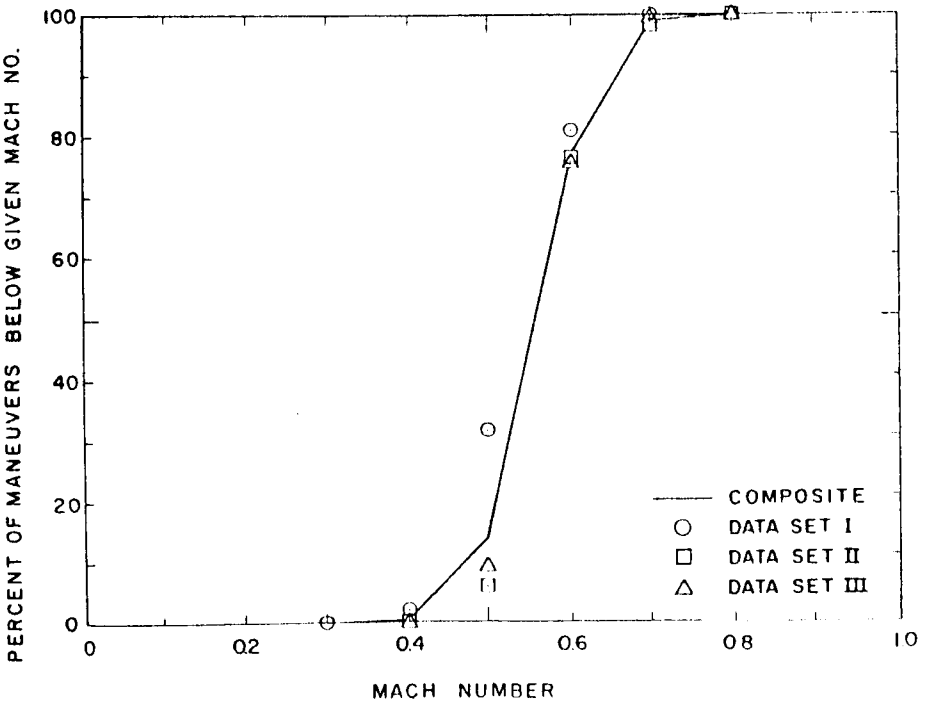

Figure 37. Graph Indicating Percentage of F-105D Descending Left Turns Below Given Mach Numbers by Data Set

The variation in the time to perform the descending left turns was due to the amount of change in heading angle which ranged from 70 to 200 degrees and to the pilot's technique, the latter being more significant. The extent of these variations are shown in Table 15 which lists the distributions of maneuvers by ranges of maneuver duration, that is, the time between the start of the roll into the turn and the peak of the role indicative of the effort to bring the wings back to level flight. Figure 38 shows the percentage of maneuvers shorter than a given duration.

TABLE 15

Distribution of Descending Left Turns by Duration

Duration (seconds)	Set I	Set II	Set III	Composite
6 to 10			4	4
10 to 14	7	13	16	36
14 to 18	16	37	52	105
18 to 22	16	29	26	71
22 to 26	10	11	13	34
26 to 30	4	5	10	19
30 to 34	5	4	2	11
34 to 38	4	5	6	15
38 to 42	1	4		5
42 to 46	2	2	1	5
46 to 50	2	4		6
50 to 54		1	1	2
54 to 58		2		2
58 to 62	1	1	1	3
Total	68	118	132	318

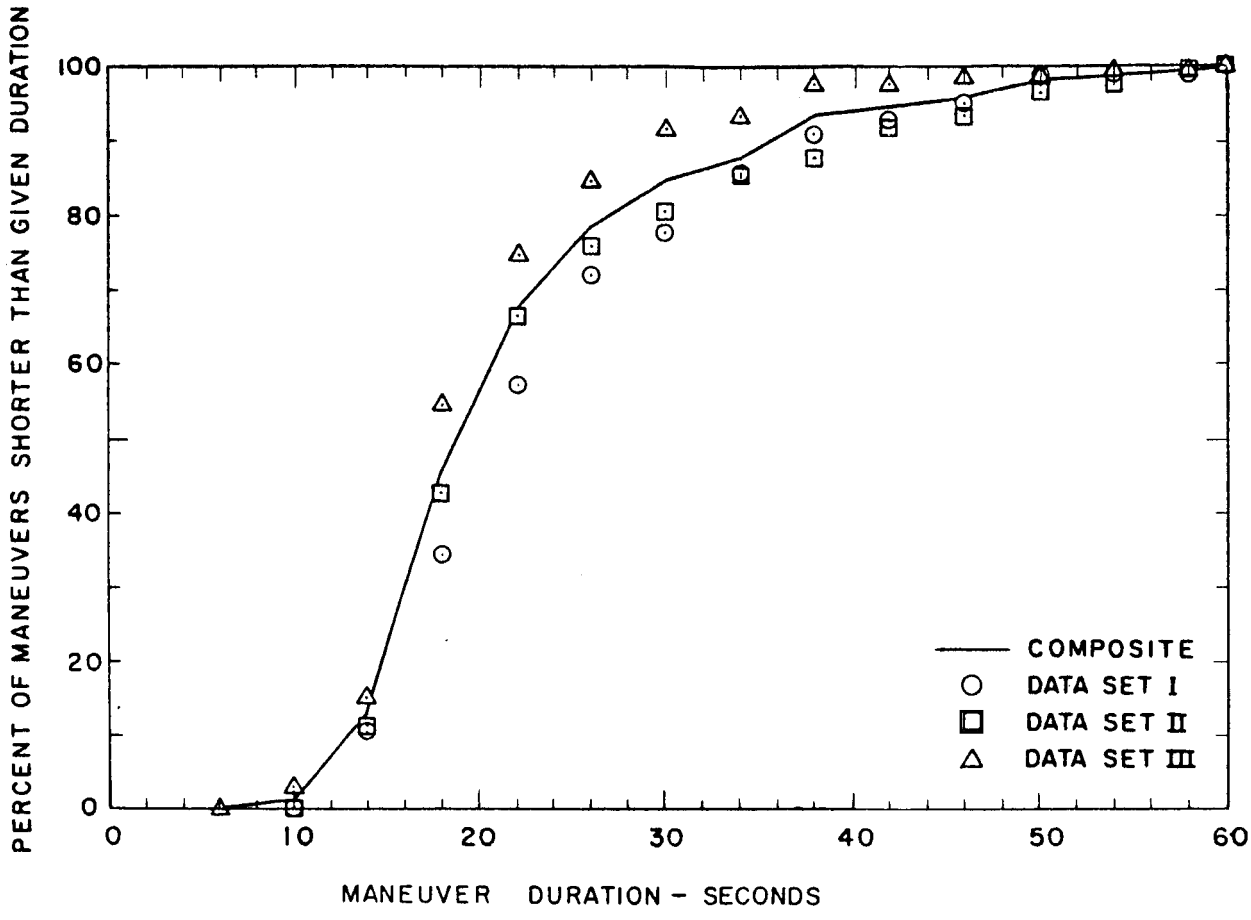

Figure 38. Graph Indicating Percentage of F-105D Descending Left Turns Shorter Than Given Durations by Data Set

APPENDIX B

PARAMETER PATTERNS FOR THE BASIC MANEUVERS

The application of the proposed statistical model to predict structural load distributions requires that maneuver types be recognizable in eight-channel data. The parameters most indicative of maneuver types are the three angular velocities, p, q, r; normal acceleration; lateral acceleration; and altitude. The airspeed and the longitudinal acceleration can sometimes support these parameters. The trace patterns indicative of the basic maneuver types are described below.

The turn maneuver may be identified by the combination of the following trace patterns: (1) a long positive peak in the normal acceleration, n_z, trace; (2) depending on the turn going either right or left, a long positive or negative peak in the yaw rate, r, trace; (3) again depending on the direction of the turn, an early positive or negative peak followed by a late peak of opposite sign in the roll rate, p, trace. In addition, a long positive peak similar to that in the normal acceleration trace appears in the pitch rate, q, trace. The trend in the altitude trace indicates that the turn is ascending, descending, or level. Figures 39 and 40 show oscillograph recordings of a descending left turn and a descending right turn, respectively.

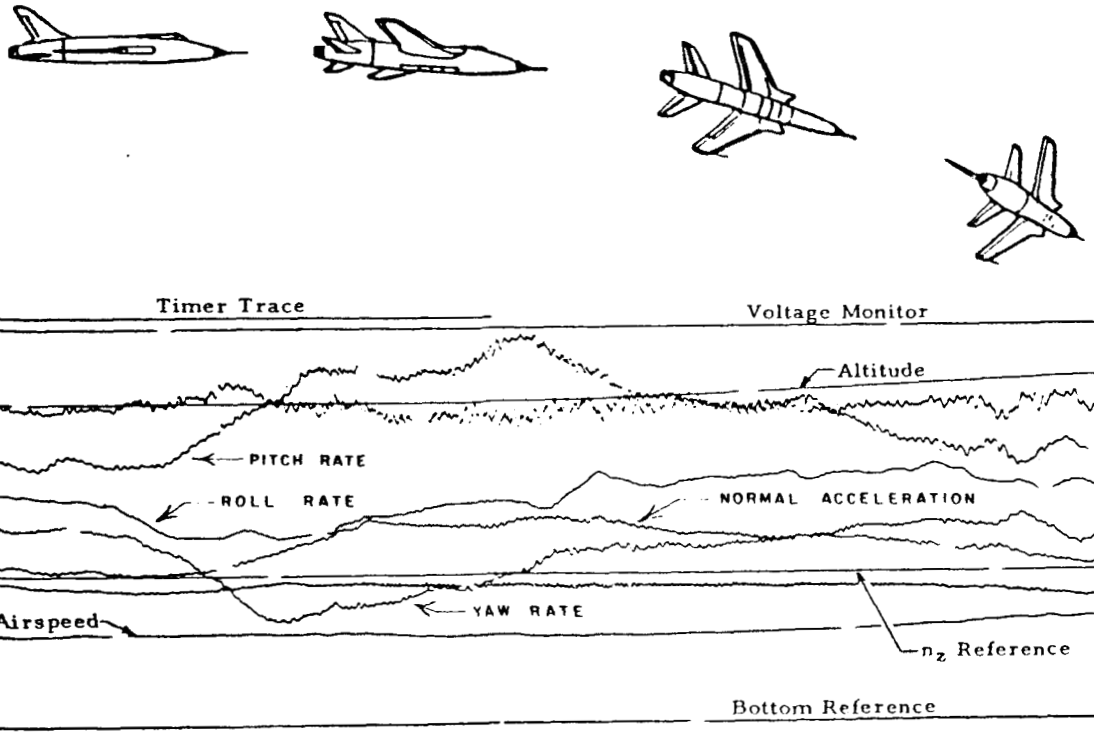

Figure 39. Oscillogram Showing Descending Left Turn

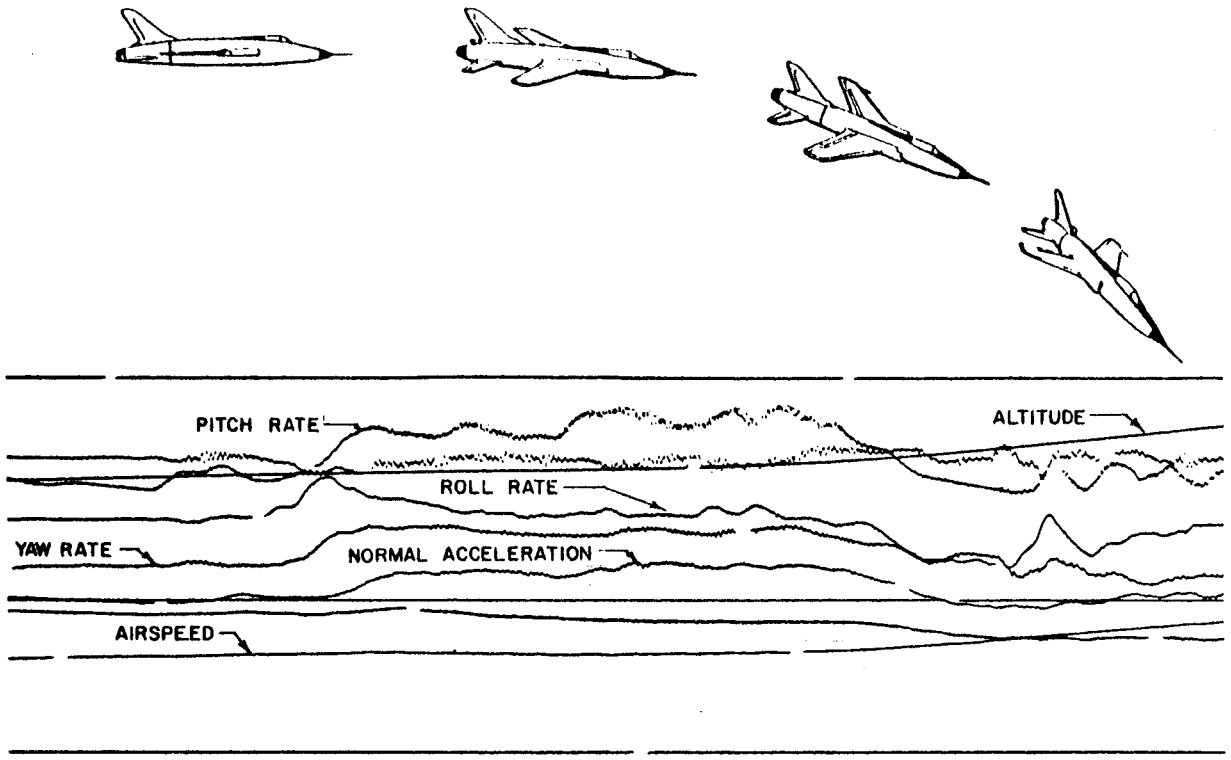

Figure 40. Oscillogram Showing Descending Right Turn

A pull-up maneuver may be classified as either a rolling or a symmetrical pull-up depending on whether or not it includes a roll rate peak. A symmetrical pull-up maneuver may be identified by the combination of the following trace patterns: (1) a large positive peak in the normal acceleration trace; (2) a large positive peak in the pitch rate trace occurring simultaneously with the former peak; and (3) an increasing rate of climb or slope of the altitude trace. Figure 41 shows an oscillograph recording of a symmetrical pull-up. Besides all the characteristic trace patterns of the symmetrical pull-up, a rolling pull-up maneuver has large positive or negative roll rate and yaw rate peaks superimposed on the normal acceleration peak. The sign of the roll rate and yaw rate peaks indicates the direction of the roll. Figure 42 shows an oscillograph recording of a right rolling pull-up. The rolling pull-up maneuver is quite similar to a symmetrical pull-up maneuver followed by an ascending turn maneuver. However, they can be distinguished by noting when the roll rate peak begins. If it begins while the normal acceleration is still high, the maneuver is a rolling pull-up. But, if the peak begins when the normal acceleration has returned close to a 1.0 value, there are two maneuvers, that is, a symmetrical pull-up and a turn.

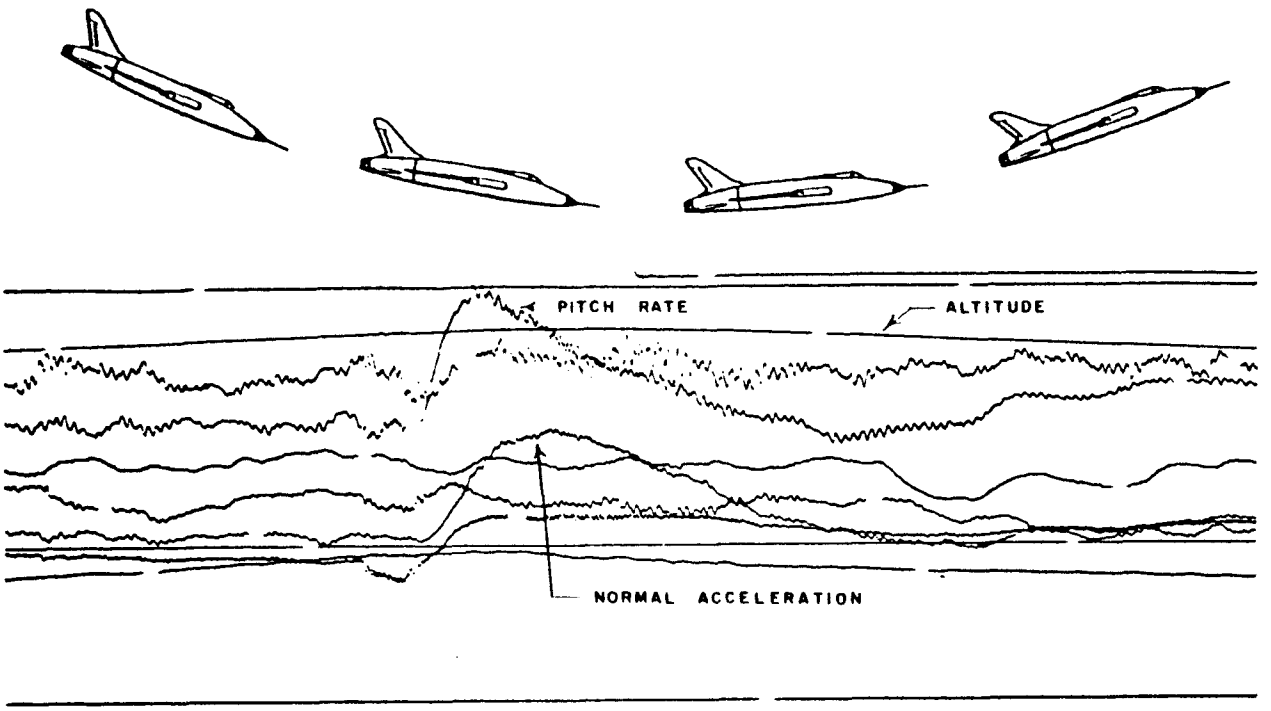

Figure 41. Oscillogram Showing Symmetrical Pull-up

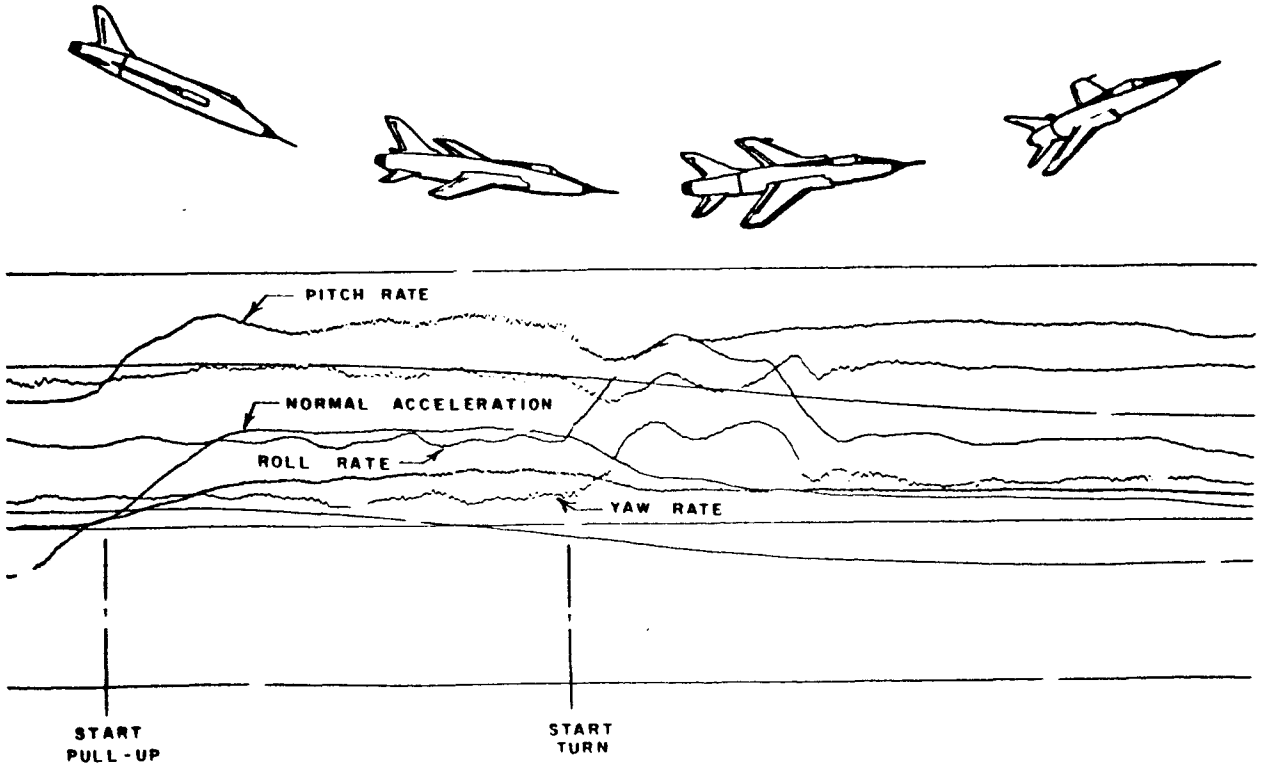

Figure 42. Oscillogram Showing Right Rolling Pull-up

The yaw maneuver is characterized by a deflection in the yaw rate trace and a large deflection in the lateral acceleration trace. None of the other parameters vary significantly. Figure 43 illustrates a yaw maneuver. In the F-105D data, a yaw maneuver was often performed early in a flight by producing a right and left yaw in quick succession to test the rudder control system (i. e., a "rudder kick").

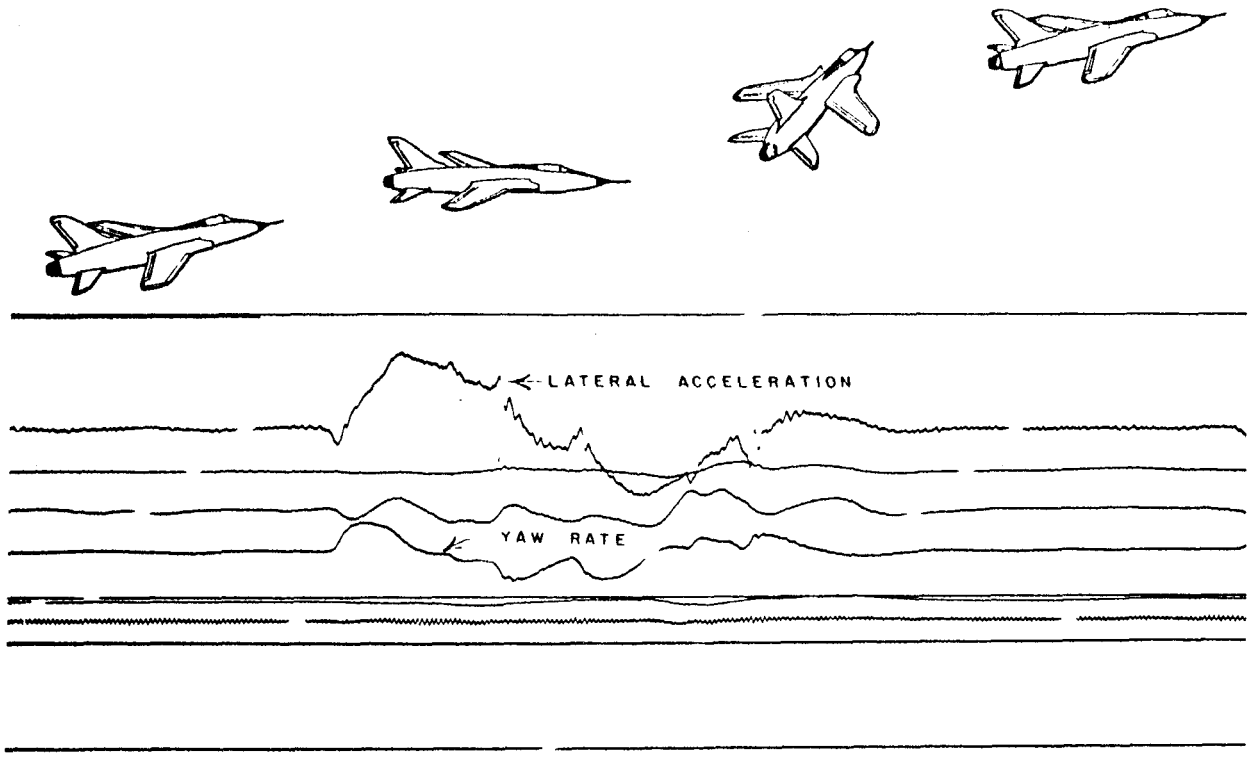

Figure 43. Oscillogram Showing Yawing Maneuver

The acceleration and deceleration maneuvers indicate an abrupt power change or the use of either an afterburner or a dive-brake system. A rapid increase or decrease of the longitudinal acceleration characterizes these maneuvers which are of relatively short duration and end as the longitudinal acceleration returns to a normal value. While the airspeed trace increases or decreases, none of the other parameters vary appreciably. Figure 44 shows a deceleration maneuver.

The barrel roll maneuver is characterized by a long peak in the roll rate trace, p. The yaw rate trace, r, will move first in one direction and then in the other because of the induced yaw and the pilot's subsequent action to correct for the induced yaw. The normal acceleration trace has no significant activity. The 180-degree roll shown in Figure 45 followed a 180-degree pitching maneuver which ended with the aircraft inverted.

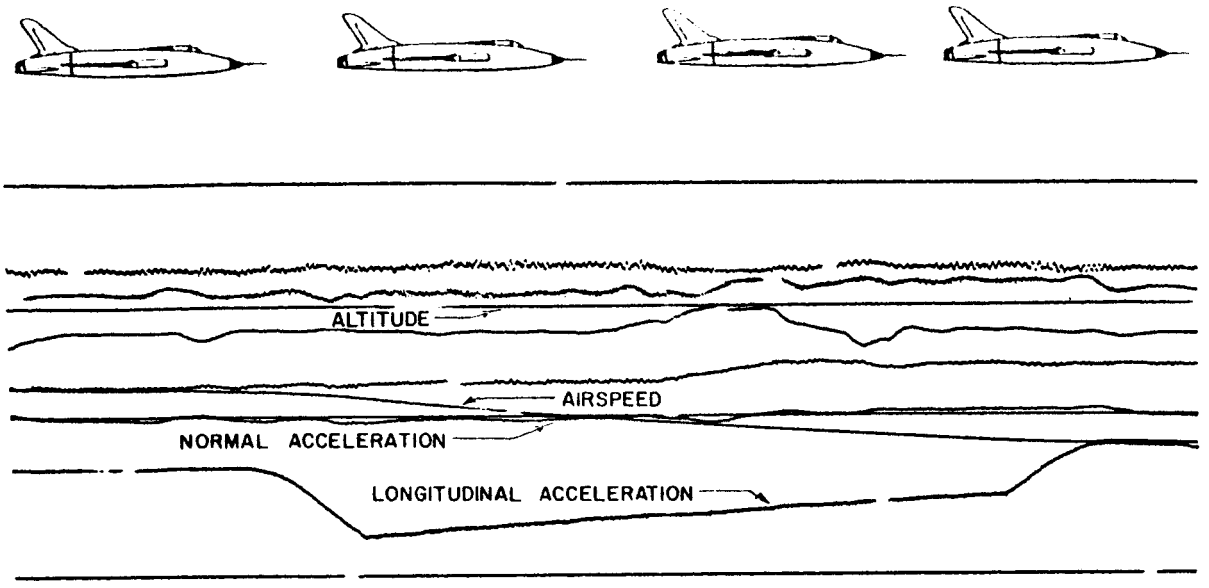

Figure 44. Oscillogram Showing Deceleration Maneuver

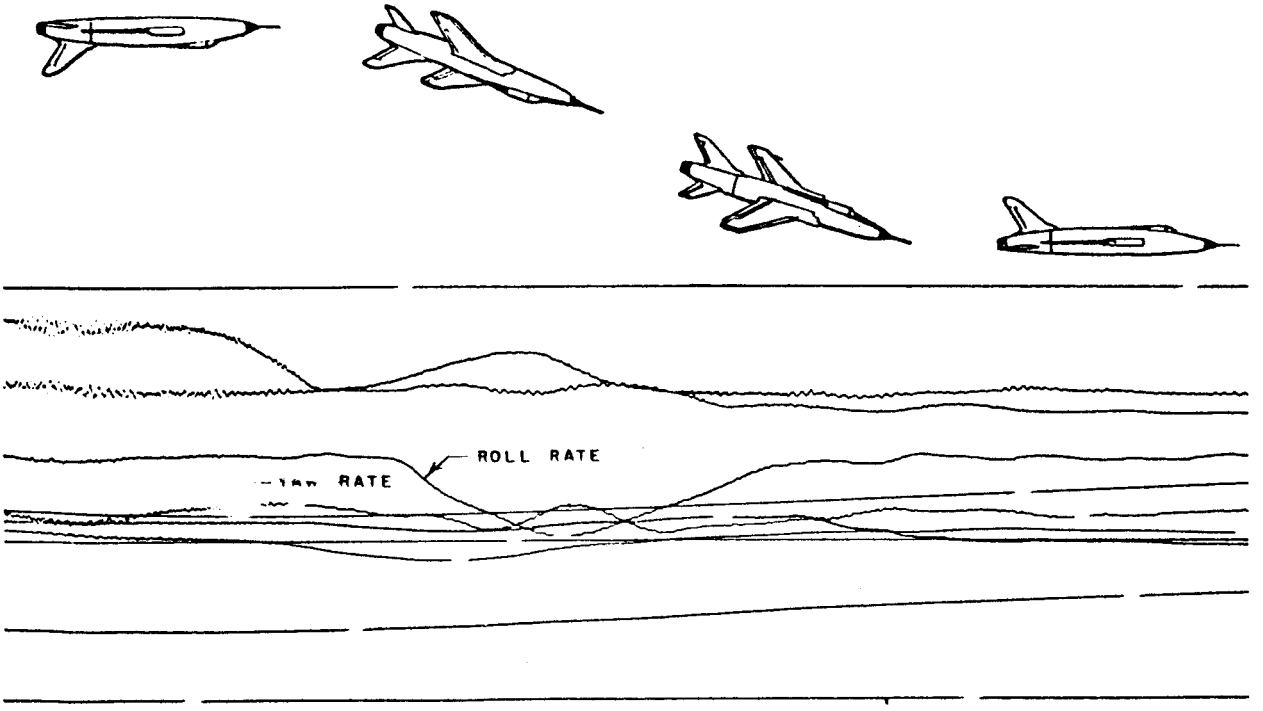

Figure 45. Oscillogram Showing Barrel Roll

Although the maneuver types described above include all those observed in the available F-105D data, maneuvers not covered by these types may be expected in other data. Then, either the description of an existing type will have to be enlarged or a new maneuver type defined.

APPENDIX C

DEVELOPMENT OF APPROXIMATE LOADS EQUATIONS FOR THE F-105D AIRPLANE

1. General Development

The airloads acting on the various surfaces of the F-105D aircraft were calculated from equations developed from the summation of the forces and moments on a rigid body. With the positive direction of the distances, forces, and accelerations as shown in Figure 46, an axis system was centered at the aircraft's center of gravity. The summation of moments and forces in this axis system results in the following equations:

$$2\Delta L_{zw} \cdot y_w - L_{yv} \cdot z_v = I_x \dot{p} - (I_y - I_z)\, qr - I_{xz}(\dot{r} + pq)$$

$$L_{zA} \cdot x_{zA} + L_{zH} \cdot x_{zH} = I_y \dot{q} - (I_z - I_x)\, pr - I_{xz}(r^2 - p^2)$$

$$L_{yA} \cdot x_{yA} + L_{yv} \cdot x_{yv} = I_z \dot{r} - (I_x - I_y)\, pq - I_{xz}(\dot{p} - qr)$$

$$L_{yA} + L_{yv} = \frac{W}{g} a_{y_{c.g.}}$$

$$L_{zA} + L_{zH} = -\frac{W}{g} a_{z_{c.g.}}$$

When solved for the air loads, these equations result in the following relationships:

$$L_{yA} = \frac{W_D}{(1 - x_{yA}/x_{yv})} \left[\frac{I_z}{x_{yv} W_D} \dot{r} - \frac{I_{xz}}{x_{yv} W_D} \dot{p} - \frac{(I_x - I_y)}{x_{yv} W_D} pq + \frac{I_{xz}}{x_{yv} W_D} qr - \frac{W}{W_D} n_y \right]$$

$$L_{zA} = \frac{W_D}{(1 - x_{zA}/x_{zH})} \left[\frac{W}{W_D} n_z - \frac{I_y}{x_{zH} W_D} \dot{q} + \frac{(I_z - I_x)}{x_{zH} W_D} pr + \frac{I_{xz}}{x_{zH} W_D} (r^2 - p^2) \right]$$

$$L_{yv} = \frac{W_D}{(1 - x_{yv}/x_{yA})} \left[- \frac{I_z}{x_{yA} W_D} \dot{r} + \frac{(I_x - I_y)}{x_{yA} W_D} pq \right.$$

$$\left. + \frac{I_{xz}}{x_{yA} W_D} \dot{p} - \frac{I_{xz}}{x_{yA} W_D} qr + \frac{W}{W_D} n_y \right]$$

$$L_{zH} = \frac{W_D}{(1 - x_{zH}/x_{zA})} \left[\frac{W}{W_D} n_z - \frac{I_y}{x_{zA} W_D} \dot{q} + \frac{(I_z - I_x)}{x_{zA} W_D} pr \right.$$

$$\left. + \frac{I_{xz}}{x_{zA} W_D} r^2 - \frac{I_{xz}}{x_{zA} W_D} p^2 \right]$$

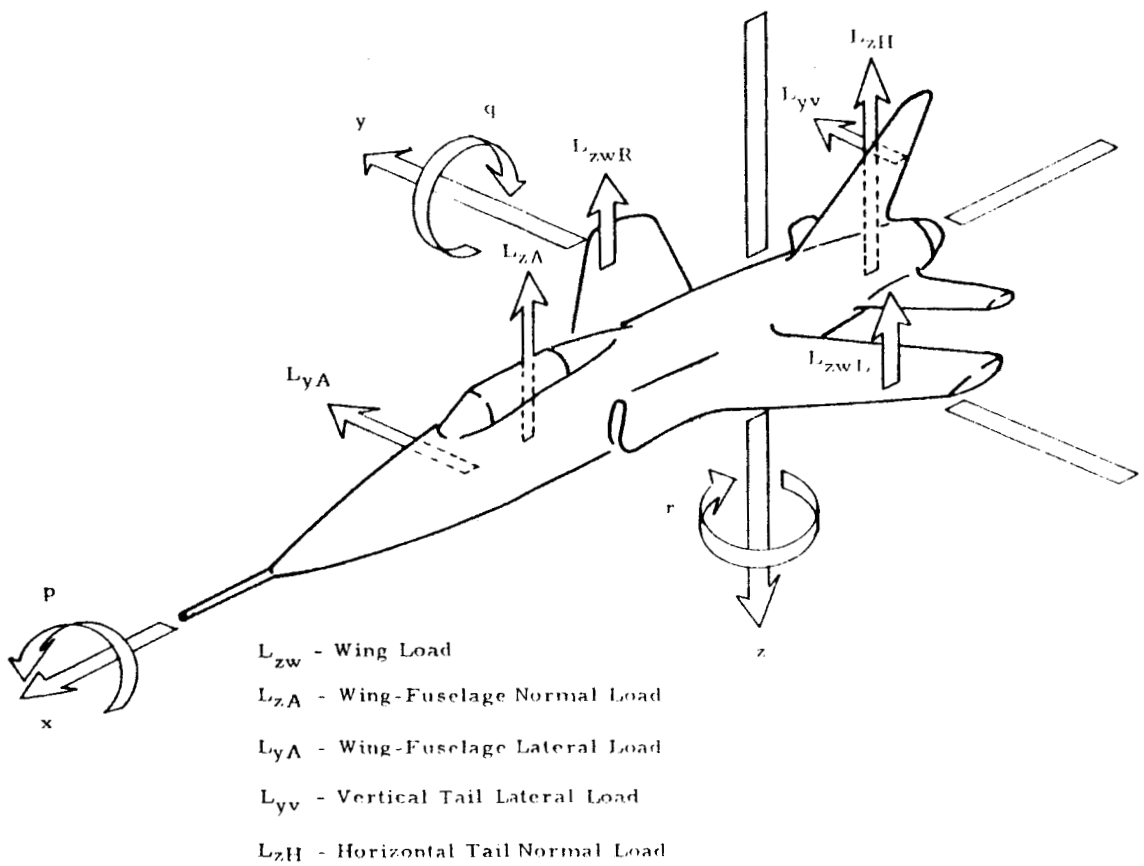

Figure 46. Drawing to Illustrate Parameter Sign Conventions and Positioning of Airloads on the Airplane

$$\Delta L_{zw} = \frac{W_D}{2y_w/b}\left[\frac{I_x}{bW_D}\dot{p} - \frac{(I_y - I_z)}{bW_D}qr - \frac{I_{xz}}{bW_D}\dot{r}\right.$$

$$- \frac{I_{xz}}{bW_D}pq + \frac{I_z}{bW_D}\frac{z_v}{(x_{yv} - x_{yA})}\dot{r} - \frac{(I_x - I_y)}{bW_D}\frac{z_v}{(x_{yv} - x_{yA})}pq$$

$$- \frac{I_{xz}}{bW_D}\frac{z_v}{(x_{yv} - x_{yA})}\dot{p} + \frac{I_{xz}}{bW_D}\frac{z_v}{(x_{yv} - x_{yA})}qr$$

$$\left. - \frac{x_{yA}}{b}\frac{z_v}{(x_{yv} - x_{yA})}\frac{W}{W_D}n_y\right]$$

The aircraft design gross weight W_D and wing span b were introduced into these equations to permit arranging the variables in nondimensional groups. Although the effect of this nondimensional grouping was not evaluated during this program, it is possible that these groups may facilitate applying the parameter peak distributions from one aircraft type to another. Since the design weight and wing span can be cancelled out of the equations, they did not affect the calculations in the present program.

In order to reduce the number of variables and achieve a neat solution, a substitution was made for the wing air loads. If it can be assumed that the wing air load is composed of a symmetrical load plus an asymmetrical load, then

$$L_{zwL} = L_{zw}/2 + \Delta L_{zw}$$

$$L_{zwR} = L_{zw}/2 - \Delta L_{zw}$$

Then, subtracting gives

$$L_{zwL} - L_{zwR} = 2\Delta L_{zw}$$

The wing air load was also combined with the fuselage air load to give the total wing-fuselage air load:

$$L_{zA} = (L_{zwL} + L_{zwR}) + L_{zF}$$

where

$$L_{zw} = (L_{zwL} + L_{zwR})$$

Since the relationship between the wing air load and fuselage air load was established from aerodynamic data, the respective air loads may be calculated whenever desired.

Given the dimensions and inertia properties of an aircraft, the air loads at any instant may be calculated through these relationships.

2. Simplified Equations

The relative magnitudes of the terms in the air loads equations were examined to determine whether any could be ignored in the present program to reduce the computational effort. The study revealed that the magnitude of some terms was relatively negligible compared with that of other terms. Consequently, such terms were dropped from the equations. As expressed below, the simplified equations were then used to calculate the air loads:

$$L^*_{zA} = \frac{W_D}{(1 - x_{zA}/x_{zH})} \left[\frac{W}{W_D} n_z - \frac{I_y}{x_{zH} W_D} \dot{q} \right]$$

$$L^*_{zH} = \frac{W_D}{(1 - x_{zH}/x_{zA})} \left[\frac{W}{W_D} n_z - \frac{I_y}{x_{zA} W_D} \dot{q} \right]$$

$$L^*_{yv} = \frac{W_D}{(1 - x_{yv}/x_{yA})} \left[- \frac{I_z}{x_{yA} W_D} \dot{r} + \frac{I_{xz}}{x_{yA} W_D} \dot{p} + \frac{W}{W_D} n_y \right]$$

$$L^*_{yA} = \frac{W_D}{(1 - x_{yA}/x_{yv})} \left[\frac{I_z}{x_{yv} W_D} \dot{r} - \frac{I_{xz}}{x_{yv} W_D} \dot{p} - \frac{W}{W_D} n_y \right]$$

$$\Delta L^*_{zw} = \frac{W_D}{2y_w/b} \left[\frac{I_x}{b W_D} \dot{p} \right]$$

3. Inertia Loads

Calculating the total load on any structural member requires determining the inertia force acting on that member. The force on each mass element i may be expressed as

$$\Delta L_i = \Delta w_i \frac{a_i}{g}$$

The a_i in each of the three orthogonal directions may be written as

$$\frac{a_x}{g} = n_x - \frac{x_a}{g}(q^2 + r^2) - \frac{y_a}{g}(\dot{r} - pq) + \frac{z_a}{g}(\dot{q} + rp)$$

$$\frac{a_y}{g} = n_y - \frac{y_a}{g}(r^2 + p^2) - \frac{z_a}{g}(\dot{p} - qr) + \frac{x_a}{g}(\dot{r} + pq)$$

$$\frac{a_z}{g} = -n_z - \frac{z_a}{g}(p^2 + q^2) - \frac{x_a}{g}(\dot{q} - rp) + \frac{y_a}{g}(\dot{p} + qr)$$

Similar to the reduction of the equations for the air loads, simplified relationships for the inertia loads were developed. As a result, the following expressions yield the primary accelerations for the major parts of the aircraft structure:

(1) wing:

$$\frac{a_z}{g} = -n_z + \frac{y_a}{g}\dot{p}$$

(2) horizontal tail:

$$\frac{a_z}{g} = -n_z - \frac{x_a}{g}(\dot{q} - rp) + \frac{y_a}{g}\dot{p}$$

(3) vertical tail:

$$\frac{a_y}{g} = n_y - \frac{z_a}{g}\dot{p} + \frac{x_a}{g}pq$$

When combined with the mass distribution of the structure, these expressions for acceleration give the inertia loads.

4. Shear Calculation

The shear load at a given wing station y may be expressed as

$$V_{y_{Airload}} = L_{zA}\int_{y}^{b/2}\omega_1(y)\,dy - \Delta L_{zw}\int_{y}^{b/2}\omega_2(y)\,dy$$

where

V_y = vertical shear at wing station y

L_{zA} = vertical air load, wing-fuselage

$2\Delta L_{zw}$ = differential wing load

$b/2$ = wing semi-span

y = lateral distance from aircraft c. g.

dy = differential element of y

$\omega_1(y)$ = percent of L_{zA} per foot of span

$\omega_2(y)$ = percent of ΔL_{zw} per foot of span

Assuming that $\omega_1(y)$ and $\omega_2(y)$ are independent of L_{zA} and ΔL_{zw}, then the equation for the shear load at wing station y may be rewritten as

$$V_{y_{Airload}} = \theta_{1y} L_{zA} - \theta_{2y} \Delta L_{zw}$$

where

$$\int_y^{b/2} \omega_1(y)\, dy = \theta_{1y} \qquad \int_y^{b/2} \omega_2(y)\, dy = \theta_{2y}$$

Derived from wind tunnel test data, the values of θ_{1y} and θ_{2y} are functions of configuration, altitude, and Mach number.

The inertia force contribution to the shear load may be written as

$$V_{y_{Inertia}} = \int_y^{b/2} \left[\frac{a_z}{g} \right] g\, m(y)\, dy$$

where

$\left[\frac{a_z}{g} \right]$ = vertical acceleration in g's at dy

$m(y)$ = mass distribution of structure per foot of span

Approximating the preceding integral by a summation of the n weight elements ω_i between y and b/2 gives

$$V_{y_{Inertia}} = \sum_{i=1}^{n} \left[\frac{a_z}{g} \right]_i w_i$$

Then V_y may be completely expressed by

$$V_y = \theta_{1y} L_{zA} - \theta_{2y} \Delta L_{zw} + \sum_{i=1}^{n} \left[\frac{a_z}{g} \right]_i w_i$$

Similar relationships may be developed for other parts of the aircraft structure.

From the simplified equations presented above and the weights and dimensions of the F-105D aircraft, shear equations were developed for the wing station 136.6, the horizontal tail root, and the vertical tail root. These equations, which were used to calculate the shear loads at the foregoing locations, are as follows:

(1) wing station 136.6 (location 6A):

$$V^{*}_{6A} = .15547\ Wn_z + .000138\ I_y\dot{q} - .000596\ I_x\dot{p}$$

$$-n_z \sum_{i=1}^{n} w_i + .01745\ \dot{p} \left(\sum_{i=1}^{n} w_i \frac{y_i}{g} \right)$$

(2) vertical tail root:

$$V^{*}_{RVT} = .1061\ Wn_y - .000741\ I_z\dot{r} + .000741\ I_{xz}\dot{p} - 889\ n_y - 3.244\ \dot{p}$$

(3) horizontal tail root:

$$V^{*}_{RHT} = -.0307\ Wn_z - .000472\ I_y\dot{q} - 349\ n_z + 3.86\ \dot{q} + .993\ \dot{p}$$

To indicate the difference between the solutions acquired from the complete and the simplified equations, Figures 47 and 48 each show for one sample maneuver two time histories of calculated loads, one derived from the complete equations (V_{6A}, V_{RVT}) and the second from the simplified equations (V^*_{6A}, V^*_{RVT}). Figure 47 giving the wing normal shear loads shows that the simplified equations yielded quite accurate load values. Although Figure 48 giving the vertical tail root shear loads shows that the values derived from the simplified equations do not compare as favorably, they are acceptable for the purposes of this study. This study was intended to demonstrate the accuracy of a statistical calculation of load distribution when compared to a time history calculation. For this purpose, it is necessary only that identical equations be used in both calculation methods, not that the calculated loads be strictly accurate.

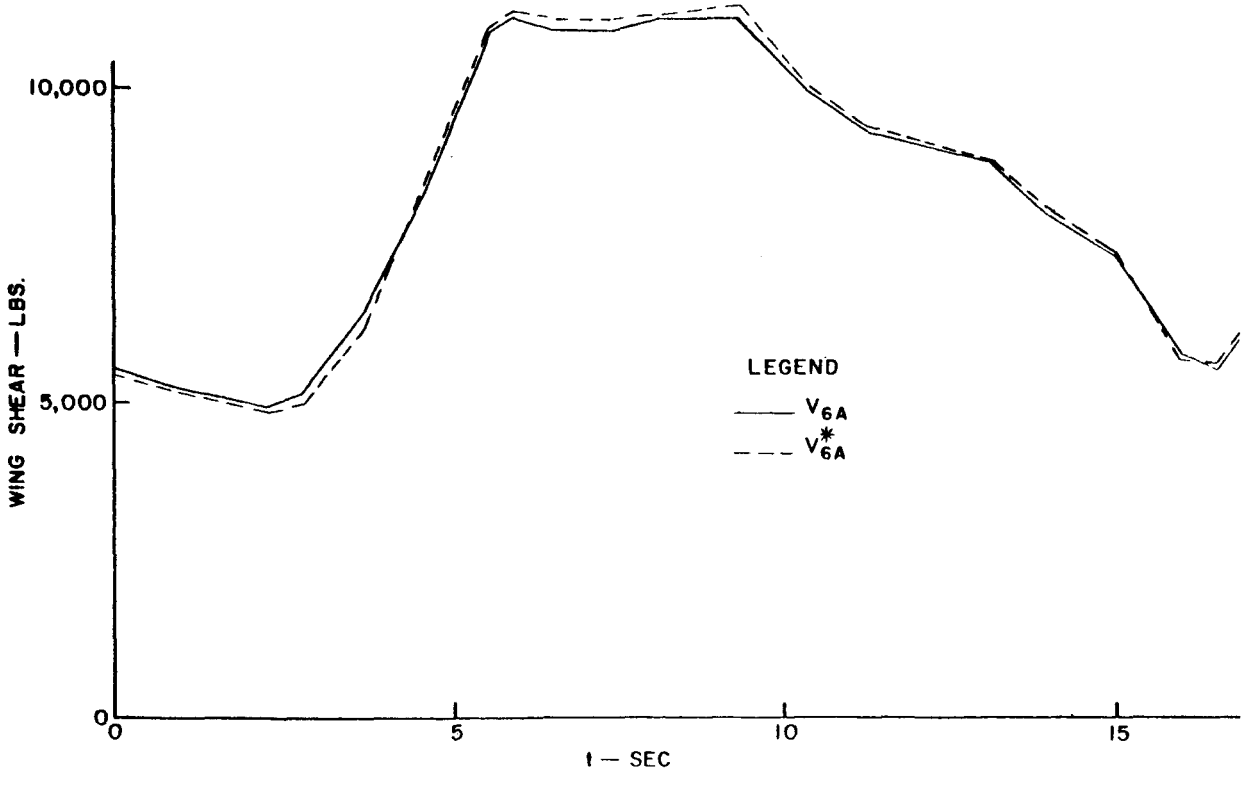

Figure 47. Time History Plots of Wing Shear Load Calculated With Complete (V_{6A}) and Simplified (V^*_{6A}) Equations

Each maneuver sample was treated individually in calculating the aircraft gross weight and moments of inertia. It was assumed that the weight and moments of inertia were constant during a maneuver. The values of the parameters, n_z, n_y, p, q, r, $\dot{p}$, $\dot{q}$, and $\dot{r}$, were taken at discrete instants from the time history of each maneuver. Then loads calculated at these instants gave a time history of the loads.

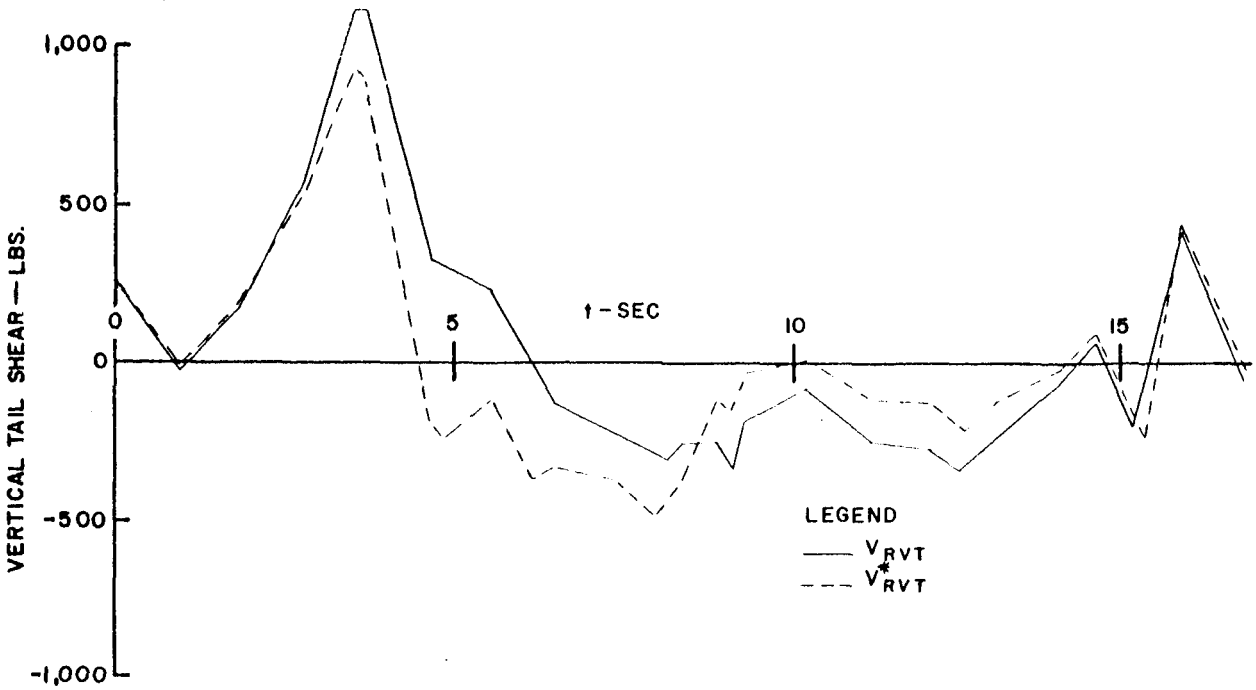

Figure 48. Time History Plots of Vertical Tail Shear Load Calculated With Complete (V_{RVT}) and Simplified (V^*_{RVT}) Equations

Dimensions Used in the Equations

Table 16 gives the dimensions locating the points at which air loads were applied as indicated in Figure 46. This table also locates the center of gravity of the vertical and horizontal tail. These dimensions were obtained from available weight and balance and aerodynamic data. The data available was not sufficient to yield dimensions for all combinations of flight envelope and loading characteristics encountered. However, the use of a set of constant dimensions was considered adequate for the purpose of the present program. To apply this method to design considerations requires including the effects of changes in the aircraft's center of gravity and centers of pressure.

TABLE 16

Constants Used in Air Loads Equations

A. Coordinate Distances to Air Load Application Point

x_{yA} = +2.500 ft - wing-fuselage lateral air load

x_{yv} = +21.052 ft - vertical tail lateral air load

x_{zA} = -1.135 ft - wing fuselage normal air load

TABLE 16 (cont'd)

x_{zH} = -19.635 ft - horizontal tail normal air load

y_w = +14.62 ft - wing normal air load

z_{yv} = -7.891 ft - vertical tail lateral air load

B. Center of Gravity Locations

1. horizontal tail

x = -20.40 ft

y = +5.25 ft

z = +1.68 ft

2. vertical tail

x = -21.55 ft

y = 0

z = 6.73 ft

3. wing (outboard of Station 136.6)

x = 0

y = 14.10 ft

z = 0

C. Wing Span = 34.925 ft

D. Design Gross Weight = 36,018 lb.

Moments of Inertia

The moments of inertia computed for each maneuver sample were assumed to remain constant during the maneuver. As listed in Table 17, the base values of the moments of inertia are those for an externally clean aircraft with internal stores and a 36,018-lb. design gross weight. The values were corrected for the various configurations of internal and external stores and for changes in the fuel supply. The 40 flight records used for the present investigation have 16 different takeoff configurations. The breakdown of the configurations includes distinguishing the full and empty external fuel tanks. However, this distinction did not appreciably increase the number of different configurations since most of the maneuvers occurred when the external tanks were empty. The various takeoff configurations are listed in Table 10 in Appendix A.

TABLE 17

Base Values of Moments of Inertia for an Externally Clean Aircraft with Internal Stores and Fuel

$I_x = 17,100 \text{ slug-ft}^2$

$I_y = 202,100 \text{ slug-ft}^2$

$I_z = 214,000 \text{ slug-ft}^2$

$I_{xz} = 2,550 \text{ slug-ft}^2$

Gross Weight

The aircraft gross weight during each descending left turn was estimated by taking the difference between the takeoff and landing gross weights and applying a linear rate of weight loss during the flight.

APPENDIX D

DATA FILTERING TECHNIQUES

Traces of parameters recorded in a flight loads program exhibit wave-like patterns having a wide range of amplitude and frequency. In some portions of the recorded flights, the patterns are very erratic while in other places they are quite smooth. In general, the frequency of the parameter trace is higher at low altitudes and high airspeeds. With the paper speed set for the recording of the F-105D eight-channel data, oscillations with frequencies up to 5 cps could be visually distinguished. However, oscillations of higher frequency were apparent in some portions of the flights. The high frequency oscillations are caused mostly by atmospheric turbulence.

Parameter responses to maneuvers are normally smooth low-frequency trace deflections whose peaks have durations of 2 seconds (which corresponds to a frequency of 0.25 cps) or more. Since a statistical description of the maneuvers was the objective of this study and, accordingly, equations to calculate only the loads due to maneuvers were developed, it was decided to ignore the high-frequency gust-induced motions in the recorded data. In the F-105D data the linear accelerations due to gusts are relatively small compared to the accelerations due to maneuvers. Although most of the gust accelerations were removed by the fixed sampling rate, as discussed below, any remaining in the data sample should not appreciably affect the larger maneuver data. However, the traces representing the aircraft angular motions presented some difficulty because large high-frequency oscillations appeared in the derived angular acceleration time histories when the small high-frequency oscillations in the angular rate traces were differentiated. Consequently, as described later, the angular rate traces were smoothed before differentiating to eliminate all the high-frequency oscillations which would otherwise have appeared in the derived angular acceleration time histories.

The sampling rate placed a frequency limitation on the measured parameter time histories. Figure 49 illustrates the frequency limitation of a sampling rate of 5 samples per second. Assuming that a parameter is sinusoidal and has unit amplitude and that the peak falls midway between two readings, the figure presents the ratio of the measured peak amplitude to the actual peak amplitude versus the trace frequency. The measured peak amplitude may be in error by 5 percent for a 0.5-cps trace and by 100 percent (or, in other words, completely missed) for a 2.5-cps trace. Thus, the sampling rate limited the frequency of the reduced data to approximately 0.5 cps.

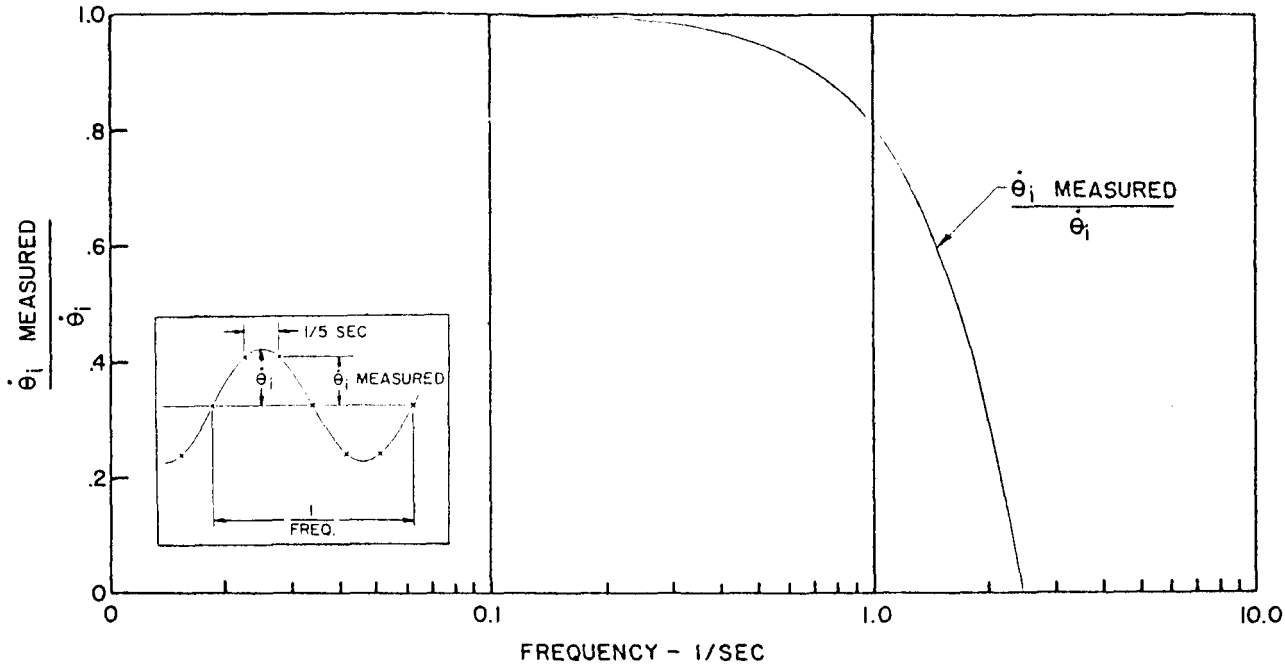

Figure 49. Graph to Indicate Effect of a Five-per-Second Sampling Rate on Frequency of Reduced Data

Two types of filtering techniques were tried to smooth the angular rate traces—a "cosine" filter and a 7-point weighted filter. When the "cosine" filter was used, the angular rate value $\dot{\theta}_i$ at each point i was replaced by a filtered $\dot{\theta}'_i$ which was calculated from the following equation:

$$\dot{\theta}_i = \frac{1}{2} (\dot{\theta}_{i-1} + \dot{\theta}_{i+1})$$

The dashed curve in Figure 50 illustrates the effect of the "cosine" filter on a sinusoidal input trace of unit amplitude sampled 5 times per second. This figure presents the ratio of $\dot{\theta}'_i$ to $\dot{\theta}_i$ versus input trace frequency where the sample point i was located at a peak of the input trace. Although this filter smoothes the data in the desired frequency range, it has two undesirable effects: (1) the phase shift which causes negative peak values at the sample point for input frequencies between 1.225 and 3.775 cps, 6.225 and 8.775 cps, etc., and (2) the resonance peaks at 2.5 cps, 5 cps, 7.5 cps, etc. Because of these two effects, the "cosine" filter was not used.

The 7-point weighted filter replaced the angular rate $\dot{\theta}_i$ at the sample point by a filtered $\dot{\theta}'_i$ which is expressed as follows:

$$\dot{\theta}_i = \frac{1}{16} (\dot{\theta}_{i-3} + 2\dot{\theta}_{i-2} + 3\dot{\theta}_{i-1} + 4\dot{\theta}_i + 3\dot{\theta}_{i+1} + 2\dot{\theta}_{i+2} + \dot{\theta}_{i+3})$$

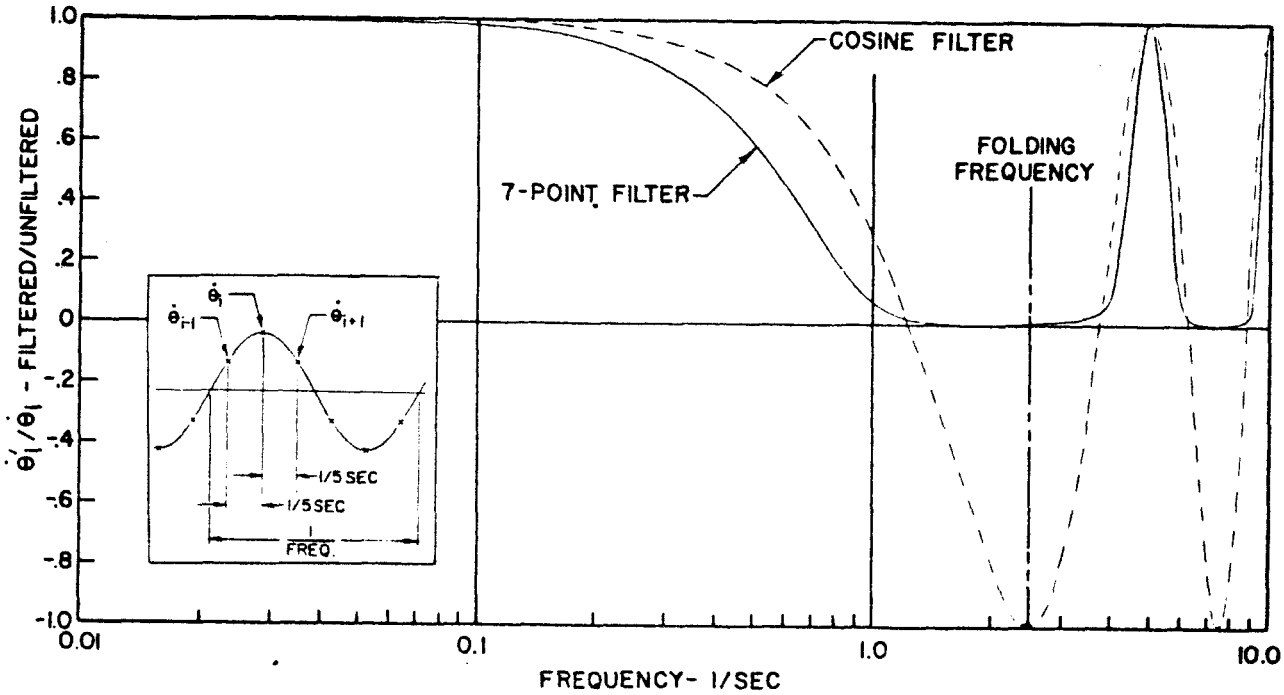

Figure 50. Graph to Indicate Effect of Filtering on Frequency of Reduced Data

The solid line in Figure 50 is the ratio of $\dot{\theta}'_i$ to $\dot{\theta}_i$ for a unit sinusoidal input trace sampled 5 times per second with sample point i located at a positive peak. Although this filter smoothes the data more severely in the low-frequency input ranges below 1.2 cps, it has the obvious advantage of not introducing a phase shift and negative peak values calculated for the positive peak at point i. The resonance peaks still present at 5 cps, 10 cps, etc., did not present any problem, however, since the data readers measured a line drawn through the mean of trace oscillations with frequencies of 5 cps and above and made no attempt to measure the actual trace in these areas.

Because of the advantages given above, the 7-point filter was used to smooth the angular rate time histories. Although this filter placed an additional frequency limitation on the angular rate data, it had no appreciable effect on data at frequencies below 0.25 cps.

Figures 51 and 52 show the effect of the smoothing on the roll rate and roll acceleration time histories for one descending left turn. The solid lines in these figures represent time histories derived from the measured values of roll rate, and the dashed lines represent time histories derived from data in which the roll rates were smoothed. The advantage of the smoothing is quite evident in the roll accelerations illustrated in Figure 52.

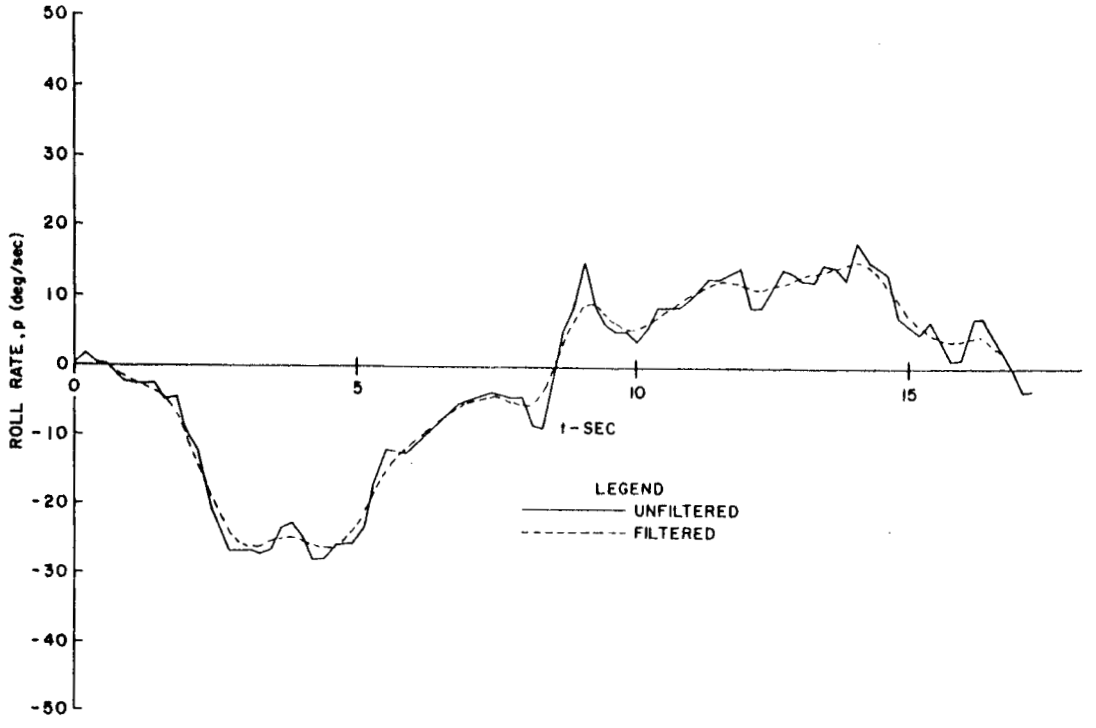

Figure 51. Filtered and Unfiltered Roll Rate Time Histories

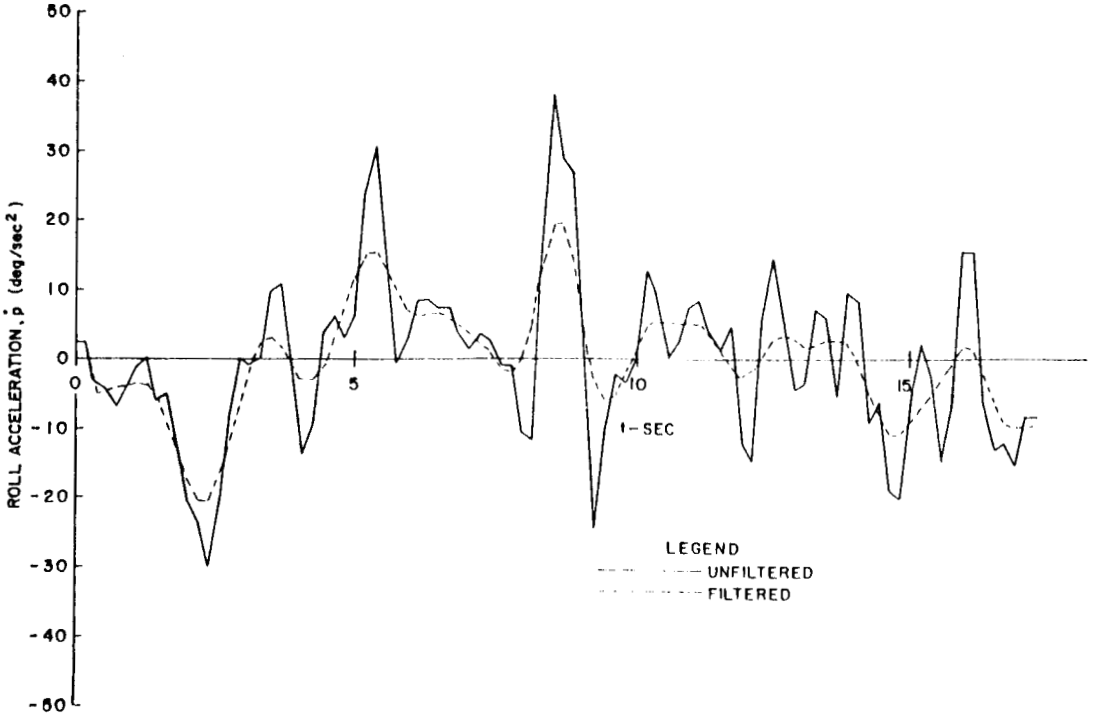

Figure 52. Plots of Roll Acceleration versus Time Derived from Filtered and Unfiltered Roll Rate Time Histories

APPENDIX E

PREDICTED AND OBSERVED PEAK LOADS DISTRIBUTIONS BY DATA SET

Since the data were processed in batches, three independent subsets of predicted and observed distributions were derived to study the effect of sample size and to check the consistency of the predictions through the comparison of data. Set I contains 68 maneuvers; Set II, 118; and Set III, 132. For each of these sets, the number of samples in the normalized distributions is the same as the number of maneuvers. However, the peak distributions and observed peak load distributions were separated into Conditions 1 and 2: Set I contains 54 maneuvers in Condition 1 and 14 in Condition 2; Set II contains 50 maneuvers in Condition 1 and 68 in Condition 2; and Set III contains 81 maneuvers in Condition 1 and 51 in Condition 2. Distributions were not derived for the 14 maneuvers in Condition 2 of Set I since this sample is too small.

Figures 53 through 64 present the predicted and observed distribution for the wing, horizontal tail, and vertical tail loads for the three subsets and the two conditions. Generally, the predicted distributions do not fit the observed distributions as well as the composites (Figures 26 to 31); nevertheless, even with the small sample sizes, the fits are obviously acceptable.

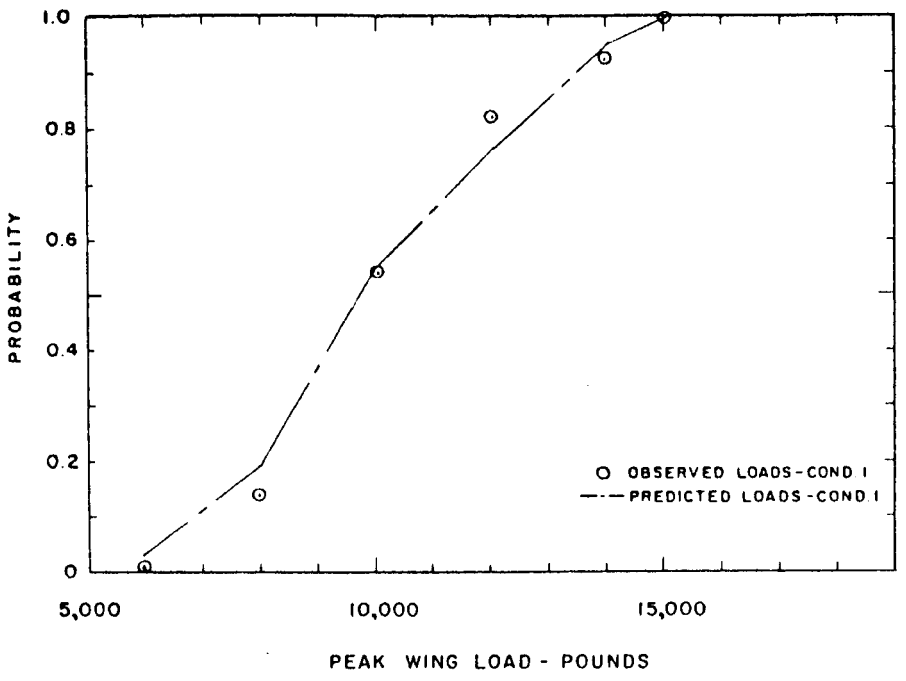

Figure 53. Predicted and Observed Cumulative Probability versus Peak Wing Load for Data Set I, Condition 1 (54 turns)

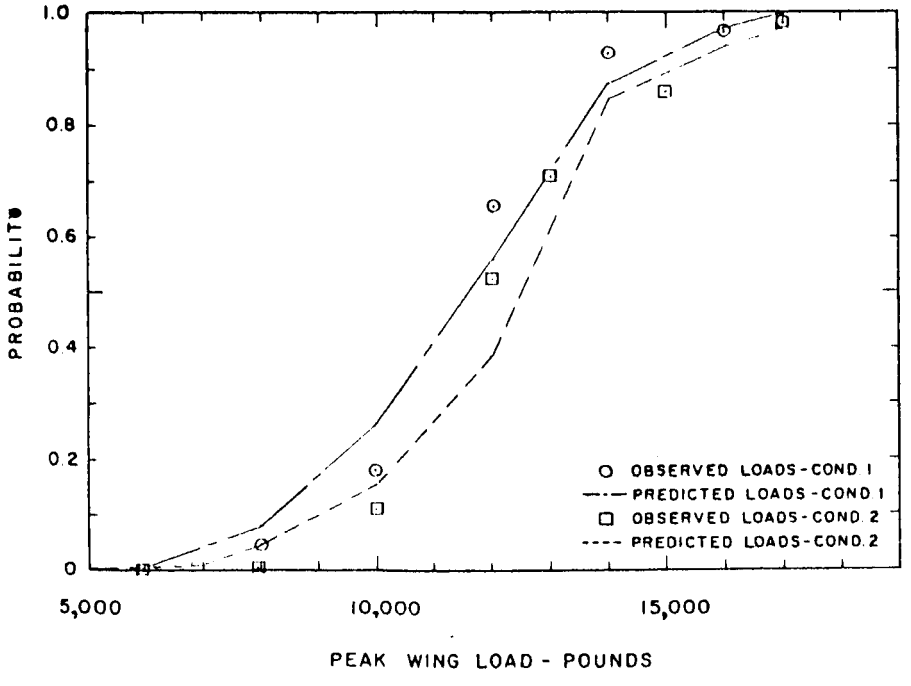

Figure 54. Predicted and Observed Cumulative Probability versus Peak Wing Load for Data Set II, Condition 1 (50 turns) and Condition 2 (68 turns)

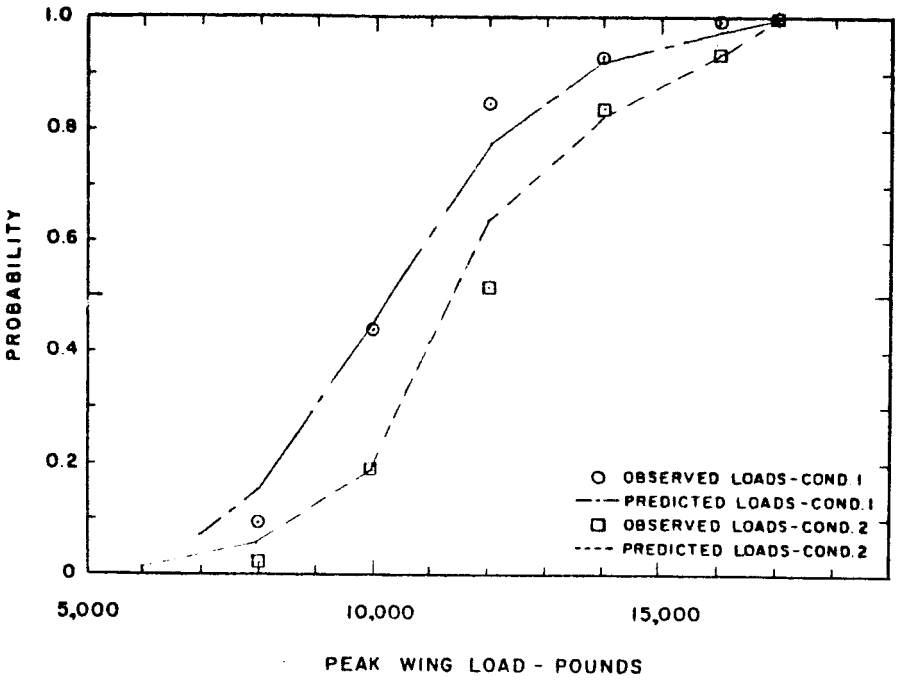

Figure 55. Predicted and Observed Cumulative Probability versus Peak Wing Load for Data Set III, Condition 1 (81 turns) and Condition 2 (51 turns)

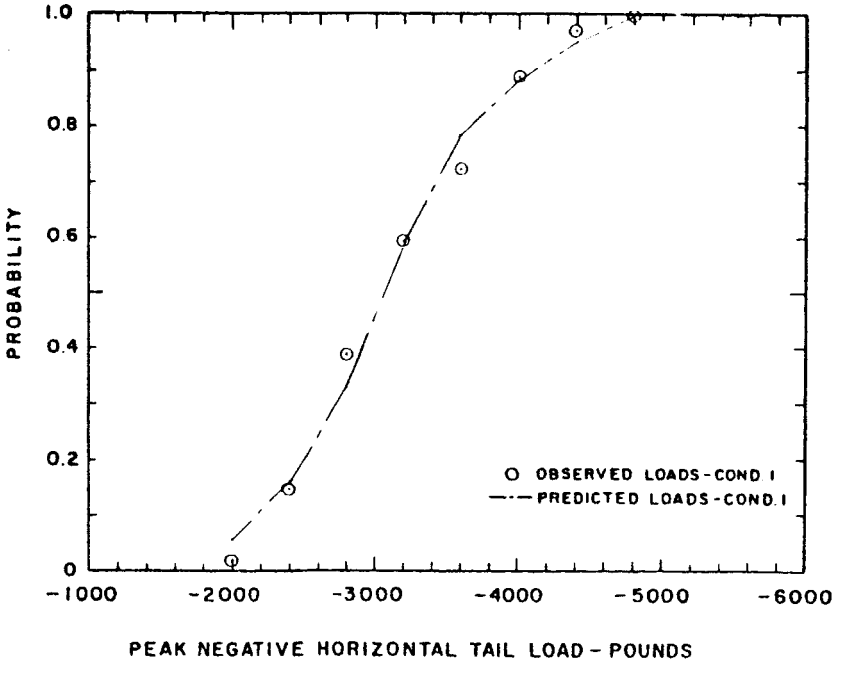

Figure 56. Predicted and Observed Cumulative Probability versus Peak Horizontal Tail Load for Data Set I, Condition 1 (54 turns)

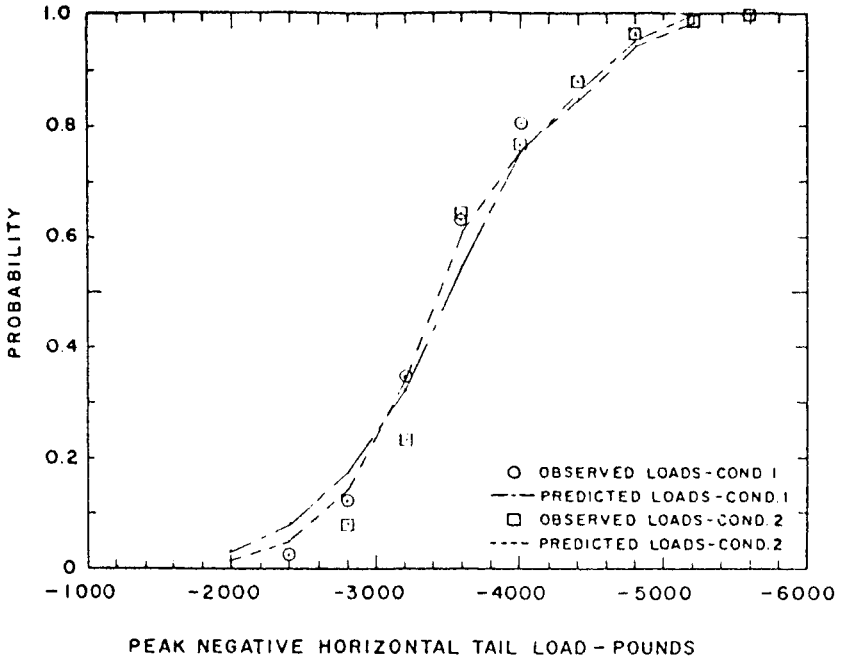

Figure 57. Predicted and Observed Cumulative Probability versus Peak Horizontal Tail Load for Data Set II, Condition 1 (50 turns) and Condition 2 (68 turns)

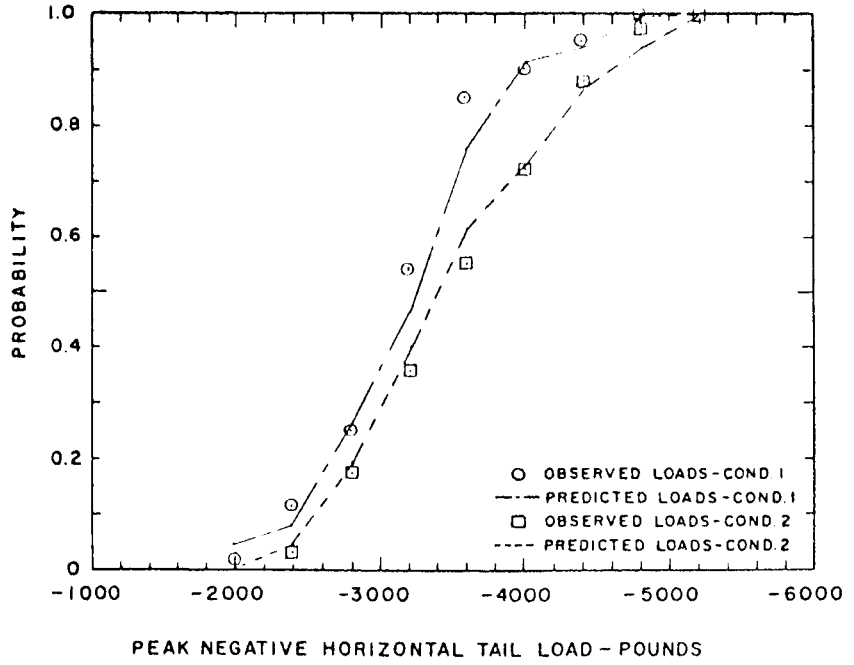

Figure 58. Predicted and Observed Cumulative Probability versus Peak Horizontal Tail Load for Data Set III, Condition 1 (81 turns) and Condition 2 (51 turns)

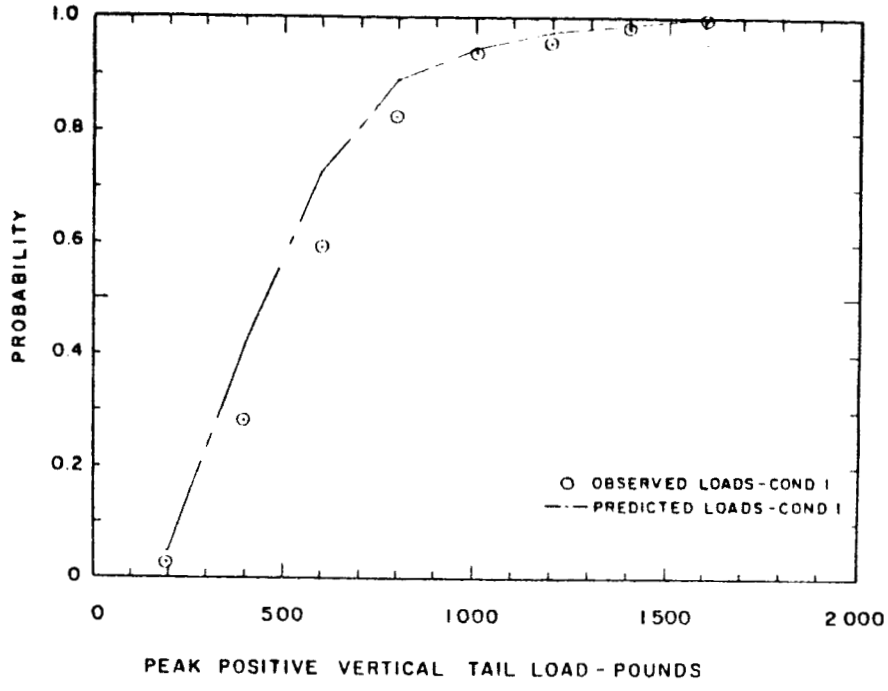

Figure 59. Predicted and Observed Cumulative Probability versus Peak Positive Vertical Tail Load for Data Set I, Condition 1 (54 turns)

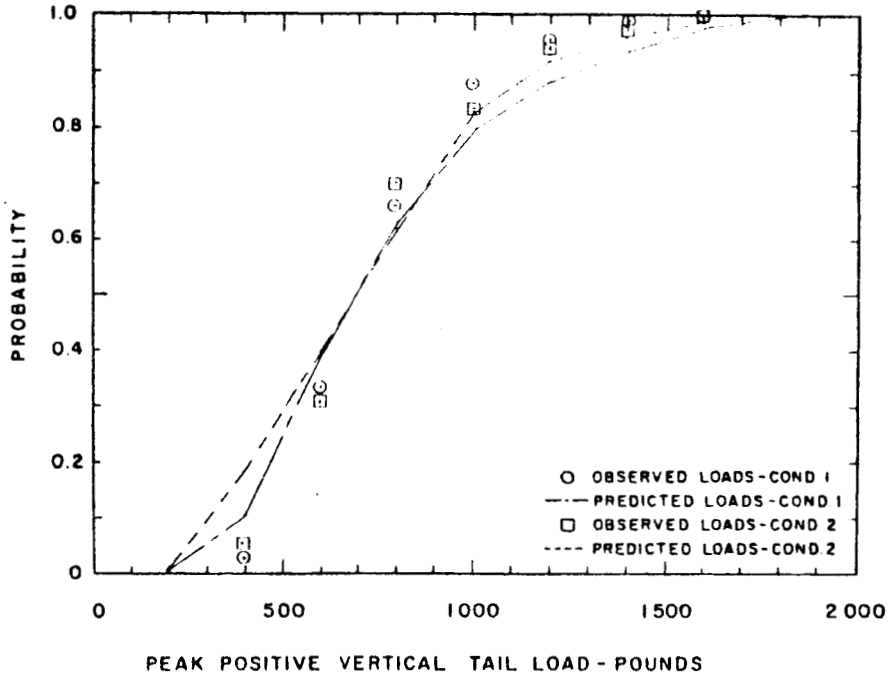

Figure 60. Predicted and Observed Cumulative Probability versus Peak Positive Vertical Tail Load for Data Set II, Condition 1 (50 turns) and Condition 2 (68 turns)

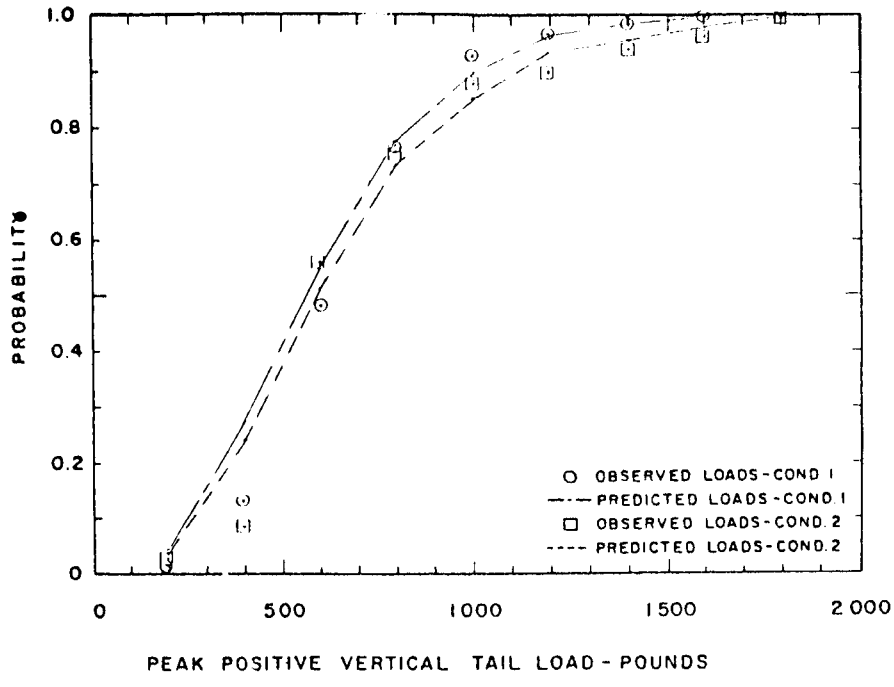

Figure 61. Predicted and Observed Cumulative Probability versus Peak Positive Vertical Tail Load for Data Set III, Condition 1 (81 turns) and Condition 2 (51 turns)

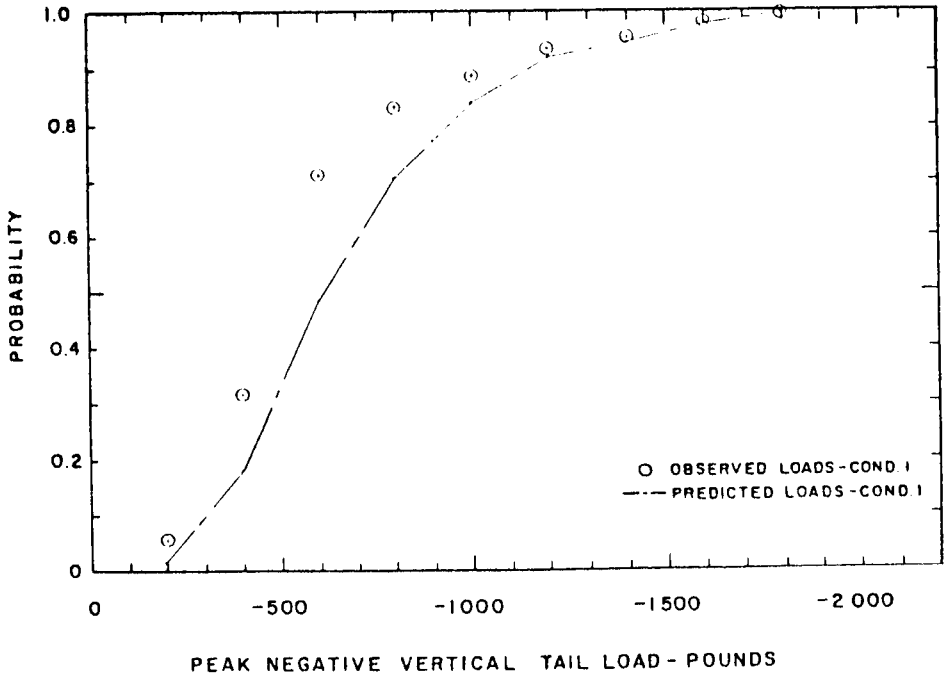

Figure 62. Predicted and Observed Cumulative Probability versus Peak Negative Vertical Tail Load for Data Set I, Condition 1 (54 turns)

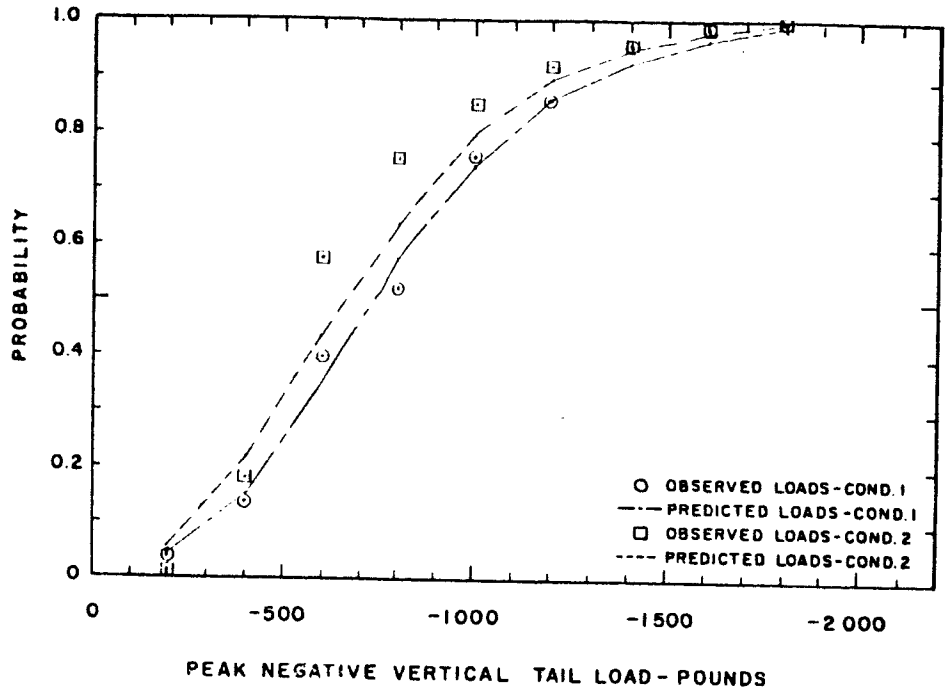

Figure 63. Predicted and Observed Cumulative Probability versus Peak Negative Vertical Tail Load for Data Set II, Condition 1 (50 turns) and Condition 2 (68 turns)

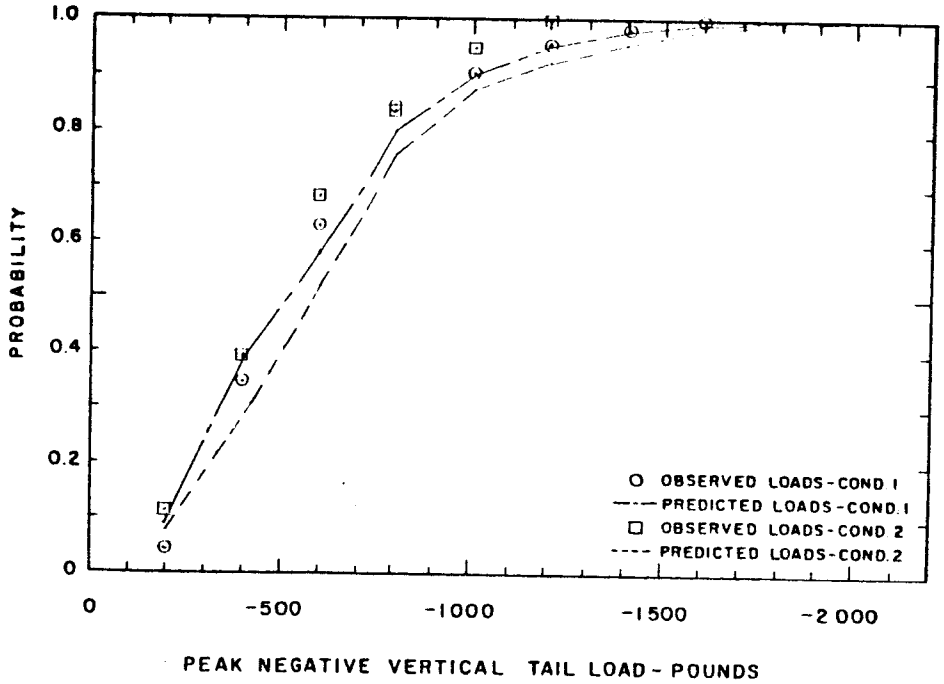

Figure 64. Predicted and Observed Cumulative Probability versus Peak Negative Vertical Tail Load for Data Set III, Condition 1 (81 turns) and Condition 2 (51 turns)